Behaviour of rare earth elements during water-rock interaction and alteration processes in volcanic lake systems

by

Georgina Ayres

A thesis submitted to the
Faculty of Geosciences of Utrecht University
in partial fulfilment of the requirements for
the degree of Master of Science

Supervisor: dr. M.J. van Bergen

Department of Earth Sciences
Petrology Research Group
August 2012

1. Abstract

The rare earth elements are widely used to study processes in many different geological environments. Although their behaviour is particularly suitable for research on water-rock interactions, volcanic lakes have received little attention so far. This thesis documents the results of a study on rare earth elements (REE) in active, crater-lake hosting volcanic-hydrothermal systems worldwide. Particular attention has been paid to Poás and Rincón de la Vieja, two Costa Rican volcanoes for which new analytical data are presented. A literature survey covers geochemical information available for volcanic lakes in Indonesia, Argentina, the Philippines, New Zealand, Japan, USA and Russia. Most of these lakes are highly acidic.

The main objective of this research was to explore how REE that are dissolved in crater lake water can be used to gain insights into water-rock interaction processes and to monitor activity in the underlying hydrothermal system. For this purpose, the newly acquired data and those from the literature compilation were evaluated to discern systematics in the behaviour of the REE and other elements, whereby the compositions of local rocks were taken in account as well.

The REE concentrations and their normalized trends show significant variations for the investigated lakes. There is a rough correlation between REE patterns of the lake waters and the local rocks, testifying that lavas and other solid volcanic products are the principal source of the REE. In general, the correspondence is best for highly acidic lakes. The observed systematics indicate that rock dissolution plays an important role but fractionation among the REE shows that complete, congruent dissolution is rare and only occurs under extreme conditions. In general, water-rock interaction in these volcanic-hydrothermal settings affects individual igneous minerals in different ways, some being more resistant than others. The collected data indicate that the REE signatures in lake waters are controlled by preferential retention or release from REE hosting phases, either primary igneous minerals or glass in volcanic materials, or secondary phases formed as alteration product.

An important discovery is the apparent role of alunite in regulating the signatures of dissolved REE in lake waters. This is surprising because this mineral is an alteration product that is commonly not stable in acidic volcanic lakes. However, as could be confirmed in PHREEQC models, the saturation state of alunite in these waters is inversely correlated with temperature. This implies that alunite can be present in hotter parts of the hydrothermal system below the lake, and that the REE signatures in the lake may be inherited from inflow of water that had interacted with alunite present at depth. Changes in REE patterns in lakes that have been monitored over longer times indicate that the influence of alunite may vary with time. This suggests that a lake may signal the stability of the mineral, and its formation or dissolution in response to changing conditions. Apart from the REE data, the potential role of alunite can be confirmed by comparing the concentrations of its main cation constituents with other dissolved cations in the lake.

Time-series results on REE concentrations in the highly dynamic crater lake of Poás provide evidence for an intermittent role of alunite in the subsurface system. Strong fluctuations in LREE/HREE ratios, observed over decades of monitoring, probably reflect variations in the stability of the mineral, induced by changing hydrothermal conditions. Changes in the REE concentrations sometimes coincided with phreatic eruptive events. Since alunite is a secondary, non-magmatic mineral, its presence or absence may affect the porosity and permeability of volcanic rocks and conduits that act as pathways for upflowing fluids. Evidence for Poás suggests that the formation of alunite has a sealing effect that reduces the influx of fluid and heat into its lake.

It is concluded that REE in volcanic lakes are a promising new instrument to study water-rock interaction and alteration processes that are active at the very present. Monitoring the REE provides a valuable parameter in assessing changes in the state of activity for volcanic-hydrothermal systems.

2. Introduction

This introduction describes the rationale for investigating the behaviour of rare earth elements (REE) volcanic areas that host magmatic-hydrothermal systems and the structure of this thesis.

2.1 REE as geochemical tracer for magmatic-hydrothermal systems

The REE in rocks, minerals and water have long been used as a geochemical indicator of geological processes and the provenance of geological materials. Their coherent behaviour makes them an excellent natural tracer, with an almost unlimited number of applications in the Earth sciences. In the past, only an incomplete set of the REE group could be measured because of analytical limitations, but recent advances have made it possible to collect accurate data for almost the complete set of elements. Despite this progress, volcanic crater lakes and hydrothermal waters (both submarine and terrestrial) have received relatively little attention so far. Exceptions are, for example, studies by Michard et al. (1986), Michard (1989), Gammons et al. (2005), and Lewis et al. (1997 and 1998).

More comprehensive studies are required to discover how the behaviour of REE can be used to explore the controls and conditions of water-rock interaction and alteration in volcanic-hydrothermal areas. Key questions that must be addressed are:

- What are the main factors that determine the REE concentrations in volcanic lakes and hydrothermal waters?
- What are the principal factors that regulate fractionation among the REE
- How do REE record water-rock interactions in the subsurface?
- Are REE data useful to monitor volcanic-hydrothermal activity?

This thesis attempts to shed light on these issues by focusing on crater lakes, the majority of which are strongly acidic. The objective of this study is to find systematics in the behaviour of the REE by compiling and interpreting literature data, supplemented by new analytical results obtained from well studied volcanoes.

The emphasis is of this research will be on Poás (Costa Rica), because is hosts one of the World's best studied crater lake. Many of its samples, covering more than 30 years of monitoring, were already analysed and interpreted by Martínez (2008). These data are supplemented by analytical results obtained on new sets of samples.

2.2 This thesis

This thesis presents a compilation of REE data from different volcanoes in different parts of the World, with emphasis on Poás and Rincón de la Vieja volcanoes in Costa Rica, for which new data were collected as well.

Chapter 3 summarizes general information on REE behaviour, anomalies and other features that might be relevant for interpreting data from water and rock samples. Brief introductions are given for the selected areas.

Chapter 4 introduces the geological setting, activities and lake properties for Poás and Rincón de la Vieja.

Chapter 5 describes the research strategy and the methods used to analyse the collected water and rock samples.

Chapter 6 describes the results with the help of time-series tends and various diagrams that are suitable to explore relationships between water, rocks and minerals, using the REE as well as major elements.

Chapter 7 presents modelling results for mineral saturation and REE species behaviour for selected samples of Poás, based on PHREEQC.

Chapter 8 discusses water-rock relationships combining REE data with major element data, time-series trends and modelling results for the investigated areas.

Chapter 9 presents a synthesis of the results and main conclusions of the study.

Analytical data of analysed water samples are given in an *Appendix.*

3. Background

This chapter provides background information as an aid in understanding the behaviour of the rare earth elements during water-rock interaction and alteration, with a main focus on volcano-hosted lake systems. Brief introductions will be given on volcanic lakes and associated hydrothermal systems, the behaviour of the REE in fresh and altered volcanic rocks, the main primary and secondary REE-hosting minerals and the investigated volcanic areas. Because special attention will be paid to Poás and Rincón de la Vieja, these volcanoes will be introduced separately in chapter 4.

3.1 Volcanic lake systems and hydrothermal areas

Volcanic lakes are surface expressions of subsurface hydrothermal systems that are often fed by a body of cooling magma. General properties and behaviour of volcanic lakes have been described by Pasternack and Varekamp (1997) and Varekamp et al. (2000). A crater lake can only exist if there is a balance between input and output fluxes of water. Input fluxes include volcanic fluids (liquid water and/or gas), meteoric water and possibly streams entering from nearby springs. Output fluxes are evaporation from the lake surface, potentially accompanied by an overflow out of the crater area or a subsurface seepage flux.

Varekamp et al. (2000) distinguished CO_2-dominated, quiescent and active crater lakes. Active crater lakes receive considerable input from volcanic gases and act as condenser vessels. Their composition is determined by the nature of the primary gas escaping from an underlying cooling volume of magma, as well as by water-gas-rock interaction processes, dilution, evaporation, precipitation of saturated minerals and the formation of secondary alteration minerals. The occurrences to be discussed belong mainly to this group of active lakes. Many are highly acidic, due to the input of gas species such as SO_2, HCl and HF.

The high acidity of the water facilitates the extraction and dissolution of elements during interaction with the surrounding volcanic rocks. This water-rock interaction usually leaves a residue of altered rock with an assemblage of indestructible igneous minerals as well as minerals that formed newly when the interaction took place. In extreme cases, complete dissolution of a rock will occur.

The interaction may take place at the interface between the lake and the surrounding rocks or in the system below the lake. Because the rocks in the lake basin have usually been altered most severely due to the long exposure to the aggressive water, their effect on the solute concentrations is rather limited. Therefore, fluctuations in the lake composition will mostly reflect changes in the composition of hydrothermal water that interacted with subsurface rocks and enters the lake at bottom vents. This water is derived from a zone immediately below the lake where two fluid phases can coexist (liquid and vapour), thus sufficiently far from the intrusive body where vapour will be dominant.

The architecture, processes and mass fluxes predict that the signatures of REE that are dissolved in the lake water largely reflect properties of inflowing water derived from the interior of the volcano, and thus record the conditions and nature of water-rock interaction processes in the subsurface.

For the study of REE in crater lakes it is therefore relevant to have a conceptual understanding of the nature and distribution of rocks and minerals present between the lake bottom and the inferred magma body. Such insights can be derived from studies investigating the distribution of alteration assemblages as observed in eroded, formerly lake-hosting volcanic edifices.

Figure 3.1 presents a schematic cross section through a lake-hosting magmatic-hydrothermal system, indicating the main features and the distribution of a number of key alteration minerals. Several of these have an important control in regulating the behaviour of the REE.

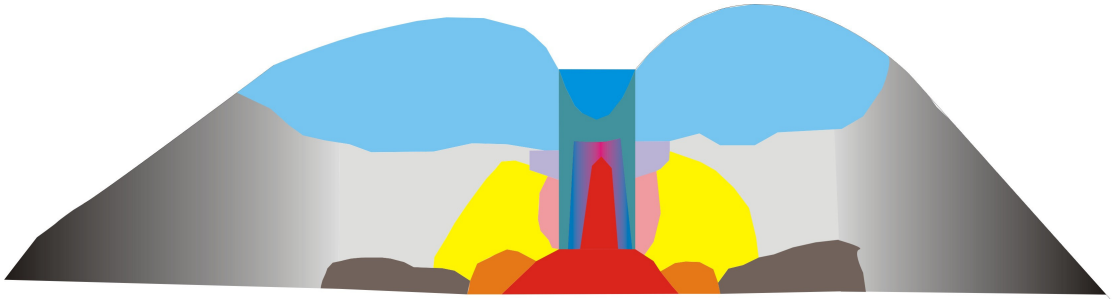

	Alunite	Chlorite	Cristo-balite	Illite	Kaolinite	Opal	Pyrite	Pyro-phyllite	Quartz	Smectite
					X	X				
			X		X		X			
	X		X				X		X	
							X	X	X	
				X			X		X	
							X			X
		X		X			X			
	Hydrothermal seal									
	2-phase vapour-liquid									
	Vapour									
	Magma									
	Unaltered rock									

Figure 3.1: Schematic cross section indicating main features and the distribution of alteration minerals in a volcanic magmatic-hydrothermal system with an active crater lake.

3.2 Behaviour of the rare earth elements (REE)

This section introduces the behaviour of REE in volcanic rocks, minerals and waters, the main REE anomalies that have been defined and the tetrad effect. These systematics form the basis in understanding the REE distribution during water-rock interaction processes.

3.2.1 General behaviour of REE

Volcanic rocks and minerals

The REE signatures of volcanic rocks are highly variable and depend on the source of the magma, the melting process and the degree of magma evolution. Figure 3.2 shows chondrite-normalized REE trends for an average basalt, andesite, dacite and rhyolite, representative for magmas at convergent plate boundaries. This is the most relevant setting in view of the volcanoes studies here. In all cases, the rocks show an enrichment of the LREE relative to the heavy REE. The LREE part is clearly steeper than the HREE part.

The REE contents of a rock are made up of different contributions of the minerals present, each having its own REE distribution. Because water-rock interaction will not affect all minerals to the same extent and at the same time, it is relevant to explore the REE concentration and distribution in the individual minerals. Figure 3.3 shows the chondrite-normalized patterns of primary and accessory minerals in magmatic rocks. There are obvious difference in the concentrations and distribution of the REE between the minerals. Of the primary minerals, amphibole (LREE enriched), clinopyroxene (HREE enriched) and orthoclase (LREE enriched) have the highest REE contents. Plagioclase

shows a strong positive Eu anomaly. The REE contents of several accessory minerals are much higher. Minerals with highest abundances include monazite, allanite, titanite and apatite.

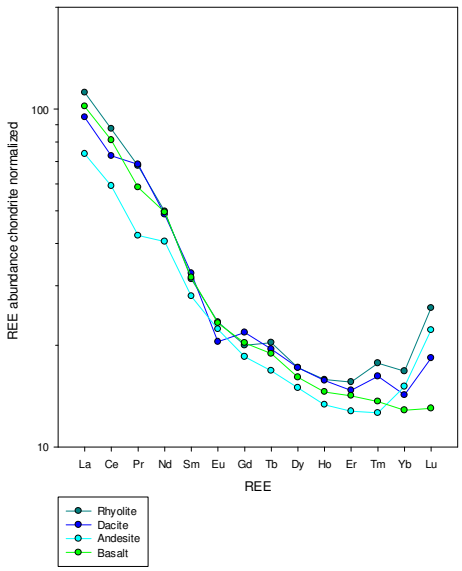

Figure 3.2: REE patterns of common volcanic rock types. The basalt is of a calc-alkaline type. Each trend represents an average of rock data from the Georoc (2010).

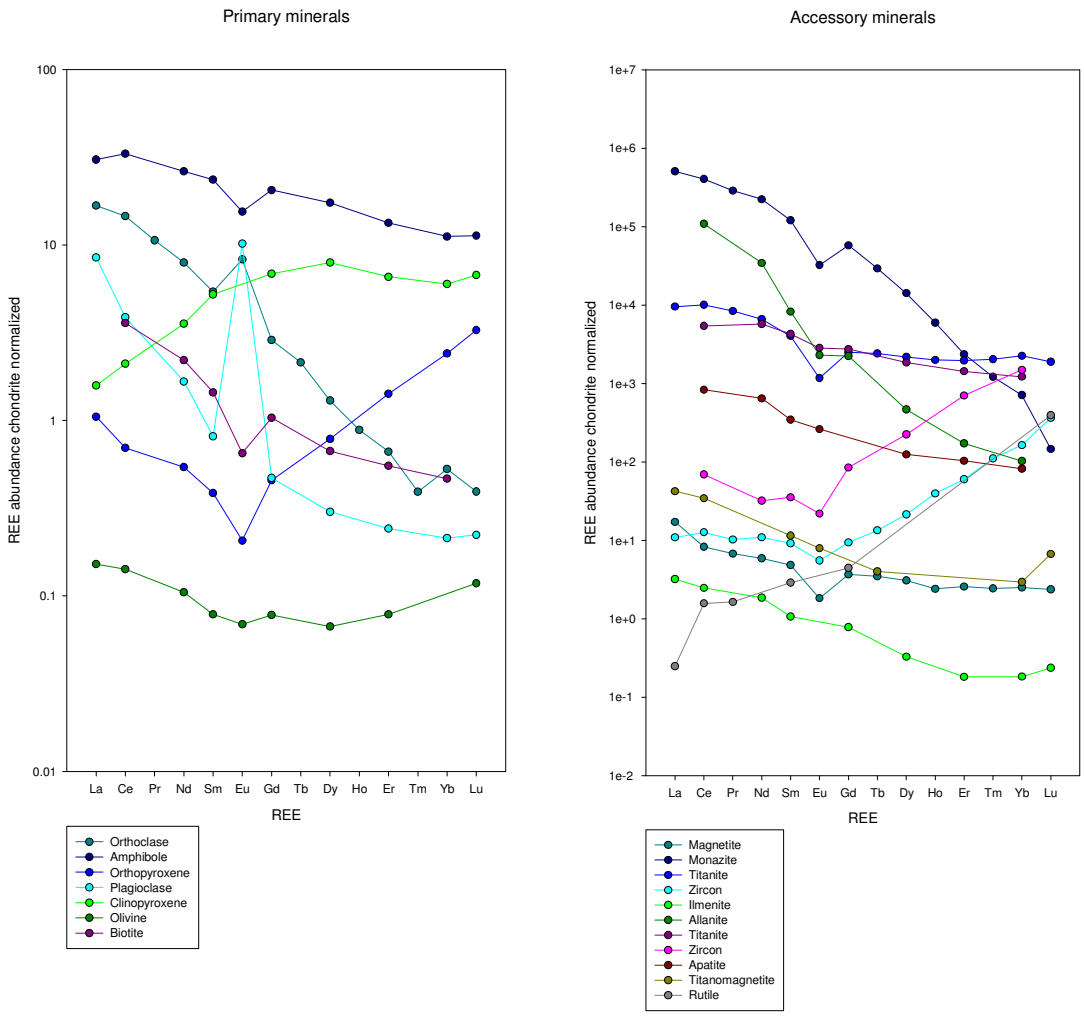

Figure 3.3: REE carrying phases grouped as primary and accessory minerals. Data from Aubert et al. (2001) (orthoclase), Ayres and Harris (1997) (monazite), Bea et al. (1994) (zircon (turquoise trend)), Bonyadi et al. (2011) (magnetite), Fujimaki et al. (1984) (amphibole, clinopyroxene, ilmenite, olivine, orthopyroxene, plagioclase), Gromet and Silver (1983) (allanite, apatite, biotite, titanite (dark pink), zircon), Heaman (2009) (titanite (blue)), Klemme et al. (2005) (rutile), Luhr et al. (1984) (titanomagnetite).

Alteration minerals

Figure 3.4 shows chondrite-normalized REE plots for a number of secondary alteration minerals that could play a role in REE distributions during water-rock interaction. They may take up dissolved REE from fluid when they form, or may add to the budget of REE in the water when they dissolve when stability conditions change. Most of the minerals as well as the alunitic rock shows a clear enrichment of the LREE compared to the HREE. An exception is calcite, which has a flat pattern with a strong negative Eu anomaly.

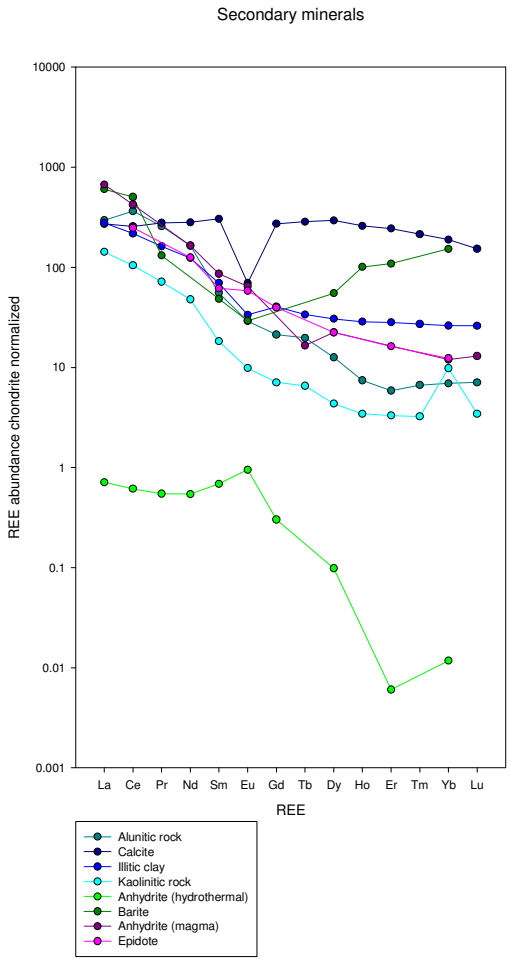

Figure 3.4: The important minerals grouped as secondary minerals. Data from Baioumy and Gharaie (2008) (illitic clay), Gromet and Silver (1983) (epidote), Guichard et al. (1979) (barite), Karakaya (2009) (alunitic and kaolinitic rock), Luhr et al. (1984) (anhydrite (magma)), Ogawa et al. (2007) (anhydrite (hydrothermal)), Schönenberger et al. (2008) (calcite).

3.2.2 Primary and secondary REE-carrying minerals

Some minerals are a more probable source of REE than others and only the most relevant minerals are described here. Figure 3.1 shows their REE plots.

Pyroxenes [$(Mg,Fe)_2Si_2O_6$ or $Ca(Mg,Fe)Si_2O_6$]

Clinopyroxene is a main REE source in fresh dolerite, basalt and gabbro (Bach and Irber, 1998). In andesite, pyroxene is one of the important REE^{3+} carriers (Bau et al., 1998), showing a negative Eu anomaly (Sanada et al., 2006 referring to McKay et al., 1994). The extent of this negative Eu anomaly is approximately the same as the positive anomaly for plagioclase (Hanson, 1980). Leaching experiments by Sanada et al. (2006) suggest that plagioclase will break down faster than pyroxene in acid solution of an andesitic rock.

Plagioclase: albite ($NaAlSi_3O_8$) – anorthite ($CaAl_2Si_2O_8$)

The REE pattern of plagioclase is convex down with a positive Eu anomaly in a chondrite normalized plot (Taylor and McLennan, 1985). When plagioclase weathers, a positive Eu anomaly and LREE enrichment in the fluid is expected (Philpotts and Schnetzler, 1968; Taylor and McLennan, 1985). The reason is that Eu can occur in a divalent state, next to a trivalent state, in which case it is more easily incorporated, since it can replace Ca^{2+} (Protano and Riccobono, 2002 referring to Henderson, 1984 and Krauskopf and Bird, 1995). During weathering plagioclase is usually replaced by kaolinite and silica (Risacher et al., 2002, referring to Arriba, 1995).

Magnetite (Fe_3O_4)

Magnetite is another common mineral in basalt and andesite that prefers LREE instead of HREE (Bau et al., 1998).

Titanite ($CaTiSiO_5$)

Titanite is HREE enriched in albitites (Biddau et al., 2002). In general, there is slight enrichment in the LREE, a negative Eu anomaly, and a flat pattern for HREE in titanites from pegmatites (Heaman, 2009). Titanite in granodiorite contains relatively high REE concentrations. This is mainly important for the MREE and the HREE, since allanite is an important host of LREE. These accessory minerals may contain almost the entire budget of the MREE and HREE in granitoid rocks (Gromet and Silver, 1983).

Alunite [$KAl_3(SO_4)_2(OH)_6$]

The general formula of alunite is $XAl_3(SO_4)_2(OH)_6$, where X can be K, Na, Ca. The mineral can be a weathering product of feldspar. Members of the group are alunite [$KAl_3(SO_4)_2(OH)_6$], natroalunite [$NaAl_3(SO_4)_2(OH)_6$], and minamiite [(Na, Ca, K)$Al_3(SO_4)_2(OH)_6$]. There is a good positive relation between K and La, Ce, Nd, but the relation between Na and La and between Ca and La is poor. Volcanic areas where sulphur-bearing gas or acidic water is released are favourable for alunite formation, because kaolinite reacts with sulphuric acid to produce alunite. Alunite, jarosite and crandallite are interchangeable by substituting components, but they form under different conditions (Kikawada et al., 2004 and referring to Abe and Takeuchi, 1967).

(Potassium-) jarosite [$KFe_3(SO_4)_2(OH)_6$]

The general formula of the alunite-jarosite group is [$AB_3(XO_4)_2(OH)_6$] where A=K,Na,Ca,Ba,S,Ag,Pb,NH_4,U, B=Al,Fe,Cu,Zn and X=S,P (Parsapoor et al., 2009 referring to Scott, 1987). Jarosite is a secondary mineral like alunite and forms under comparable conditions. Potassium can be substituted by LREE implying that jarosite is a LREE enriched mineral (Fulignati et al., 1999 and Kikawada et al., 2004). REE^{3+} do not substitute for Fe^{3+} since their ions have a larger size, but they can substitute for K^+ like in alunite (Welch et al., 2007 referring to Dutrizac, 2004).

Gibbsite [$Al(OH)_3$]

Clay minerals show LREE enrichments when normalized to PAAS (Bao and Zhao, 2008). Gibbsite is a secondary clay mineral.

Other clay minerals

Clay minerals that are residual products of strong weathering are more enriched in LREE than in HREE. On the other hand, moderately weathered granodiorite shows HREE enrichment (Taylor and McLennan, 1985). LREE are also more weakly sorbed onto the surfaces of clay minerals than HREE (Coppin et al., 2002). Eu^{3+} can be adsorbed to some clay minerals like montmorillonite (Okada et al., 2007 and references therein). REE sorption of kaolinite is more pH dependent than the REE sorption of smectite. Kaolinite and smectite surfaces sorb HREE more strongly than LREE at high ionic strength (Coppin et al., 2002).

Kaolinite [$Al_2Si_2O_5(OH)_4$]

During advanced stages of weathering, cerium is fixed on kaolinite and cerianite, causing a positive Ce anomaly in altered subalkaline granite. Kaolinite often replaces plagioclase (Risacher et al., 2002): $2NaAlSi_3O_8 + H_2O + 2H^+ \rightarrow Al_2Si_2O_5(OH)_4 + 2Na^+ + 4SiO_2$ (Karimzadeh Somarin and Lentz, 2008).

Barite ($BaSO_4$)

Deep-sea barites show a V-shape sea water normalized REE pattern, with a negative Eu anomaly but no negative Ce anomaly (Guichard et al., 1979). Barite generally favours Eu^{3+}at low temperatures and Eu^{2+} at high temperatures. This implies that hydrothermal and metamorphic barite has a positive Eu anomaly (Sverjensky,

1984). Since Ba and Eu are both divalent there is no charge compensation needed. The large ionic radius of Ba^{2+} (1.50 Å) allows the uptake of Eu^{2+} (1.33 Å) which is bigger than REE^{3+}. Under strongly acidic hydrothermal conditions (pH lower than 2) barite can be dissolved (Parsapoor et al., 2009).

Fe-hydroxides

At pH < 5 REE do not adsorb significantly on Fe-oxyhydroxides (Verplanck et al., 2004 and Bau, 1999). Because HREE starts to sorb at a lower pH, it is preferentially sorbed to the Fe-oxyhydroxide surfaces (Welch et al., 2009)

The description of the minerals summarized

Minerals with a positive Eu anomaly are plagioclase, hydrothermal and metamorphic barite, and some clay minerals. Negative anomalies can be found in pyroxene, titanite, and deep-sea barite. The Eu anomaly of plagioclase and pyroxene are opposite and of the same order of magnitude. Plagioclase, magnetite, jarosite and gibbsite may show LREE enrichment. HREE enrichment is found in pyroxene, Fe-hydroxides, and clay minerals.

3.2.3 REE Anomalies

Eu

Eu occurs in two valency states: Eu^{2+} and Eu^{3+}. Hydrothermal and metamorphic conditions will favour Eu^{2+} if temperatures are high (> 250°C). Eu^{2+} is present in unaltered igneous rocks, where plagioclase is commonly the main host. Eu^{3+} will be dominant under near-surface conditions where temperatures are low (Sverjensky, 1984).

However, low temperatures do not necessarily imply that Eu^{3+} is always present, because it will not be stable under highly reducing conditions Eu^{3+}:

$Eu^{2+}{}_{(aq)} + H^{+}{}_{(aq)} + ¼\ O_{2\,(aq)} \Leftrightarrow Eu^{3+}{}_{(aq)} + ½\ H_2O_{(l)}$

Another reaction may also be important near mid-oceanic ridges:

$Eu^{3+} + Fe^{2+} \rightarrow Eu^{2+} + Fe^{3+}$ (Sverjensky, 1984)

Eu anomalies in minerals can either be positive or negative. The formula used in this thesis to calculate the Eu anomaly is: $Eu/Eu^{*}=2Eu_N/(Sm_N+Gd_N)$, following Martínez (2008). Hydrothermal and metamorphic K-feldspar, plagioclase and barite show a positive anomaly (Hanson, 1980; Sverjensky, 1984; Lewis et al., 1997; Fulignati et al., 1999). Olivine does not show an anomaly, whereas clinopyroxene, hornblende, apatite and sphene usually show negative anomalies (Hanson, 1980). A negative Eu anomaly in natural water can result from the dissolution of minerals, but it can also be explained by removal via oxides and carbonates (Négrel et al., 2000).

Positive Eu anomalies are characteristic for high-temperature and Cl-dominated hydrothermal fluids, but no or negative Eu anomalies are found for hydrothermal fluids from alkaline and sulphate dominated rocks (Michard and Albarède, 1986; Michard, 1989). An explanation could be that plagioclase dissolves slower than the source of the other REE (Bach and Irber, 1998). The nature of water-rock interaction is important, given the fact that an Eu anomaly will be larger when the permeability and porosity of a rock increases (Whitford et al., 1988).

La

The anomaly is positive in shale-normalized REE patterns of seawater and marine precipitates (Bau and Dulski, 1996; Bau, 1996 and references therein). Bolhar et al. (2004) used this feature to infer a seawater signature for banded iron formations (BIF).

Ce

The existence of Ce anomalies is due to the different oxidation states in which the element can occur. Under oxidising conditions Ce^{4+} may form instead of Ce^{3+}. Because of the poor solubility of Ce^{4+}, its behaviour is different from the other REE. Fe and Mn oxides can remove Ce^{4+} (Négrel et al., 2000). In hydrothermal conditions it is not likely to have Ce^{4+} because of the high temperature (Bau et al., 2003 referring to Bilal and

Müller, 1992). Ce oxidation is preferred at high pH, which means that a Ce anomaly will be pH dependent (Biddau et al., 2002 referring to Goldstein and Jacobsen, 1988 and Elderfield et al., 1990). No significant anomalies are seen in felsic or mafic volcanics and sedimentary rocks (Leybourne et al., 2000). Positive anomalies are seen for weathered subalkaline granite samples like weathered dolerite, intermediate and felsic rocks. This anomaly is due to adsorption on kaolinite or cerianite (Scheepers and Rozendaal, 1993). Silicic alteration will also create a positive Ce anomaly (Parsapoor et al., 2009). It should be noted that there are different ways to calculate a Ce anomaly (see Ohta and Kawabe, 2001; Leybourne et al., 2000; Bao and Zhao, 2008; Smedley, 1991; Meen, 1990; Leybourne and Johannesson, 2008; Sholkovitz, 1995).

Pr

Friend et al. (2008 and references therein) explained how the presence of La enrichment can be deduced by combining a possible Ce anomaly with a possible Pr anomaly. Bau and Dulski (1996) proposed to calculate the Pr anomaly as: $Pr/Pr^*=Pr_{SN}/(0.5Ce+0.5Nd)_{SN}$

Gd

A negative Gd anomaly is sometimes found in near-neutral to slightly alkaline environments, for example seawater (Bau et al., 1998 references therein) and mangrove sediment (Prasad and Ramanathan, 2008). A positive anomaly may appear when land-use is changed or by human activities (Prasad and Ramanathan, 2008). However, many references in Bau (1996) also report a positive anomaly for marine precipitates. Also, shale normalized seawater shows a positive anomaly (Fee et al., 1992 referring to de Baar et al., 1985b). Positive anomalies in groundwater in basalt aquifers and some in sedimentary aquifers may be attributable to sorption and co-precipitation (Tweed et al., 2006). The anomaly is calculated using the formula: $Gd/Gd^* = Gd_{cn}/[0.33Sm_{cn}+0.67Tb_{cn}]$ (Bau and Dulski, 1996). The presence of a Gd anomaly means that any inferred Eu anomaly will depend on a calculated Gd value (Tweed et al., 2006). Because Gd is used in nuclear medicine, fresh water in densely populated areas shows a positive anomaly (Naya and Lahiri, 1999 referring in Merten and Büchel, 2004). There is generally a small positive anomaly in oceans, but this is still under discussion because measurement techniques may have questionable accuracies (Mayanovic et al., 2007; see also Fee et al., 1992).

Tb

Lottermoser (1990) claims that Tb anomalies reflect poor analytical accuracy. Fee et al. (1992, referring to de Baar et al., 1985ab) found a negative anomaly in seawater relative to shale, but emphasized that there is still an ongoing debate about the behaviour of Gd and Tb.

Dy

Gammons et al. (2005) reported a negative anomaly for Lake Caviahue near Copahue volcano, Argentina, which they considered to be an analytical artifact. The lake is acidic and oxic. Fee et al. (1992) found a positive anomaly in some waters and sediment samples (e.g. saline to hypersaline and acidic Lake Tyrrell, Australia), but could not verify this.

Ho

A Ho anomaly was detected in shale-normalised data obtained from a flattened W-shape pattern with Ho anomalies in groundwaters from a sand aquifer (Texas, USA) probably reflects analytical errors according to Tang and Johannesson (2005). Fee et al. (1992) found a positive anomaly for seawater.

Yb

The dissolution of organic and sulphide phases may produce a pronounced positive Yb anomaly (Yan et al., 1999). Below pH 6, there is an anomalous behaviour of Yb, but the reason is not known (Piasecki and Sverjensky, 2008).

Lu

There is a negative Lu anomaly in seawater and other near-neutral/slightly alkaline environments (Bau et al., 1998). The positive anomaly found in groundwater aquifers of basalt and some sediments may be due to sorption or co-precipitation effects (Tweed et al., 2006).

The REE anomalies summarized

The only important anomaly relevant for this research on REE behaviour in crater lake settings is the europium anomaly. The other anomalies are important for near-neutral to slightly acidic seawater (La), weathered subalkaline igneous rocks (Ce), oxidation, temperature and pH change in (near-)surface waters (Ce), near-neutral to slightly alkaline environments such as seawater (Gd, Lu), dissolution of organic and sulphate phases (Yb).

Tetrad effects in REE patterns

A tetrad effect is visible in a REE plot if a subdivision into the following four groups appears:
I La-Nd
II Pm-Gd
III Gd-Ho
IV Er-Lu
The first and second tetrad groups have some problems. The possible presence of Ce^{4+} or Eu^{2+} creates anomalies, and Pm is not stable in nature. There are two different tetrad shapes: M (convex) and W (concave) (Bau, 1996; Monecke et al., 2002 referring to Masuda et al., 1987; Veksler et al., 2005; Bortnikov et al., 2008; Schönenberger et al., 2008). How much of a 4f-subshell is filled determines this appearance: I: ¼, II: ½, III: ¾, and IV: completely filled. The repulsion of the electrons is responsible for the tetrad pattern. The ratio with the neighbouring element is more important than the absolute concentration (Bau, 1996; Veksler et al 2005).

Igneous rocks like Li-F granites and their hydrothermally altered equivalents like greisens and pegmatites show very clear tetrad patterns. This can be explained by fractionation of F-rich fluids from the igneous rock, but also by aluminofluoride complexes. The tetrad patterns in some sedimentary rocks and seawater are weak (Veksler et al 2005 and referring to Masuda and Ikeuchi, 1978; and Monecke et al., 2002).

A tetrad pattern is visible for synthetic cryolite (Na_3AlF_6), but there is no explanation for its occurrence in this rare mineral (Veksler et al., 2005). High temperature tourmalines from aplite, granite and pegmatite show the most pronounced M- and W-type of tetrads. The tourmalines demonstrate the importance of pH, because their REE contents are higher in a quartz-feldspar vein than in a tourmaline-quartz vein, which is explained by a more elevated alkalinity (Bortnikov et al., 2008). Veksler et al. (2005) stated that only silicate melts have M-type patterns. They have also been found in granites with their accessory fluorite (Monecke et al., 2002). Most chlorites show M- or W-type of tetrads, which can be explained by complexation during the hydrothermal stage. The mobility of REE is aqueous media depends on temperature, pH, eH and the mineral (Bortnikov et al., 2008).

The theory of tetrad patterns is not universally accepted. Supporters (e.g. Masuda and co-workers) support their existence, while others (e.g., McLennan, 1994) believe that tetrad patterns reflect analytical errors.

3.3 Crater lakes and hydrothermal alteration areas

The lakes and hydrothermal areas studied here were selected on the basis of available REE data. The areas are briefly introduced below. Main characteristics of the lakes are summarized in table 3.1. Poás and Rincón de la Vieja are treated in more detail in chapter 4.

Volcano	Name	Volume (m^3)	Depth (m)	Diameter (m)	pH	Temperature (°C)	References
Poás		3.7×10^3 – 1.7×10^6 (1993-1997)	Up to 55	Up to 320	-0.87 – 1.75	22 - 94	Martínez (2008)
Rincón de la Vieja		Not found	Not found	Not found	0.35 – 0.53	36 - 45	Appendix A
El Chichón	El Chichón Crater Lake	Max 3.5×10^4-6×10^5	1-3.3	November 1982: 650 length, 200-450 width	0.56-2.7	26 (2006) -58 (1983)	Rouwet et al. (2009); Casadevall et al. (1984); Armienta et al. (2000); Taran et al. (2008); Morton-Bermea et al. (2010)
Copahue		Not found	Not found	300 width	0.2-1.1	21-54	Varekamp et al. (2009) and references therein; Venzke et al. (2002-)
Yellowstone	Norris Geyser Basin	Not found	0-unknown	Not found	2.8-3.5	81-90	Morgan et al. (2009); Lewis et al. (1997)
	Gibbon Geyser Basin	Not found	Not found	Not found	2.0-3.0	73-93	Lewis et al. (1997)
	Upper Geyser Basin	Not found	0-unknown	Not found	3.0	75	Morgan et al. (2009); Lewis et al. (1997)
Ruapehu		9.0×10^6 (1991, depth about 134 m)	300	oval shaped, average 500	0.63-1.78	10-60	Christenson and Wood (1993); Christenson et al. (2010)
Keli Mutu	TAP	5.3×10^6	64	400 x 330	1.7-1.9	20.4-22.4	Pasternack and Varekamp (1994)

Volcano	Name	Volume (m^3)	Depth (m)	Diameter (m)	pH	Temperature (°C)	References
Keli Mutu	TiN	6.4 x 10^6	127	430 x 306	0.3-0.5	29.3-32.7	Pasternack and Varekamp (1994)
	TAM	4.2 x 10^6	67	357 x 260	2.9-4	18-20.45	Pasternack and Varekamp (1994)
Patuha	Kawah Putih	Not found	8-17	Not found	<0.5-1.3	26-35	Sriwana et al. (2000) and references therein
Kawah Ijen		3.0 x 10^7 (2004)– 4.35 x 10^6 (1922)	182-200	Not found	0.09-0.39	33.8-44	Takano et al. (2004) and references therein; Delmelle et al. (2000)
Kelut		2.5 x 10^6 - 40 x 10^6	34	Not found	5.9-6.5	30.7-42.8	Bernard and Mazot (2004); Thouret et al. (1998); Badrudin (1994)
Telaga Bodas		Not found	Not found	Not found	0.40	Not found	Moore et al. (2008)
Telaga Warna		Not found	Not found	Not found	Not found	Not found	
Pinatubo		6.5 x 10^7 - 2.5 x 10^8	Not found	Not found	3 - 5.5	26-40	Stimac et al. (2004) and references therein
Kusatsu-Shirane	Yugama	Not found	Not found	120 x 200 – 270 x 350	0 - 1.84	-0.5 – 26.7	Ohba et al. (2008) and references therein
Maly Semiachik		Not found	117	550	0.7 – 1.4	30-34	Takano et al. (2000) and references therein

Table 3.1: Abbreviations TAP, TiN, and TAM: see below *Keli Mutu, Indonesia*.

El Chichón Volcano Crater Lake, Mexico ([1] = Taran et al., 1998; [2] = Morton-Bermea et al., 2010)

This volcano is part of the small Chiapanecan Volcanic Arc between the Trans-Mexican volcanic belt and the Central American volcanic arc (CAVA). Because both volcanic chains consist of calc-alkaline rocks, it is expected that El Chichón produced calc-alkaline rocks. In reality, its products are trachyandesitic. The pyroclastic material ejected during the 1982 eruption was anhydrite-bearing trachyandesite. The occurrence

of K-alkaline rock has been explained by the location near the triple junction between the North American, Caribbean and Cocos plates. According to others, of the rock composition is related to the subduction of the Cocos plate under the North American plate [1, 2 and referring to Damon and Montesinos (1978)]. The lake has been sampled irregularly. The data base includes REE analyses of 25 lake-water samples (including six samples from three different dates).

Copahue, Argentina ([1] = Varekamp et al., 2001; [2] = Venzke et al., 2002-)

Prior to 2000 the lake waters of Copahue had compositions suggesting near-congruent rock dissolution. Between 1992 and 1995 hydrothermally altered rock debris was ejected, as well as siliceous dust, pyroclastic sulphur, and rare juvenile fragments[1, 2]. Magmatic eruptions occurred between July and October 2000 and changed the properties of the lake since then. A detailed study has been done on the behaviour of REE in an acid stream originating in the summit area near the lake [1].
The lake has been sampled irregularly. The data base includes REE analyses of 12 lake water samples.

Yellowstone, USA (Morgan et al., 2009 summarized)

Yellowstone has at least 20 large (> 100m in diameter) hydrothermal craters. Comparison of the crater sizes of Yellowstone with those of active geyser basins and thermal areas indicate that the events creating this hydrothermal activity occur at a much bigger scale than elsewhere. The explosive hydrothermal systems require hydrothermal fluids around boiling temperature to flow along interconnected, well-developed joints and fractures in a water-saturated system. In Yellowstone, active deformation of the caldera, active faulting and moderate local seismicity are among the processes that influence the hydrothermal system. Due to their low permeabilities, the hydrothermal fluids flow along the edges of rhyolitic lava flows. The Lava Creek Tuff consists of high-silica rhyolite ignimbrites. The caldera was formed by the catastrophic eruptions at 2.05, 1.3, and 0.64 Ma. There are more than 10000 active hot springs, geysers, fumaroles, and mud pots in the Yellowstone caldera, which is is 45 by 85 km in size.

The hydrothermal waters have been sampled frequently but the data base includes REE analyses of only 14 water samples.

Ruapehu, New Zealand

Rhyolite is the main lithology in this zone, and frequently displays hydrothermal alteration. The length of the thermal cycle varies between 4 and 16 months (Christenson et al., 2010). Between the disappearance of the lake in 1945 and its re-establishment in 1946, numerous phreatic and phreatomagmatic eruptions had occurred. In the 1960s and 1970s fresh pumiceous andesite was ejected and the activity was lower in the 1980s. The pH of the crater lake was higher during 1971-1973 period (1.18-1.78), than 1988-1990 period (0.63-0.87) (Christenson and Wood, 1993). The big eruption occurred on 23 September 1995, and a synopsis of events between November 1994 and August 1996 is given by Christenson (2000). In the sampling period of 1994-1996 the pH changed between 0.63 and 1.2 (Christenson, 2000).There have been other eruptions afterwards: March 1996 (uncertain), June - September 1996, October 1997, October 2006 and September 2007. The eruption of 25 September 2007 was a phreatic eruption without warning. The lake was relatively cool (13 °C) and the seismicity was low (Venzke et al., 2002-).

The lake has been sampled regularly but the data base includes REE analyses of only three lake water samples.

*Keli Mutu, Indonesia (*Pasternack and Varekamp, 1994 summarized)

Keli Mutu is a stratovolcano on Flores. It produced hydrothermal eruptions between 1860 and 1870. The phreatic eruptions probably deposited the bedded ashes and lapilli on the walls.

There are three lakes in the summit area, situated in steep craters: Tiwu Ata Polo (TAP), the southeastern lake, Tiwu Nua Muri Koohi Fah (TiN), the central lake, and Tiwu Ata Mbupu (TAM), which fills a pit crater inside a large crater. The lakes have been sampled irregularly. The data base includes only one REE analysis of lake water from unknown.

Kawah Putih, Indonesia (Sriwana et al., 2000 summarized)
Kawah Putih lake is situated in the summit of Patuha volcano in West Java. Lavas produced by this volcano are medium-K basaltic andesite with 54-58 wt% SiO_2 and 5-6 wt% MgO. Although there have not been magmatic or phreatic activity since 1600 AD Sriwana et al., 2000 referring to Neumann van Padang, 1951, the volcano should is categorized as potentially active.

The lake has been sampled irregularly. The data base includes REE analyses of four lake water samples.

Kawah Ijen, Indonesia

Kawah Ijen is an active stratovolcano with a basaltic to andesitic composition, situated in East Java (e.g. Palmer et al., 2011; Van Hinsberg et al., 2010; Delmelle et al., 2000 and references therein). Its crater lake is part of a caldera complex. According to their SiO_2 and K_2O contents, the erupted products belong to the calc-alkaline island arc series (Delmelle and Bernard, 1994). This crater lake is the largest natural body of hot hyperacid brine. It formed 50,000 years ago when the Ijen volcano collapsed, producing a 20 km wide caldera (Van Hinsberg et al., 2010 referring to Kemmerling, 1921 and Sitorus, 1990). Kawah Ijen is the only active crater of the caldera.

During the last major magmatic eruption in 1817 the lake was completely expulsed (Van Hinsberg et al., 2010 and referring to Bosch, 1858 and Kemmerling, 1921; Delmelle et al., 2000, referring to Newhall and Dzurisin, 1988). The last two eruptions in early August 2002 and early September 2000 are uncertain (Venzke et al., 2002-). Preceding eruptions were in June 1999, February 1994, and July 1993. Since 1817 the activity has been phreatic and geyser-like (Delmelle et al., 2000 referring to Newhall and Dzurisin, 1988). Over at least 50 years the lake is generally marked by quiet conditions suggesting a dynamic equilibrium (Delmelle and Bernard, 2000).

The crater wall exposes layered pyroclasts and lava flows covered by sulphur-bearing mud from the recent activity. On the outside close to the rim, altered phreatic and phreato-magmatic material discordant on magmatic deposits is found. On the outside, scoria layers and small lava flows are exposed. In general, all rocks show some degree of alteration when in contact with the acid fluid, for example along the Banyu Pahit stream that originates on the Western flank of the crater (e.g. Delmelle and Bernard, 2000; Van Hinsberg et al., 2010).

The lake has been sampled frequently. The data base includes REE analyses of 3 lake water samples.

Other volcanoes Indonesia

Kelut volcano (East Java) is highly active and erupted in the last century in 1901, 1919, 1920, 1951, 1966 and 1990. The latest eruption was in 2007. Lahars, nueés ardentes, and pyroclastic falls are associated with its eruptions (Venzke et al., 2002-; Badrudin, 1994). Eruption products are mostly basaltic andesite (Bourdier et al., 1997; Badrudin, 1994). In contrast to most of the other lakes studied here, the lake water of Kelut is not acidic but has a near-neutral pH (Bernard and Mazot, 2004). The lake area is marked by extensive CO_2 emissions (Caudron et al., 2012). Since late 2007, there is no lake anymore due to the extrusion of a lava dome in the central part of the crater.

The Telaga Bodas crater lake is situated on the flank of the Galunggung Volcano (West Java), ca. 15 km east of the city of Garut. The volcano erupted five times since 1822 and the eruption in 1984 is the most recent (Moore et al., 2008). Rocks of the volcano include basalt to basaltic andesite. However, older lavas are dominantly andesite to dacite (Moore et al., 2008).

Telaga Warna is a multicoloured lake in the area of the Dieng Plateau (Central Java). It occurs in volcanic terrain but is not associated with an obvious volcanic edifice. Escaping bubbles demonstrate the underlying activity. Little is known about its particular features.

Whereas Kelut has been extensively monitored, sampling of Telaga Bodas, and Telaga Warna has been erratic till date. For each lake, only one sample with REE data is included in the data base.

Pinatubo, Philippines ([1] = Di Muro et al., 2008; [2] = Luhr, 2008; [3] = Venzke et al., 2002-; [4] = Stimac et al., 2004)

The Pinatubo volcanic complex is the northernmost of the volcanic system related to subduction at the Manila Trench [4]. Seismic activities were recorded before the 1991 phreatic explosions [4]. The large 1991 eruption can be divided into three phases: 1) phreatic explosions, 2) extrusion of an andesite dome alternating with short-lived explosions, 3) dacite plinian eruption which formed a small summit caldera [1, 2, 4]. The phreatic explosions created a 1.5 km long line of craters on the upper slope of the volcano [4]. The eruptions ended in 1992 with the extrusion of the second andesite dome on the caldera floor. The main type of magma was medium-K dacite. Other Pinatubo eruptions and the Buag period (500kyr) have indistinguishable andesite and dacite compositions. Hence, the Buag rocks are used in this thesis for interpretation purposes [1,4]. There has also been an eruption in 1993 [3], but the data from rocks of the two other eruptions are taken here.

The lake has been sampled irregularly. The data base includes an REE analysis of only one lake water samples.

Kusatsu-Shirane, Honshu, Japan and Nishiki-numa iron-spring, Hokkaido, Japan
Kusatsu-Shirane: (Ohba et al., 2008 summarized) and Nishiki-numa: (Bau et al., 1998 summarized)

Kusatsu-Shirane is an andesite volcano at the volcanic front on Honshu Island in Japan. In 1882 the first historical eruption occurred and there were steam-driven explosions in 1982 and 1983. The largest eruption was in 1932 and a small eruption occurred in 1989. The crater lakes are Yugama, Mizugama, Karagama, and Yumiike.

The Nishiki-numa iron-spring is included to understand the REE behaviour, because there is no clear description concerning the REE for the Kusatsu-Shirane water.

Maly Semiachik, Russia ([1] = Kersting and Arculus, 1995; [2] = Takano et al., 2000; [3] = Takano et al, 2004; [4] = Venzke et al., 2002-)

Not much is known about this volcano. The geology is not extensively described and, to my knowledge, there is only one set of REE data published[3]. The last known eruption was in 1952 [4]. The Maly Semiachik volcano is situated on the Kamchatka peninsula in the central part of the Eastern Volcanic Front [1,2].

4. Geological setting, activity and lake properties of Poás and Rincón de la Vieja

Volcanism in Costa Rica is associated with a convergent plate boundary where the Cocos plate is subducting below the Carribbean plate (Carr et al., 2007a).

The volcanoes in Costa Rica are not all the same. There are three main types based on the morphology (Van Wijk de Vries et al., 2007):

1) Shield-like volcanoes, for example Rincón de la Vieja and Tenorio.
2) Small, steep stratocones, for example Arenal and Chato.
3) Volcanoes with low slope angles and broad tops, for example Poás, Irazú and Platanar.

Three petrographic types have been distinguished (Alvarado, 1985):

1) Sub-alkaline lavas. Volcanoes of this type are for example calc-alkaline Rincón de la Vieja and Irazú.
2) Andesite to high alumna basaltic-andesite lavas. Volcanoes of this group are for example Arenal and Chato.
3) Tholeiitic lavas. Volcanoes of this type are Poás and Platanar.

4.1 Poás and Rincón de la Vieja - volcanic setting, rocks and minerals

Poás

Poás is located at 10°12'N, 84°14'W. The height of the volcano is 2704 m above sea level. It is composite stratovolcano with collapse craters (Weyl, 1980: summary of different references). The volcano is part of the Central Cordillera, which can be divided into two groups with Poás and Platanar on one side and Irazú on the other. Poás and other volcanoes are trending from west-northwest to east-southeast. The group of Irazú show a fissure east-northeast to the Poás group. On the southern slopes of Poás is the Alajuela fault (Weyl, 1980; Van Wijk de Vries et al., 2007 and referring to Borgia et al., 1990). Rock compositions of the volcano point to an enriched mantle source (Carr et al., 2007a).

The rocks of Poás are basalt, dacite, and andesite. The main phenocryst in the basalts is plagioclase, but magnetite and augite are also present. In some basalts there is orthopyroxene and in some there is olivine. Removal of clinopyroxene and plagioclase of less silicic basaltic andesite forms dacite. The andesites contain pyroxenes, plagioclase, and magnetite. Pyroxene mantels olivine in glomeroporphyritic clusters of the phenocrysts where olivine is rarely found. Hornblende is sometimes found and on the south flank of Poás are pigeonite rims in the most siliceous samples (Prosser and Carr, 1987 and referring to Prosser, 1983; Cigolini et al., 1991).

Rincón de la Vieja

Rincón de la Vieja volcano is located at 10°49'N, 85°20'W. The height of the volcano is 1806 m above sea level. Rincón is a composite stratovolcano with six craters. It is part of the Guanacaste Cordillera which trends northwest-southeast. The important volcanoes of this volcanic chain are Rincón de la Vieja and Orosí. Weyl (1980) described the activity of Rincón as occasionally occurring steam and ash eruptions. Kempter et al. (1996) stated that magma mixing is the possible trigger of the oldest group of eruptions involving pyroclastic flows and tephra. The groups are described in table 4.2.

The rocks are generally dacite, labradorite rhyodacite, hypersthene-augite-andesite (Weyl, 1980, with summary of other references). The recently erupted rocks are andesitic. Pumice of the volcano is dacitic. The andesite of the youngest group contains plagioclase, augite, and magnetite as phenocrysts. Plagioclase, augite, hypersthene, and Fe-Ti oxides are commonly present in the lavas (Carr et al., 1985 and referring to Kussmaul et al., 1982; Kempter et al., 1996). Secondary minerals are anhydrite, alunite, and kaolinite and, further away from the active crater, iron-sulphate and oxy-hydroxide minerals like jarosite and goethite (Kempter and Rowe, 2000 referring to Hayba et al., 1985 and Rowe et al., 1995).

Alvarado (1985) compared the mineralogical composition of Poás and Rincón de la Vieja as follows:

	Phenocrysts	Plagioclase	Of which Anorthite	Olivine	Clino-pyroxene	Ortho-pyroxene
Poás	0 - 42	0 - 27	38 - 79	0 – 2.5	0 - 5	0 - 10
Rincón de la Vieja	30 - 60	17 - 50	45 - 65	0 – 3.5	2 - 7	0.5 - 5

Table 4.1: Mineralogical comparison of Poás and Rincón de la Vieja (Alvarado, 1985). All values in wt.%.

Group	Products	Minerals
1 (< 3500 yr B.P.)	Lapilli pumice	Plagioclase, orthopyroxene, and rare hornblende
2 (3500 – 27000 yr B.P.)	Tephra	Plagioclase, augite, hypersthene, opaques
3	Tephra and andesite lava	Hyperstene, augite, rare hornblende, plagioclase
4	Andesite lava	Plagioclase, augite, hypersthene, Fe-Ti oxides

Table 4.2: The eruption history of Rincón de la Vieja, subdivided into four groups (Kempter et al., 1996 summarized and referring to Kempter and Benner, 1989).

4.2 Properties and behaviour of the crater lakes of Poás and Rincón de la Vieja

The crater lake of Poás

The crater lake of Poás is highly acidic (pH<2) and among the most active ones in the world. Its highly dynamic behaviour and numerous eruptions have been extensively documented (Martínez, 2008 and referring to Martínez et al., 2000; Venzke et al., 2002-; OVSICORI open reports, and many references therein). The activity included persistent fumarolic degassing and periods of enhanced phreatic activity in the lake. The latest phreato-magmatic eruption occurred in 1953-1954. The activity changes are expressed in the chemical and physical properties of the lake, such as volume, depth, pH, temperature and concentrations of dissolved components. Martínez (2008) distinguished five different periods (stages) in the lake's activity since the late 1970s. They are illustrated by time-series trends for relevant parameters until early 2008 in Figures 4.1 and 4.2, while Figure 4.3 extends the trends for selected parameters monitored between 2006 and 2009. Martínez (2008) inferred that the Poás system has a 6–10 years cycles of alternating quiet and active intervals.

Tables 4.3 and 4.4 present historic overviews of the activity of Poás and main observations in the crater and the lake.

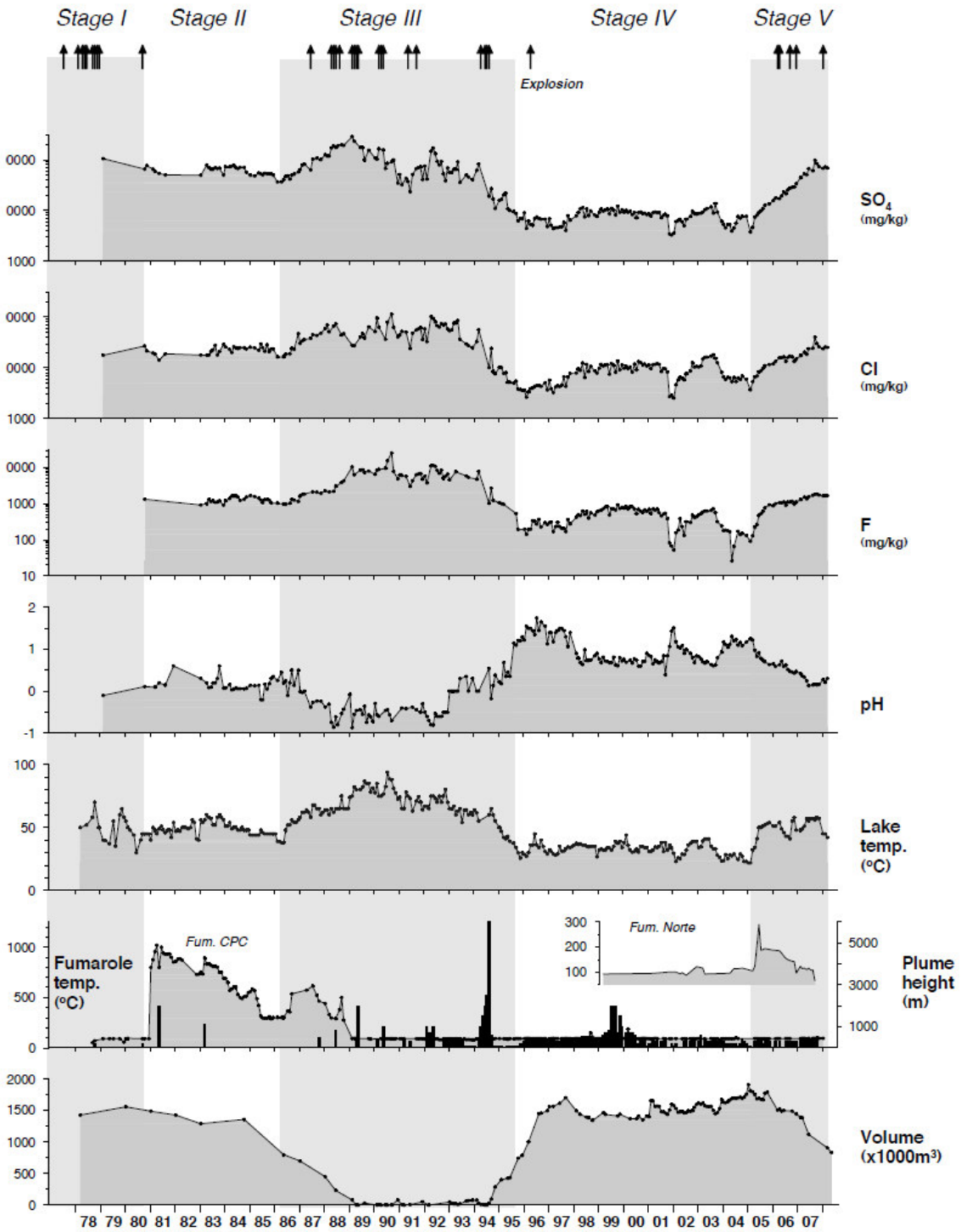

Figure 4.1: Time series plots of major parameters illustrating the evolution of Poás lake over 30 years (1978-2008). Figure from Martínez (2008).

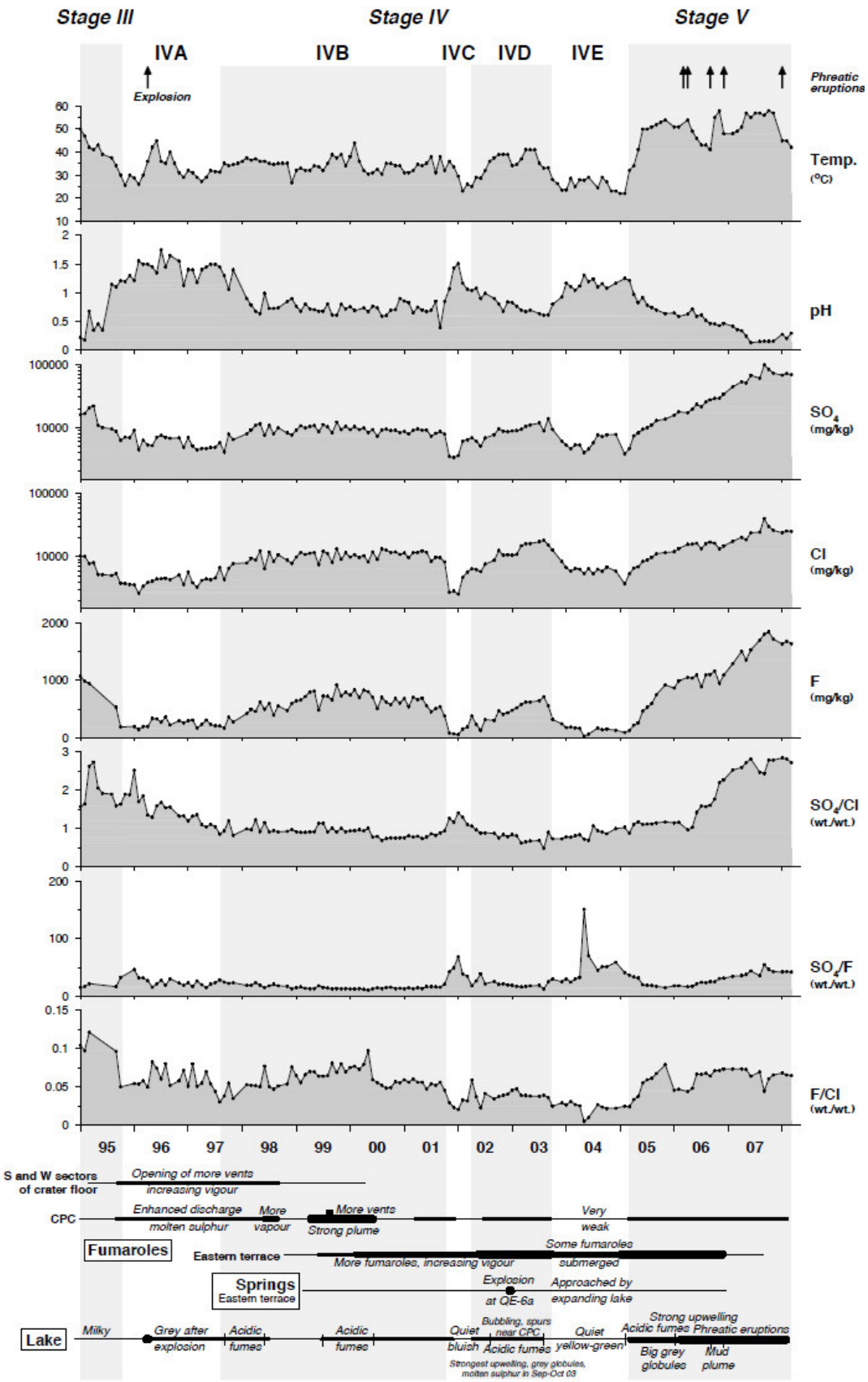

Figure 4.2: Time series plots of major parameters illustrating details in the recent evolution of Poás lake (1995-2008). Figure from Martínez (2008).

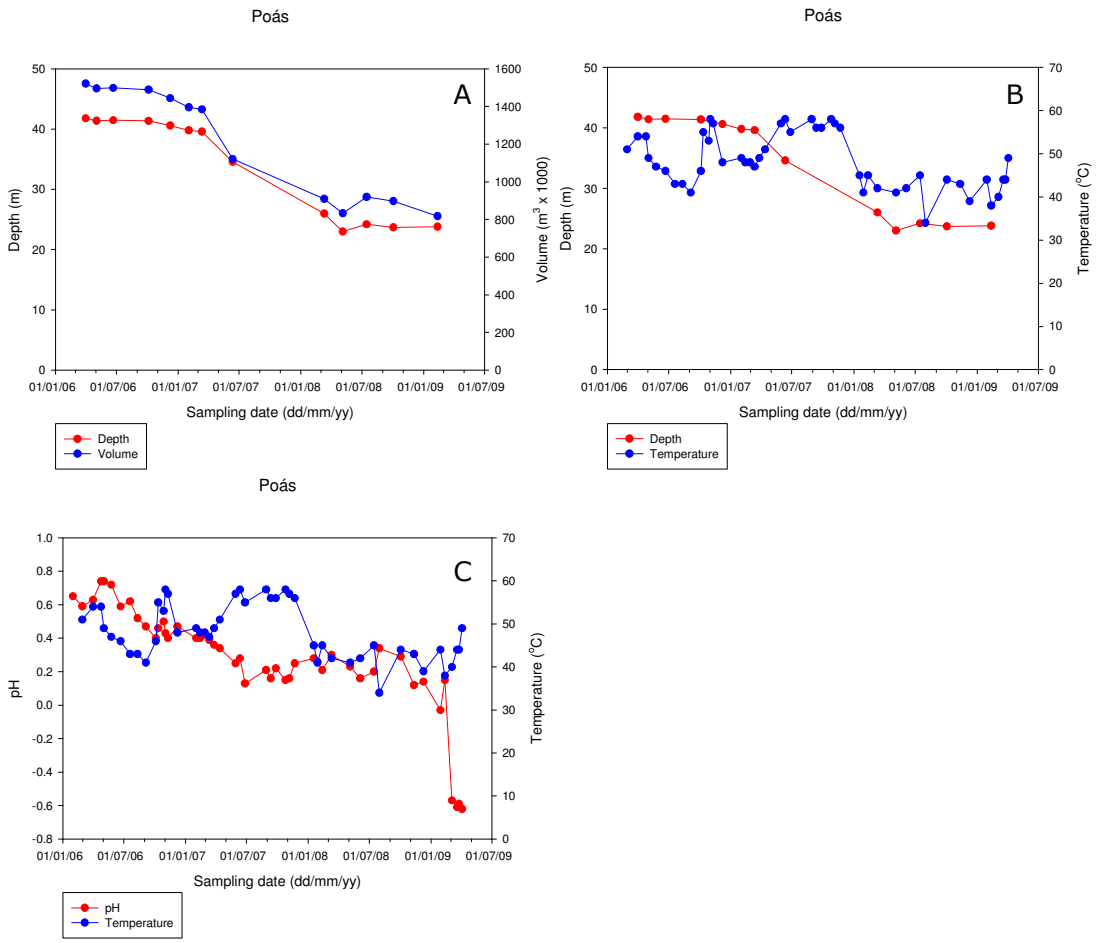

Figure 4.3: Time-series trends for depth, volume, temperature and pH for the lake of Poás for the period 2006-2009 (data collected by OVSICORI). Note the gradual decrease in depth, volume and pH, and the strong fluctuations in temperature. In all 3 graphs: red corresponds to the left y-axis and blue for the right y-axis.

Figure 4.3A shows that between April 2006 and March 2007 the lake volume did not change, but a significant decrease can be seen between March 2007 and May 2008. Following a minor increase, there was a further reduction until February 2009.

After a period of low temperatures (about 20-30ºC) in 2004-2005, the temperature had risen to more than 40ºC by early 2006, reaching more than 50 ºC in October-November and in large parts of 2007. In 2008 and 2009 the temperatures dropped in the 40s. The temperature trend (April 2006 - February 2009) is shown in figure 4.3B.

The pH of the lake decreased from April 2006 to February 2009, with an exception in May 2006 (figure 4.3C).

A phreatic eruption occurred in April 2006 and again in September and December of 2006. In 2007 no major activity was recorded and the only event in 2008 was an eruption in January. Early 2009 was more active with an earthquake in early January followed with an eruptions a few days later, while in March there was another eruption again.

Martínez (2008) already discussed some systematics in the REE signatures of the lake. The REE content is generally high and varied between 340 and 5000 ppb. Highest concentrations were observed during stage III when temperatures and acidity were highest as well. Chondrite-normalized REE patterns for this stage were close to those of the lavas, suggesting that REE abundances are created by interaction with the rocks of Poás and can be explained by (near-) congruent dissolution. The correspondence was less during the other periods, indicating that water-rock interaction must have been more complex when the lake properties were less extreme and the activity was lower. Martínez (2008) further observed that negative Eu anomalies are virtually absent in the lake waters (except for some of the analysed Stage III samples), despite their presence

in the lavas. This suggests that specific conditions and mineralogical controls may regulate the behaviour of individual REEs.

Table 4.3: Historic overview of main features in the lake-hosting active crater of Poás, subdivided into five stages according to Martínez (2008)

Stage	**Period**	**Remarks**
Before I	1830 - 1970	Single sample of lake water with incomplete data.
I	1972 – August 1980	Moderate to strong fumarolic discharge and occasional phreatic explosions within the lake.
II	September 1980 – April 1986	Relative quiescence in the lake, no phreatic activity despite strong discharge of high temperature fumaroles through the CPC (composite pyroclastic cone).
III	May 1986 – August 1995	Vigorous subaqueous fumarolic discharge, strong volume decrease and drying out of the lake, intense phreatic activity from the lake area.
IV	September 1995 – February 2005	Relative quiescence in the lake, opening of subaerial fumaroles and springs around the lake.
V	March 2005 – early 2008 (end of research)	Strong fumarolic discharge into the lake, from the North-eastern inner crater wall and from the CPC in 2005, renewal of phreatic activity and a steady decrease of lake volume from March 2006 on.

Stage	**Eruption and other important events**
Before I	1834 strong eruption, other eruptions for example: 1838, 1860, 1879-1880, 1884, 1889-1890, 1895, 1899-1901, 1903, 1905, 1908, 1910 Largest phreatic eruption reported over the last 2 centuries: 25 January 1910. Small to moderate intermittent geyser-like explosions over following ca. 40 years: 1910, 1914-1916, 1925, 1929, 1941-1946, and 1948-52 Magmatic activity 1953-1955 1969: phreatic eruptions
I Period with phreatic eruptions	1972-1980: fumarolic degassing and intermittent geyser-like phreatic eruptions late 1977 1978
II	Shallow magmatic intrusions beneath acidic crater lake: sometime in 1985

Stage	Eruption and other important events
III Period with phreatic eruptions	April 1988 May-June 1988 Lake dried out several occasions 1 May 1989: Unusual powerful steam jets. Dry ash and steam eruptions continued intermittently for several weeks Dry lake: April 1989-May 1989, but disappeared again during the dry seasons (rain: May-December) of 1990 and 1991 Phreatic eruption resumed in March 1990 Shallow magmatic intrusions beneath acidic crater: 1994 Phreatic eruption 25 April 1994 30 April 1994 2 June 1994 Between 24 & 31 July 1994 peak phreatic activity (largest: 31-7) 4 August 1994 mid-August 1994: new lake started up, more stable at very end 1994, early 1995
IV	Shallow magmatic intrusions beneath acidic crater: 2002
V Period with phreatic eruptions	minor phreatic eruptions between end March and April 26 26 April 2006: small explosion 25 September 2006 December 2006: small phreatic eruption

Table 4.4: The eruptive history, main events and other features during the different stages in the evolution of the crater lake of Poás, summarized from the compilation in Martínez (2008)

The crater lake of Rincón de la Vieja

The acid lake of Rincón de la Vieja is chemically similar to that of Poás, but less is known in detail because monitoring has been infrequent. Recorded pH values are extremely low pH (<1.2) and concentrations of dissolved elements are equally high (Kempter and Rowe, 2000; Tassi et al., 2005; OVSICORI, unpublished data).

The lake size did not change much between 1996 and January 2010. The size decreased noticeably only after the phreatic activity of November 1996. In July 2001 it was lower again, but without an obvious explanation. The lake size decrease of April 2002 is caused by a dry period. There was also a decrease in April 2007.

Between 1993 and January 2010 the lake temperature was 30-50°C, whereas a maximum of 58°C was recorded in July 2001.

The most recent eruption occurred in early November 1995. There is still seismic activity in the area.

5. Strategy and methods

This thesis focuses on the REE behaviour of acid crater lakes. New data are presented for the Costa Rican volcanoes Poás and Rincón de la Vieja. Together with previous results, the available data sets for these two volcanic lakes are the most extensive, allowing to evaluate temporal changes in detail. The crater lakes of El Chichón (Mexico), Copahue (Argentina), Ruapehu (New Zealand), Kawah Ijen, Kawah Putih, Keli Mutu, Kelut, Telaga Bodas, Telaga Warna (all in Indonesia), Pinatubo (Philippines), Kusatsu-Shirane (Japan) and Maly Semiachik (Russia) were selected for this study, because of the availability of REE data and their (predominantly) acidic nature. In addition, Yellowstone (USA) was selected to obtain a contrasting view on the REE behaviour from a hydrothermal area. Vulcano (Italy) does not host a crater lake, but presents an interesting case because here the behaviour of REE during alteration processes has been studied previously in rocks. With few exceptions, the properties of the selected areas are well documented in the literature.

To gain insight into the effects of water-rock interaction, literature data on water and rock compositions were compiled in a database. This contains the main properties of the lake waters as well as the major element concentrations together with the REE. Because publications sometimes use different units, all concentration data in the database were converted into the same unit. Because eruptive events might influence the element concentrations, these events were also included in the database. For each area, water and rock compositions were compared and evaluated in a set of diagrams (e.g., ternary diagrams, normalized REE plots, time-series trends). The PHREEQC routine (version 2.17) was used to explore the mineral saturation states and REE speciation. For evaluating differences between the LREE and HREE, La and Yb have been taken to represent the former and latter group, respectively. Furthermore, Eu anomalies were used to investigate differences in behaviour between bivalent and trivalent europium.

In addition to the literature compilation, new data were obtained by analyzing lake waters from Poás and Rincón de la Vieja. The 48 newly analyzed samples from Poás were collected between 28 February 2006 and 3 April 2009 at approximately monthly intervals by OVSICORI (Martínez, pers. comm.). These samples extend the results discussed in Martínez (2008) that cover a ca. 30-year period up to November 2005 and include REE data. The seven new samples from Rincón de la Vieja were collected between 2004 and 2008 at approximately 0.5-1 year time intervals, and were treated following the same methods as adopted for the Poás samples. Earlier major-element data from Rincón de la Vieja were taken from the literature but concentration data on the REE are lacking for this period.

A lava block expelled from the lake area during a phreatic eruption at Poás was studied to explore potential mineralogical effects of the interaction between the volcanic rocks and acidic water as far as they are relevant for the behaviour of the REE.

5.1 Samples of an ejected lava block from Poás

This sample of altered rock was collected inside the Poás crater on one of the terraces bordering the lake. It is presumably derived from a vent near the centre of the lake from which it was expelled during one of the phreatic eruptions.

Figure 5.1: Thin section of sample PV-102.

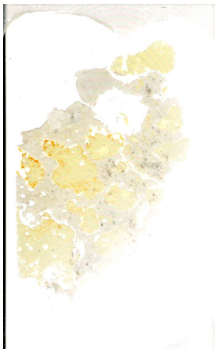

Figure 5.2: Thin section of sample PV-202.

Because colour differences in the several-decimeter-sized block suggested the presence of different minerals, light and dark parts were separated for individual analysis. They have been labelled as PV-102 and PV-202, respectively. Both sub-samples were crushed with a mortar for XRD (X-ray diffraction) analysis, which was carried out at room temperature using a Bruker-AXS D8 Advance powder X-ray diffractometer in Bragg-Brentano mode, a divergence slit and a PSD Våntec-1 detector. Because not all minerals could be determined by XRD, electron probe micro-analysis (EPMA) was used to identify minerals in thin sections (figures 5.1 and 5.2) from their chemical composition. Resin is used to fix the rock, since the minerals are very loose in the rock. The analyses were performed with a JXA-8600 superprobe using EDS techniques.

5.2 Water samples of Poás and Rincón de la Vieja

The samples were generally treated in the same way as the samples previously analyzed by Martínez (2008). The ICP and ICP-MS analyses were also performed in the laboratory at the Department of Earth Sciences of Utrecht University. Prior to analysis, the water samples were filtered with a 0.45 μ filter and diluted 100 or 200x by weight for ICP analysis. For ICP-MS analysis, the samples were diluted 50 and 100x by weight. Because the Poás and Rincón de la Vieja samples have different compositions, dilutions of the two sets of samples were not necessarily the same. A few samples were analyzed in duplicate to test the accuracy of the methods used. The IC, pH and temperature data were collected by OVSICORI (Martínez, pers. comm.).

6. Results

This chapter presents the results of the analysis of waters, rocks and minerals from Poás and Rincón de la Vieja volcanoes, as well as an overview of relevant data on other crater lakes and associated rocks, assembled from the literature.

6.1 Mineralogy of an ejected block collected in the crater of Poás

Explosive phreatic eruptions centered at the Poás lake have occasionally expelled rock fragments from the sub-lake vent area. Because they could provide insight into the mineralogical changes induced by water-rock interaction, the results of a mineralogical investigation of one of these ejecta are presented here first. Two different parts of the same rock have been studied separately: a brighter part (labelled PV-102) and a darker part (labelled PV-202).

6.1.1 X-ray diffraction results

The XRD spectra of Figures 6.1 and 6.2 indentify the main minerals present in the two different parts of the block. Cristobalite, tridymite, sulphur and alunite were detected. Minerals associated with some minor peaks could not be identified.

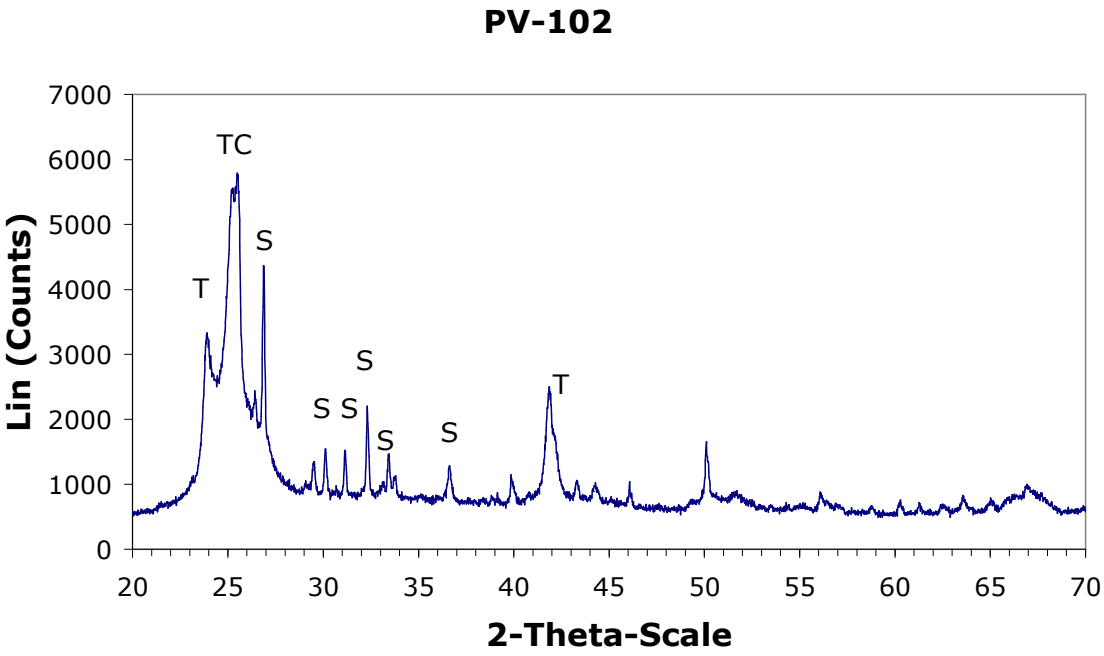

Figure 6.1: X-ray diffraction pattern for a bright part of an ejected block from Poás (PV-102) showing cristobalite (C), sulphur (S), tridymite (T), and an unspecified mineral.

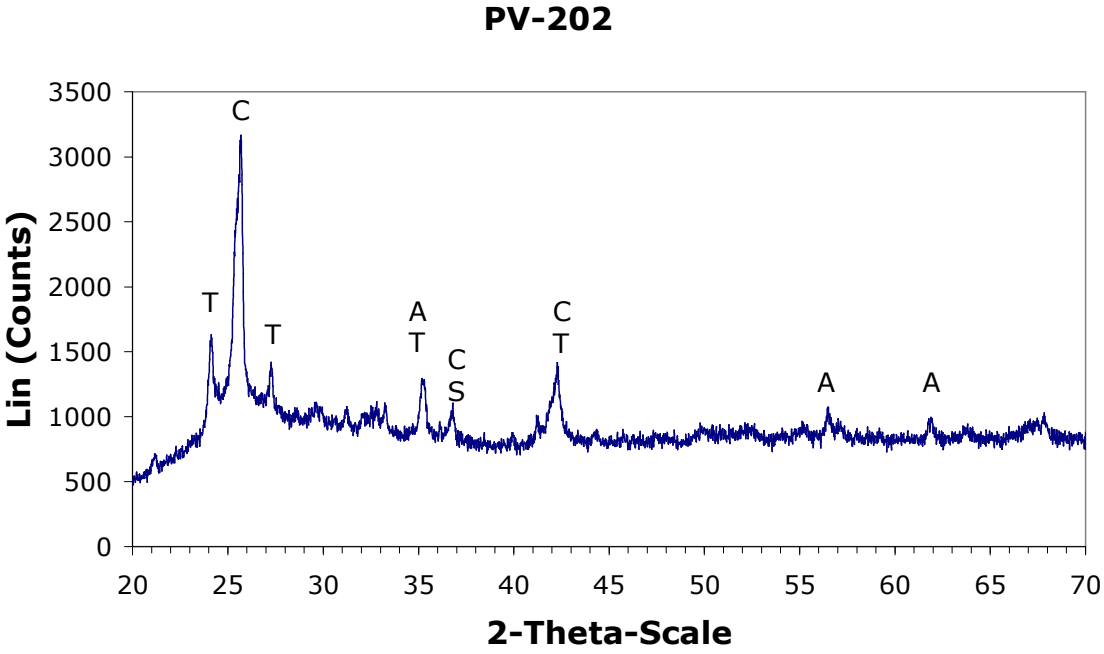

Figure 6.2: X-ray diffraction pattern for a dark part of an ejected block from Poás (PV-202) showing the presence of at least cristobalite (C), sulphur (S), tridymite (T), and alunite (A).

6.1.2 Electron microprobe results

Figures 6.3-6.6 show electron back-scatter images of PV-102 and PV-202 obtained by the electron microprobe. Different gray-scale intensities, combined with EDS surveys, provide a good impression of textures and allow mineral identification based on chemistry.

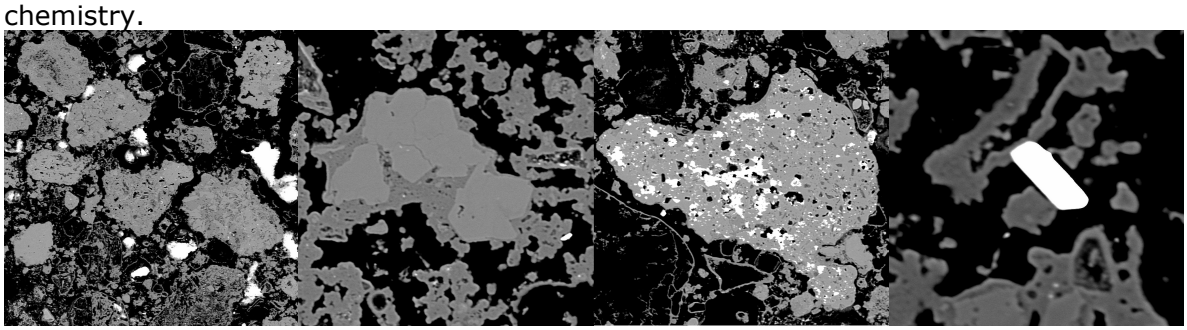

Figure 6.3: PV-102 overview. Figure 6.4: PV-202 overview. Figure 6.5: PV-102 TiO_2 in mineral. Figure 6.6: PV-202: barite grain.

Except for the bright grains and patches, virtually all grey parts are almost silica, independent of the shape, size or texture of the particle. Some grains show the texture of pumice. One of the overviews shows that TiO_2 is found in minerals (figure 6.5). Barite is found outside the minerals (figure 6.6).

PV-102 contains pyrite, barite, titanium oxide, sulphur. PV-202 contains: a KCl mineral, barite, titanoxide with sometimes considerably Sr in the mineral, probably pyroxene, K-silicate, pyrite, volcanic glass, chrome-bearing spinel, Na-Ca silicate. PV-102 contains probably more barite than PV-202. Possibly more sulphur is in this sample, which does not mean that there is more sulphur found in the lighter parts.

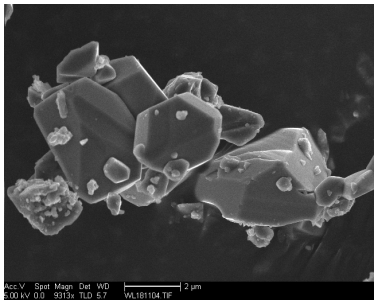

Figure 6.7: SEM image of alunite. (Rodríguez, 2011 personal communication) Scalebar represents 2 µm.

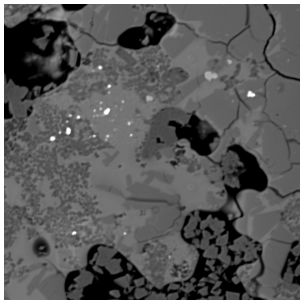

Figure 6.8: alunite grains in voids. (Rodríguez, 2011 personal communication) Width: 13.2 x 13.2 cm

Alunite has also been detected in a white part of a white and black layered rock found on the eastern terrace of the crater (Rodríguez, 2011, pers. comm.). Figure 6.7 shows a SEM image of the alunite, and figure 6.8 an EMP backscatter image. This finding further confirms the presence of the mineral in the Poás crater as identified independently by XRD, SEM, and EMP methods.

6.2 Changing compositional variations at Poás and Rincón de la Vieja

Time series trends indicate that the compositions of Poás and Rincón de la Vieja water samples are highly variable. Figure 6.2.9 illustrates this for Al and Mg as representative cations and Cl as major anion. For Poás, the subdivision into stages up to stage V is based on the properties and activity of the lake since the late 1970s (Martínez, 2008). The new samples from 2006 on are grouped by year, because a subdivision in terms of recent changes in activity is still unclear. Overall, the concentrations of the selected elements show strong fluctuations with time. Peak concentrations were observed during stage III, but relatively high, variable values also mark intervals around 1999-2001 (stage IV B), 2003-2004 (stage IV D) and 2007. Interestingly, Al and Cl follow roughly similar trends, but in detail their relative proportions do not remain constant. The Mg contents largely follow the same pattern, although the fluctuations of this element seem less strong. But this might be due to the scale.

The monitoring data for the Rincón de la Vieja lake water, collected since 1998, show clear change around 2001. The Cl concentration started to increase strongly and remained very high in the following years. In 2004 it dropped but remained at relatively high levels compared to the period before 2001. The Al concentration has also remained high since 2004. It is unknown if peak levels were reached in 2001-2004, since data are lacking for this interval. The time series for Mg shows roughly the same trend but contrasts before and after 2001 are small. The highest concentration was found in 2002, thus in the interval when peak values for Cl were observed.

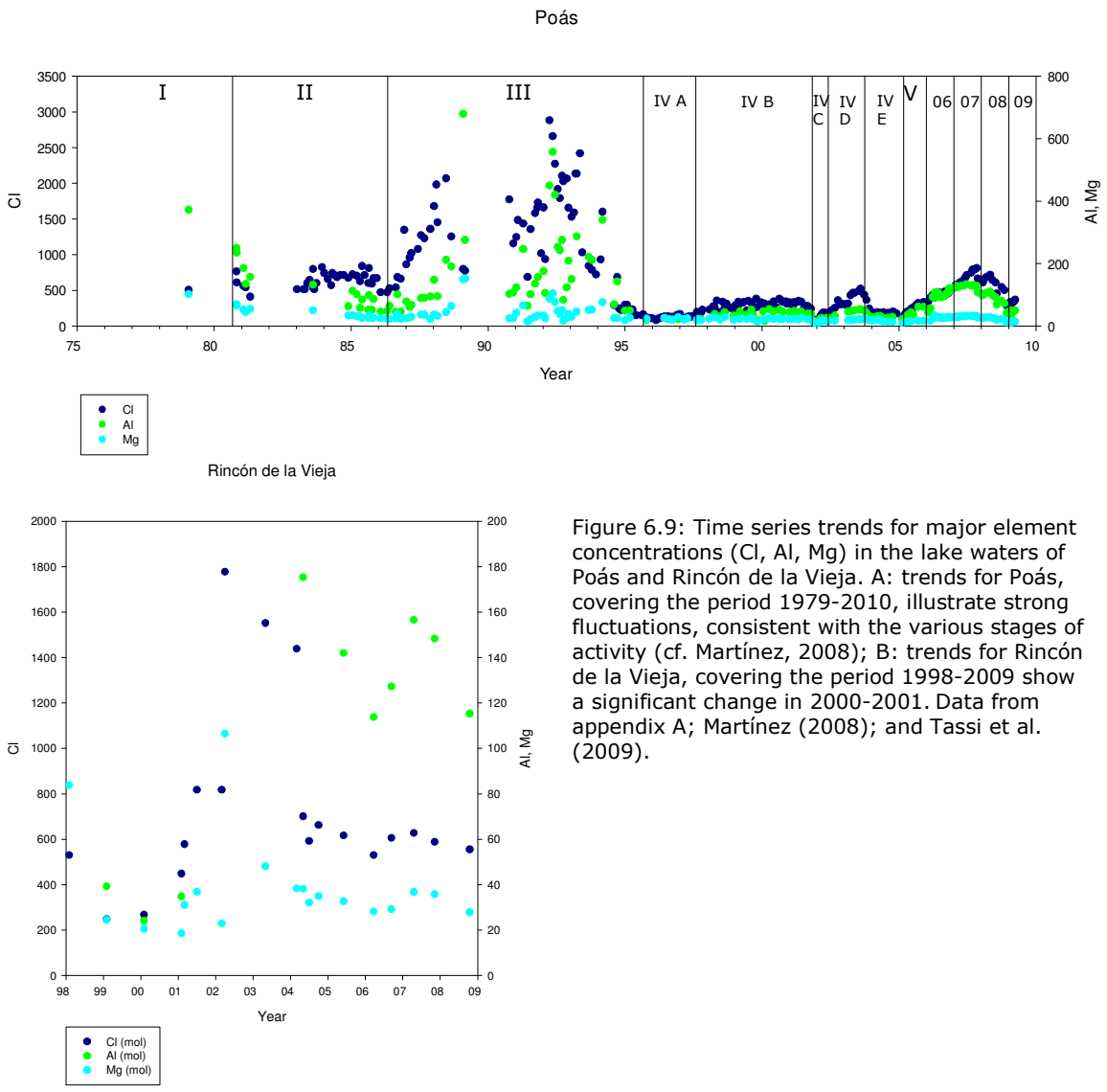

Figure 6.9: Time series trends for major element concentrations (Cl, Al, Mg) in the lake waters of Poás and Rincón de la Vieja. A: trends for Poás, covering the period 1979-2010, illustrate strong fluctuations, consistent with the various stages of activity (cf. Martínez, 2008); B: trends for Rincón de la Vieja, covering the period 1998-2009 show a significant change in 2000-2001. Data from appendix A; Martínez (2008); and Tassi et al. (2009).

6.3 Compositional variations in ternary diagrams for Poás, Rincón de la Vieja and selected volcanoes worldwide, illustrated in ternary diagrams

The investigated lake water compositions are plotted in Mg-Al-F, Mg-K-Na, Mg-K+Na-Al ternary diagrams, together with representative rock compositions and hypothetical compositions of minerals that potentially played a role in determining the water chemistry, such as alunite and feldspars

Poás and Rincón de la Vieja

Compositional variations of the crater lake waters from Poás and Rincón de la Vieja are illustrated in the ternary diagrams of figures 6.10 and 6.11. Poás stage II-V data are from Martínez (2008). The 2006-2008 data are new (this work, appendix A). Figures 6.10A and 6.11A are Mg-Al-F ternary diagrams, wherein the Poás data show two connected trends. One represents mainly stage IV and V and the other (part of) stage III and 2006-2008 samples. The new data (2006-2008) are comparable to stage III, but plot closer to the average rock composition. These samples and some of stage III follow a trend between gas (F) and the average rock composition. Substages IV A, C, and E plot furthest away from the line connecting gas and rock, while substage IV B, D, and stage V are closer. None of the samples follow a trend towards or away from alunite. The three samples of Tassi et al. (2009) are the only data points in the Rincón de la

Vieja diagram. These samples deviate from the line between the gas and host rock composition. There is no indication of an alunite control.

The Mg-K-Na ternary diagrams are shown in figures 6.10B and 6.11B. The Poás data show two trends. One represents a more recent period ((part of) stage IV E, V, 2006-2009), and runs towards the average rock composition, while the other represents an earlier period (I, III, IV A-(part of) E) and runs away from it. The combined water (both groups) and rock samples define a trend that runs towards natro-alunite and K-feldspar. The Rincón de la Vieja data show a single trend. There is a compositional gap between the data of Tassi et al. (2009) and the new data (2004-2008). The combined water and rock samples are on a trend with natro-alunite.

The Mg-K+Na-Al ternary diagrams are given in figures 6.10C and 6.11C. The Poás data follow a single trend. There is a small gap between the data for stage IV A (and some of stage IV B) and the rest of the data. The compositions for Stage I and for the most recent period (2006-2009) plot near the average rock composition. Stage III compositions fall on both sides of the rock and sometimes close to it. The combined water and rock samples follow a trend that runs towards alunite. Two trends are visible in the Rincón de la Vieja data. The most recent interval (2004-2008) represents new data (appendix A) which show different behaviour relative to the data of Tassi et al. (2009) that cover an earlier period. These samples follow a trend towards alunite, whereas the data of Tassi et al. (2009) plot much further away. The new compositions presented in this study (2004-2008) plot close to the rock samples.

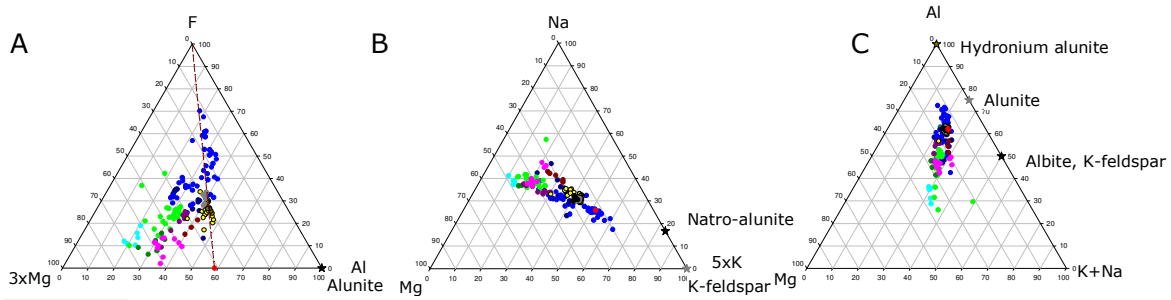

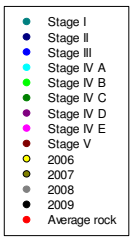

Figure 6.10: Ternary diagrams showing compositions of lake waters from Poás, together with compositions of local rocks and potentially relevant minerals. A) Water samples of part of stage III and the most recent period (2006-2008) fall on a trend line between F (representing the gas phase) and the average local rock, suggesting whole-rock dissolution during these periods. B) Many of the water samples form a trend line suggesting that alunite had an important control on their compositions. C) Trend indicating that alunite was not the only Al-bearing phase controlling water compositions or that its composition was relatively close to the hydronium endmember. Data from appendix A, Martínez (2008) and Prosser and Carr (1987) and appendix B.

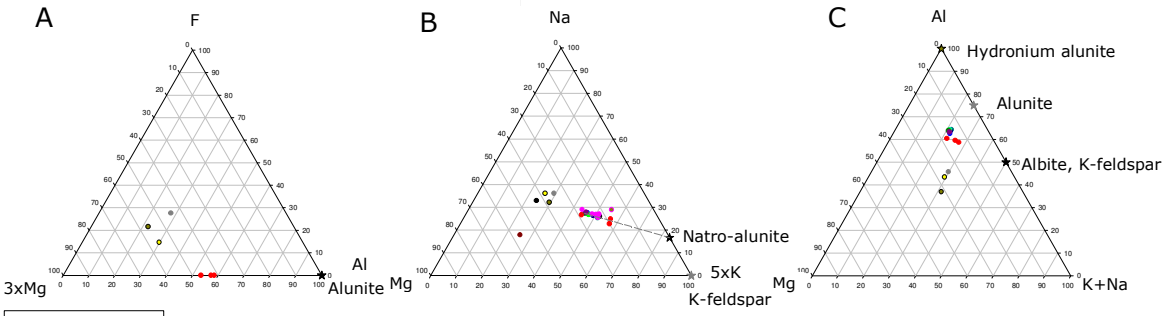

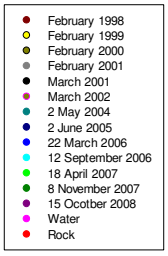

Figure 6.11: Ternary diagrams showing compositions of lake waters from Rincón de la Vieja, together with compositions of local rocks and potentially relevant minerals. Note that data sets are incomplete. B) and C) point to similar behaviour as inferred for Poás in figure 6.10, suggesting alunite precipitation controlling the older samples (1999-2001) and whole-rock or alunite dissolution the younger samples (2004-2008). Data from appendix A, Tassi et al. (2009), and Soto et al. (2003 and reference to Tomadas de Kempter (1997).

Other volcanoes

Ternary diagrams for *El Chichón* are given in figure 6.12. In the Mg-Al-F ternary diagram the data follow a single trend at relatively low Al concentrations. The compositions do not trend towards or away from alunite. In the Mg-K-Na and the Mg-K+Na-Al diagrams no clear trend towards or away from the rock samples is visible.

Figure 6.13 presents ternary diagrams for *Copahue*. The Mg-Al-F diagram shows two trends. The earlier samples (6 January 1999 and 26 November 1999) plot on the trend between F and the average rock composition. The other, more recent data fall on a different trend that does not seem to be controlled by alunite. Both in the Mg-K-Na diagram and in the Mg-K+Na-Al only a single trend is visible. The earlier water samples (15 March 1997 – 16 July 2000) plot close to the rock samples.

The data for *Yellowstone* show mainly scatter in the ternary diagrams (figure 6.14). In the Mg-Al-F diagram they fall in four different areas. The rock samples are relatively rich in Al, whereas almost all water and rock samples contain little or no Mg.

The three ternary diagrams for *Ruapehu* (figure 6.15) show a gap between two monitoring periods (1988-1995 and 1995-1996). The gap represents 2.5 months in 1995. In all cases the compositions follow a single trend. The data for the earlier period tend to fall on a line connecting the gas phase and the rock composition in the Mg-Al-F diagram, and they plot close to the rocks in the Mg-K-Na and Mg-K+Na-Al diagrams. The combined samples follow trends away from (natro-)alunite.

The *Kawah Ijen* ternary diagrams are presented in figure 6.16. The Mg-Al-F ternary diagram shows a single trend. The water samples fall on a whole-rock dissolution trend. Water samples are partly surrounded by rock samples in the Mg-K-Na ternary diagram. Some of the plotted water samples contain relatively less Na than the rock samples. The Mg-K+Na-Al ternary diagram shows water samples close to the rock samples.

The ternary diagrams for *Kawah Putih* (figure 6.17) show a single trend, which does not run towards or away from alunite. The Mg-K-Na ternary diagram only shows a single spot. The water samples plot close to a line connecting rock and natro-alunite. A single spot is also shown in the Mg-K+Na-Al ternary diagram. The water samples plot between the rock samples and (hydronium) alunite.

The ternary diagrams (Mg-Al-F, Mg-K-Na, Mg-K+Na-Al) for *Keli Mutu* are shown in figure 6.18. The samples show mainly scatter. There is no clear trend.

The Mg-K-Na ternary diagram for *Kelut* (figure 6.19) shows one trend. The water samples do not point to alunite and K-feldspar as controlling minerals.

The single trend of the Mg-K-Na ternary diagram for *Pinatubo* (figure 6.20) does not suggest an important role for alunite or K-feldspar.

Figure 6.21 displays two ternary diagrams for *Kusatsu-Shirane*. The periods are described in Ohba et al. (2008). Period I is from 1966 to 1981, period II is 1982-1989, period III covers 1990-1995, and period IV is from 1996 to 2005. The Mg-K-Na ternary diagram shows one trend. The earlier samples (period I) fall on one side close to the rock. There is a gap between period I and the other periods. The more recent periods (II, III, IV) fall on the other side of the rock. All water samples follow a trend suggesting a natro-alunite relation. Period II samples plot furthest away from the mineral, whereas period IV compositions are closer to the rock (and thus closer to the mineral as well). Like the Mg-K-Na diagram, the Mg-K+Na-Al diagram indicates a single trend. Period II compositions fall closest to the rock samples. There is a gap between period I data and those from the more recent periods (II-IV). The water samples follow a trend that runs towards (hydronium) alunite.

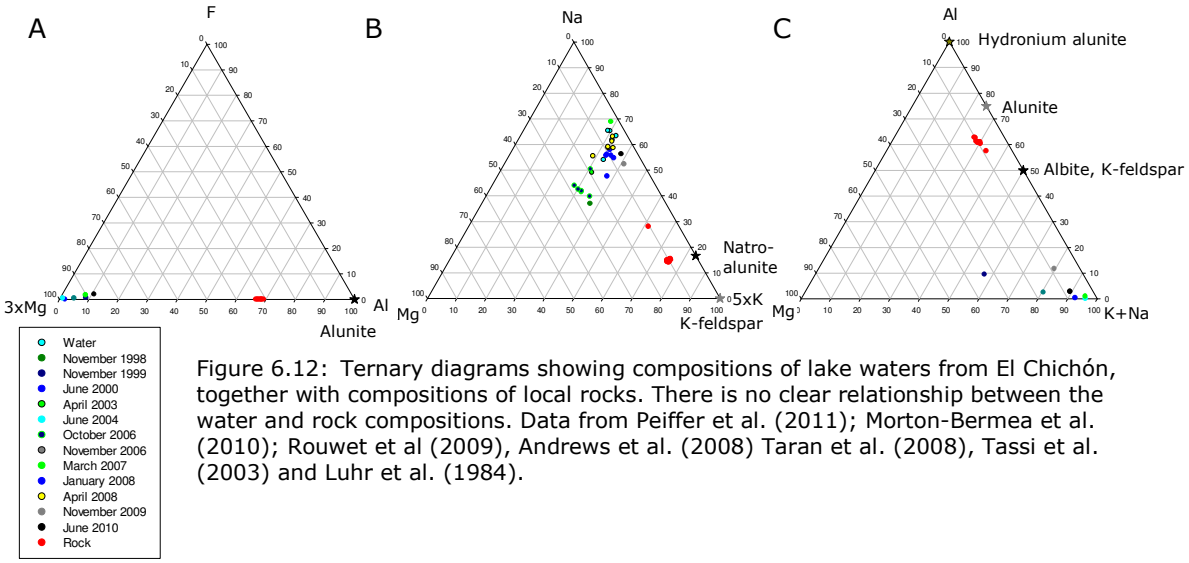

Figure 6.12: Ternary diagrams showing compositions of lake waters from El Chichón, together with compositions of local rocks. There is no clear relationship between the water and rock compositions. Data from Peiffer et al. (2011); Morton-Bermea et al. (2010); Rouwet et al (2009), Andrews et al. (2008) Taran et al. (2008), Tassi et al. (2003) and Luhr et al. (1984).

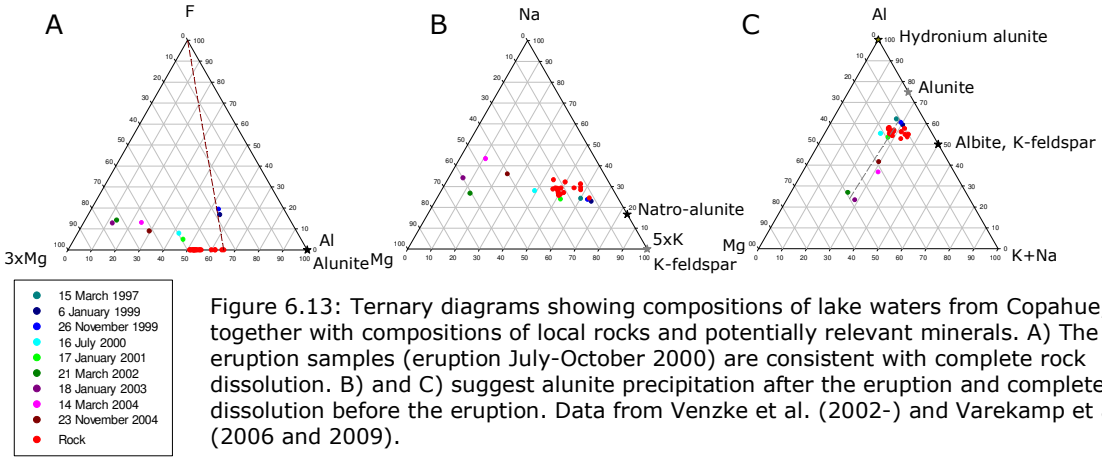

Figure 6.13: Ternary diagrams showing compositions of lake waters from Copahue, together with compositions of local rocks and potentially relevant minerals. A) The pre-eruption samples (eruption July-October 2000) are consistent with complete rock dissolution. B) and C) suggest alunite precipitation after the eruption and complete rock dissolution before the eruption. Data from Venzke et al. (2002-) and Varekamp et al. (2006 and 2009).

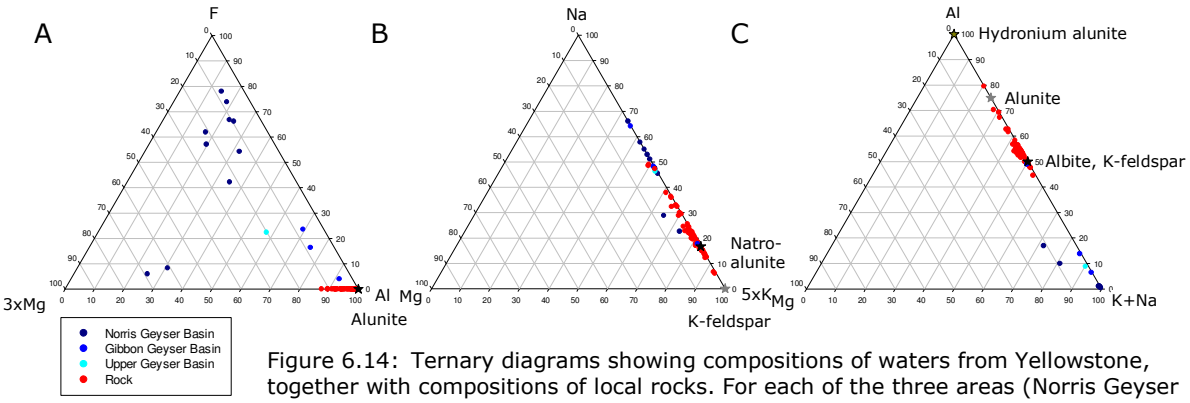

Figure 6.14: Ternary diagrams showing compositions of waters from Yellowstone, together with compositions of local rocks. For each of the three areas (Norris Geyser Basin, Gibbon Geyser Basin, and Upper Geyser Basin) there is no obvious relationship between water and rock compositions. Data from Lewis et al. (1997) and Beeson and Bargar (1984).

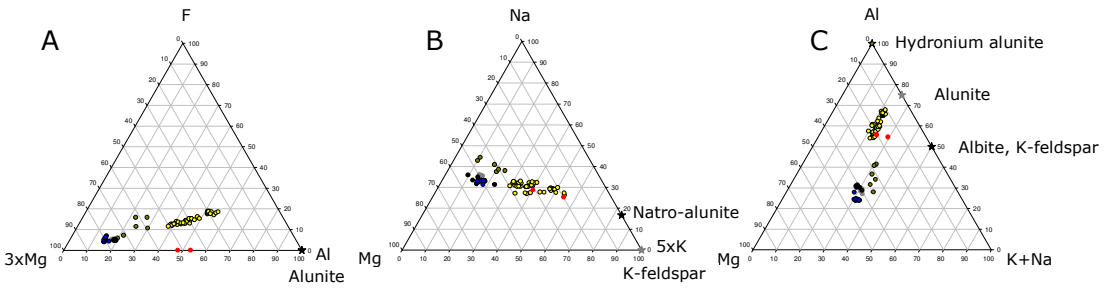

Figure 6.15: Ternary diagrams showing compositions of lake waters from Ruapehu, together with compositions of local rocks and potentially relevant minerals. A) suggests no relevant relation. B) and C) suggest an alunite control. The set of earliest samples (before the September 1995 eruption) plots close to the rocks suggesting whole rock dissolution; the samples from later periods are consistent with alunite precipitation. Data from Christenson et al. (2010); Christenson (2000); and Christenson and Wood (1993).

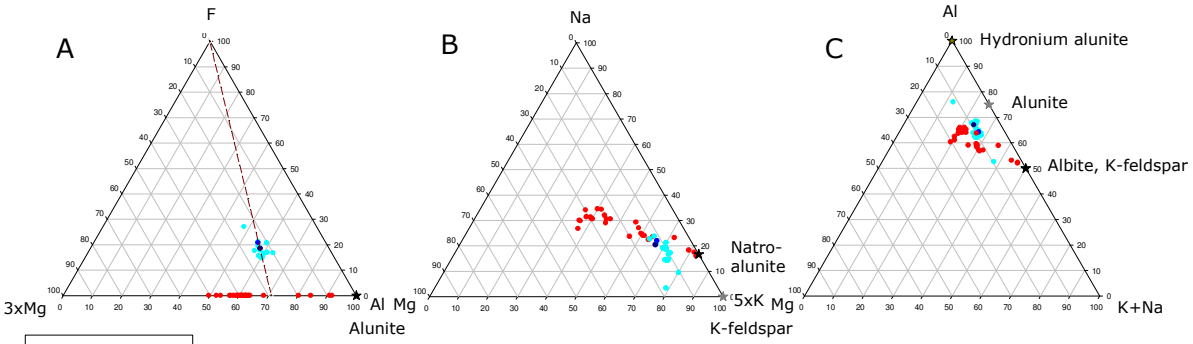

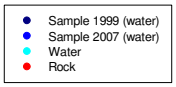

Figure 6.16: Ternary diagrams showing compositions of lake waters from Kawah Ijen, together with compositions of local rocks and potentially relevant minerals. A) The water samples of 1999 and 2007 indicate whole rock dissolution. B) and C) are not very clear in supporting a possible alunite control. Data from Van Hinsberg et al. (2010); Handley et al. (2007) and referring to Sitorus (1990); Delmelle et al. (2000 and 1994).

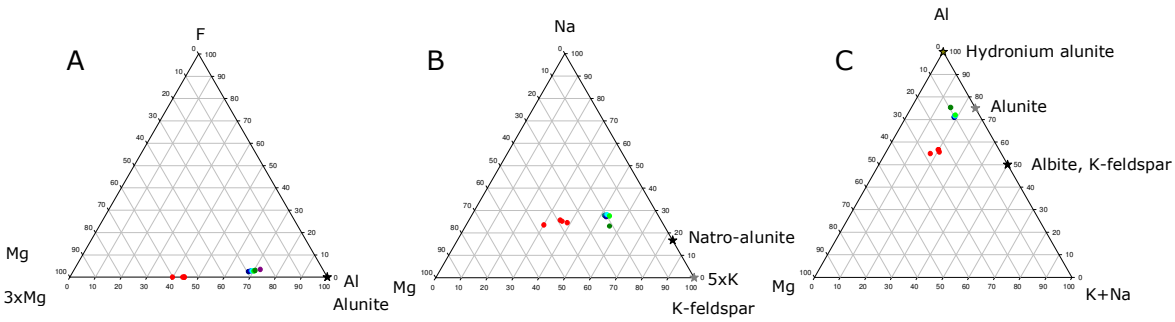

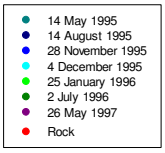

Figure 6.17: Ternary diagrams showing compositions of lake waters from Kawah Putih, together with compositions of local rocks and potentially relevant minerals. B) and C) are consistent with a possible alunite control. Data from Sriwana et al. (2000).

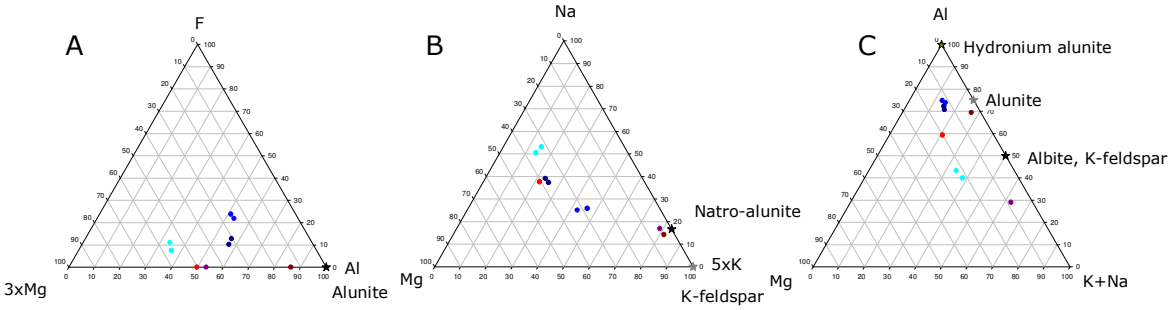

TAP water
TiN water
TAM water
TAM ash-f
TAM ash
KM scoria

Figure 6.18: Ternary diagrams showing compositions of waters from the three lakes of Keli Mutu, together with compositions of local pyroclastic rocks and potentially relevant minerals. There are no clear relationships between water and rock compositions, but alunite might (partly) control the TAP and TiN waters. Data from Pasternack and Varekamp (1994).

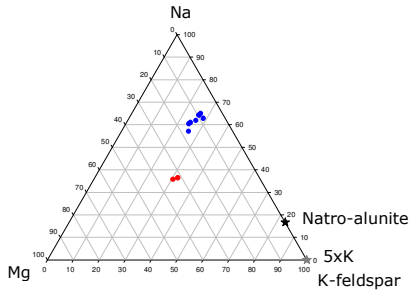

Water
Rock

Figure 6.19: Ternary diagrams showing compositions of lake waters from Kelut, together with compositions of local rocks and potentially relevant minerals. There is no evidence for a control by alunite. Data from Bourdier et al. (1997) and Badrudin (1994).

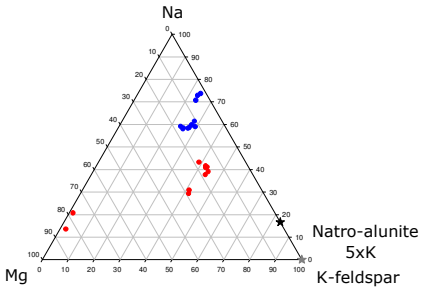

Water
Rock

Figure 6.20: Ternary diagrams showing compositions of lake waters from Pinatubo, together with compositions of local rocks and potentially relevant minerals. No alunite relation is suggested. Data from Castillo (1999) and Stimac et al. (2004).

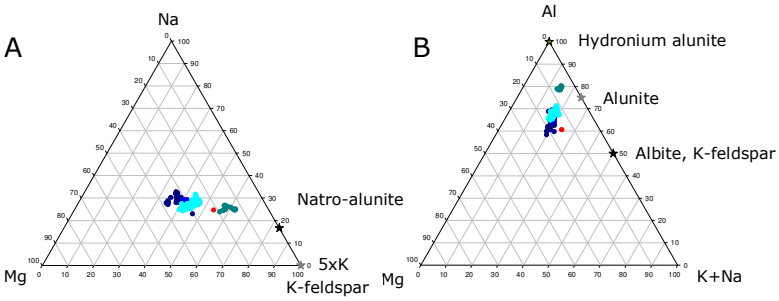

Period I (1966-1981)
Period II (1982-1989)
Period III (1990-1995)
Period IV (1996-2005)
Rock

Figure 6.21: Ternary diagrams showing compositions of lake waters from Kusatsu-Shirane, together with compositions of an average andesite and potentially relevant minerals. Both diagrams point to an alunite control. Not that compositions from Period I (1966-1981) plot closer to alunite than those from the other periods. Data from Ohba et al. (2008) and references therein.

6.4 REE patterns

REE diagrams were constructed to illustrate properties of the lake waters, to explore differences in the behaviour of the individual rare earth elements and to compare the chemical signatures of the investigated lakes. Chondritic values from Sun and McDonough 1989 were used to normalize the measured REE concentrations for diagrams shown on the left, whereas values from local volcanic rocks or from average andesite were taken to normalize the concentrations in the lake waters for diagrams shown on the right. The latter allow a direct comparison between rocks and waters in terms of REE signatures.

Poás and Rincón de la Vieja

REE patterns for waters and rocks from Poás (figure 6.22) and Rincón de la Vieja (figure 6.23) show overall similarities but differences exist in details. Chondrite-normalized trends for the Poás waters show enrichment of the LREE over the HREE. The LREE part of the trends is relatively steep, while the HREE part is close to flat. The trends for all analyzed samples available are generally parallel, with some exceptions, notably for the samples taken in 2006, 2007, and 2008 that show minor deviations in the HREE. Highest concentrations were observed in Stage III and the lowest in Stage IV (see Martínez, 2008). The new data, representing samples taken since 2006, fall between these extremes. There are no obvious anomalies in the patterns.

Chondrite-normalized trends for the rocks of Poás (data from appendix B) are comparable to those of the waters as far as enrichment of LREE over HREE concerns. The difference is that the rock patterns are not entirely parallel, since the LREE show more variation than the HREE.

The rock-normalized REE abundances in the lake water samples show a clear depletion of the LREE relative to the HREE, and a positive Eu anomaly. The trends are parallel, again with the exception for HREE parts in samples from 2006, 2007, and 2008 that tend to be steeper.

Chondrite-normalized trends for the Rincón de la Vieja waters (appendix A) show LREE enrichment over HREE. The LREE part is relatively steep and the HREE part close to flat. Highest concentrations are from the May 2004 sample and lowest from the October 2008 sample. There are no obvious anomalies in the trends.
Chondrite-normalized trends for the rocks (data from Soto et al., 2003) also show relatively steep LREE and close to flat HREE parts in addition to a negative Eu anomaly. The rock-normalized trends for the waters are close to flat with a slight depletion in the lightest REE, particularly La.

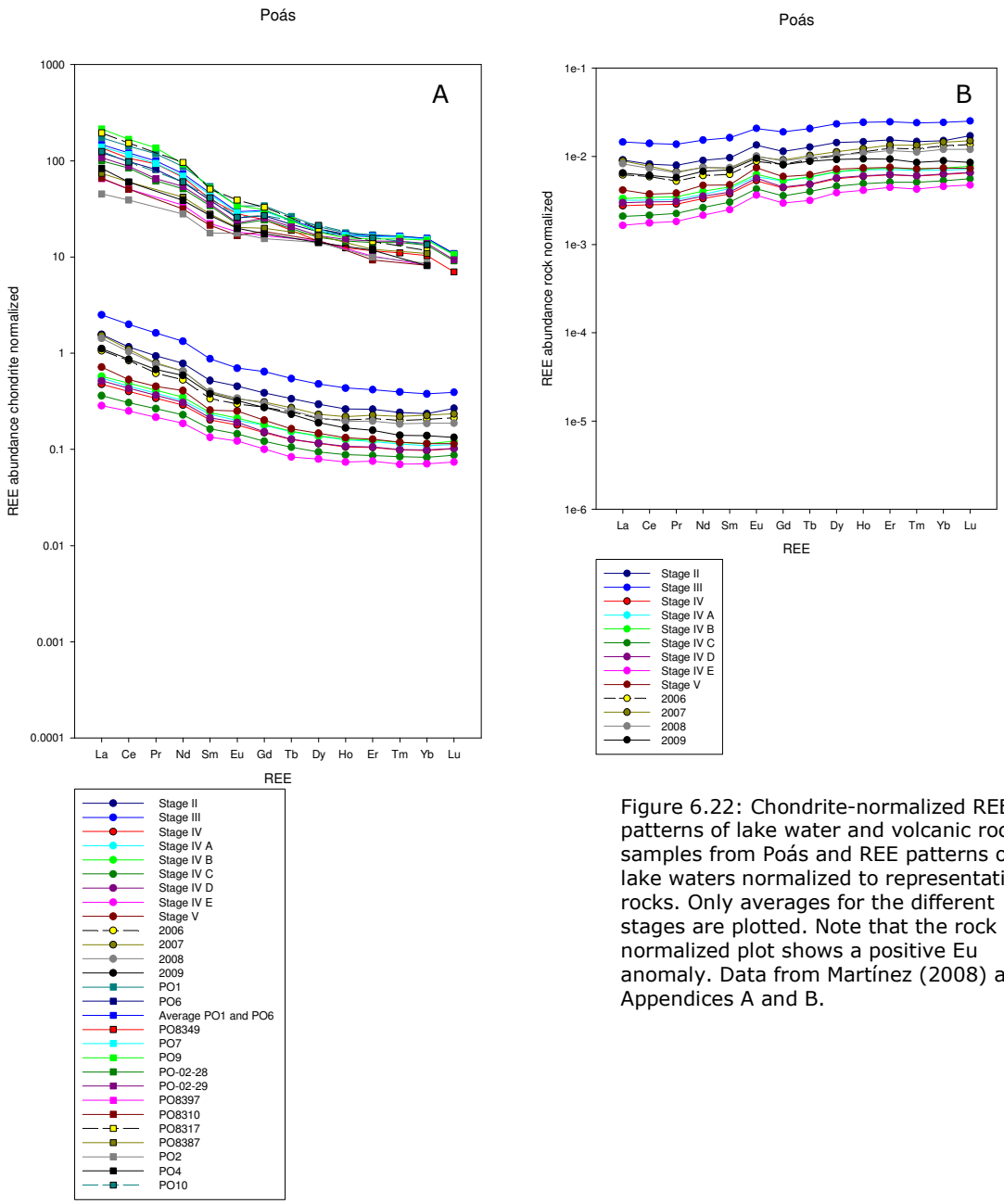

Figure 6.22: Chondrite-normalized REE patterns of lake water and volcanic rock samples from Poás and REE patterns of lake waters normalized to representative rocks. Only averages for the different stages are plotted. Note that the rock normalized plot shows a positive Eu anomaly. Data from Martínez (2008) and Appendices A and B.

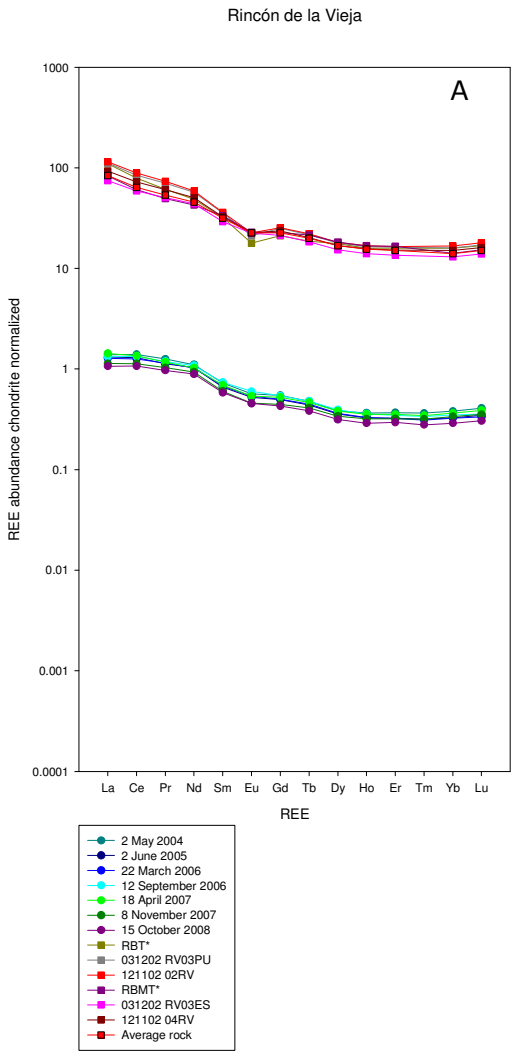

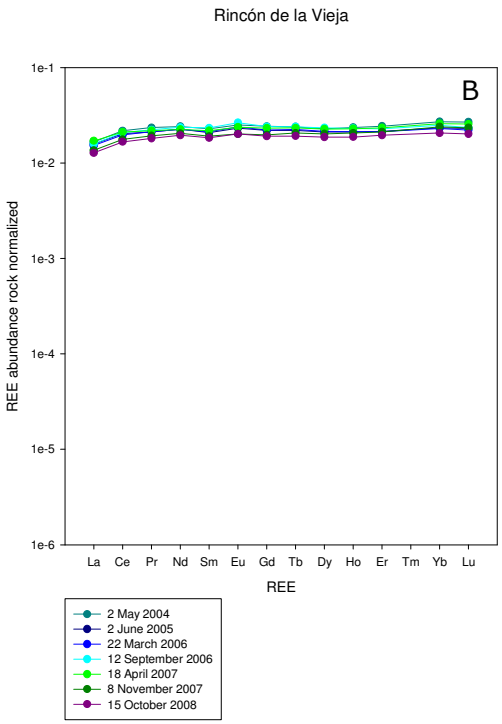

Figure 6.23: Chondrite-normalized REE patterns of lake water and volcanic rock samples from Rincón de la Vieja (A) and REE patterns of lake waters normalized to representative rocks (B). Note that the rock-normalized plot highlights a depletion in La and Ce relative to the other REE. Data from appendix A and Soto et al. (2003).

Other volcanoes

The other volcanoes can be divided into groups of different behaviour. One group consists of El Chichón (figure 6.24) and Yellowstone (figure 6.26). Another groups shows the normalized REE patterns of Copahue (figure 6.25) and Ruapehu (figure 6.27). The Indonesian volcanoes (figure 6.28) and the NW Pacific volcanoes (figure 6.29) have only one sample of every lake, except for Kawah Ijen and Kawah Putih. These different groups are made on basis of the rock normalized plots. Copahue and Ruapehu are more or less flat, El Chichón and Yellowstone are more scattered. The Indonesian group and NW Pacific volcanoes are groups on basis of geography.

Chondrite-normalized trends for El Chichón waters (data from Peiffer et al., 2011; Morton-Bermea et al., 2010; and Taran et al., 2008) show a decreasing trend from La to Lu. April 1998 is the highest observed concentration, some samples of April 2008 show the lowest plotted concentration. There are no obvious anomalies in the trends. The rocks in the same chondrite-normalized plots for El Chichón (data from Morton-Bermea et al., 2010; Andrews et al., 2008; and Luhr et al., 1984) show a steep LREE trend and a close to flat HREE.

Rock-normalized REE trend for Rincón de la Vieja have close to flat trend, but there is a broad range of the different trends.

Copahue waters (data from Varekamp et al., 2009; Gammons et al., 2005; and Takano et al., 2004) when normalized to chondrite show a relatively steep LREE and a close to flat HREE. Three of the plotted trends show a different pattern. Two samples, 18 January 2003 and 14 March 2004, have almost the

same values. The LREE trend is also steep, but HREE increases instead of a close to flat pattern. Sample 23 November 2004 show a lower value than the general trend and there is a more decreasing trend from La to Lu. The general trend shows a negative Eu anomaly. The rocks (data from Gammons et al., 2005) in the same plot show a steep LREE trend and a close to flat HREE. Sample c shows in general the same trend, but lower and has a negative Eu anomaly. The rock-normalized REE show a close to flat pattern, except for 18 January 2003 and 14 March 2004 show a dip in the LREE trend and an increasing HREE trend. Sample 23 November 2004 show a lower value than the general trend and has a lower LREE trend.

Chondrite-normalized trends for Yellowstone waters (data from Lewis et al., 1997) show a decreasing trend from La to Lu, and a negative Eu anomaly. The trend of the water is very broad. Chondrite-normalized trend for Yellowstone rocks (data from Lewis et al., 1997) are comparable to the Yellowstone water samples as far as the shape of the REE trend. Rock-normalized waters for Yellowstone show a relatively low LREE and a close to flat HREE.

The Ruapehu waters (data from Takano et al., 2004) when chondrite-normalized trends for show a steep LREE and close to flat HREE (10 February 1989 and 2 March 1995) and a close to flat REE trend for 27 March 1998. The rocks (data from Hannigan, 2005; Gamble et al., 1999; and Gamble et al., 1993) in the same figure are comparable to the older water samples (10 February 1989 and 2 March 1995). Some samples show however a small negative Eu anomaly. Sample TVZ-16 shows a slightly different trend. This sample does not have a complete data set. Old rock-normalized waters (10 February 1989 and 2 March 1995) show close to flat LREE and a slightly steep HREE. The sample of 27 March 1998 shows an increasing trend of LREE and a close to flat HREE trend.

Chondrite-normalized trends for Indonesian volcanoes waters (data from Van Hinsberg et al., 2010; Takano et al., 2004 and references therein; Sriwana et al., 2000) show steep LREE and close to flat HREE for Kawah Ijen (KI), Keli Mutu, Kelut, and Telaga Warna and a decreasing trend from La to Lu for Kawah Putih (KP). The Telaga Bodas trend is not very clear with a low La. There is a small negative Eu anomaly for KI and Keli Mutu has a low La and Ce. Chondrite-normalized trends for Indonesian volcanoes rocks (data from Geochemical Earth Reference Model (2011); Van Hinsberg et al., 2010; Sriwana et al., 2000) show steep LREE and close to flat HREE for Kawah Ijen (KI), Kawah Putih, and average andesite world. The Kawah Ijen rock samples suggest a possible small negative Eu anomaly. Indonesian volcanoes when rock-normalized show close to flat REE for Kawah Ijen, a slightly decreasing trend from La to Lu for Kawah Putih (KP), close to flat LREE with low La and Ce and at a higher value a higher close to flat HREE for Keli Mutu, a close to flat REE for Kelut, an increasing REE trend of Telaga Bodas and a steep LREE and a close to flat HREE for Telaga Warna.

Chondrite-normalized trends for NW Pacific volcanoes waters (data from Takano et al., 2004) show decreasing trend from La to Lu for Pinatubo and the same trend, but less steep for Kusatsu-Shirane and a close to flat REE trend for Maly Semichik. The rocks in the same figure (Geochemical Earth Reference Model (2011); Di Muro et al. (2008); Castillo and Punongbayan (1996); and Daag (1996)) show decreasing trend from La to Lu for Pinatubo, except for two samples indicated as old lava, basement basalt. The average andesite world shows a similar trend. The NW Pacific volcanoes plot of rock-normalized waters show a close to flat pattern of Pinatubo with a small negative Eu anomaly. Maly Semiachik shows a slightly increasing LREE and a close to flat HREE and the shape of the trend of Kusatsu-Shirane is somewhere between Pinatubo and Maly Semiachik.

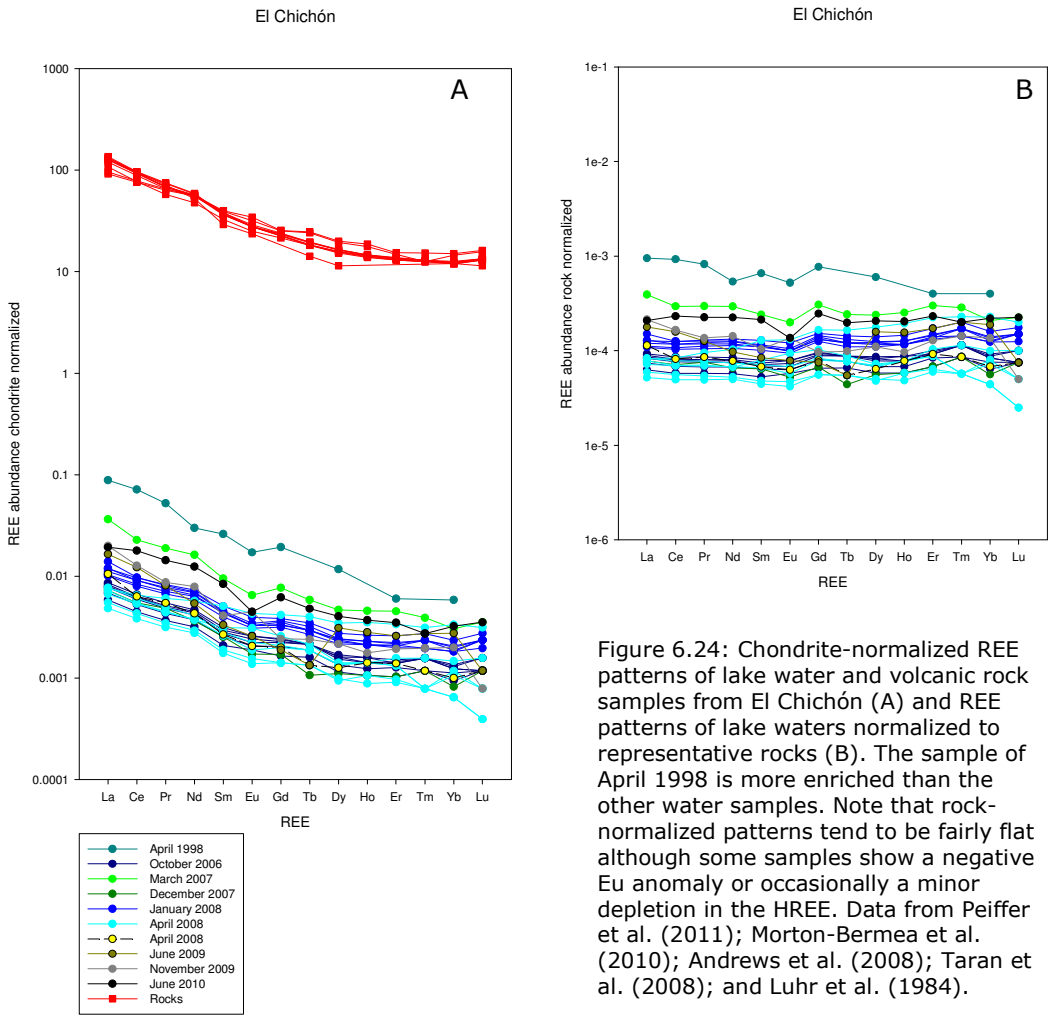

Figure 6.24: Chondrite-normalized REE patterns of lake water and volcanic rock samples from El Chichón (A) and REE patterns of lake waters normalized to representative rocks (B). The sample of April 1998 is more enriched than the other water samples. Note that rock-normalized patterns tend to be fairly flat although some samples show a negative Eu anomaly or occasionally a minor depletion in the HREE. Data from Peiffer et al. (2011); Morton-Bermea et al. (2010); Andrews et al. (2008); Taran et al. (2008); and Luhr et al. (1984).

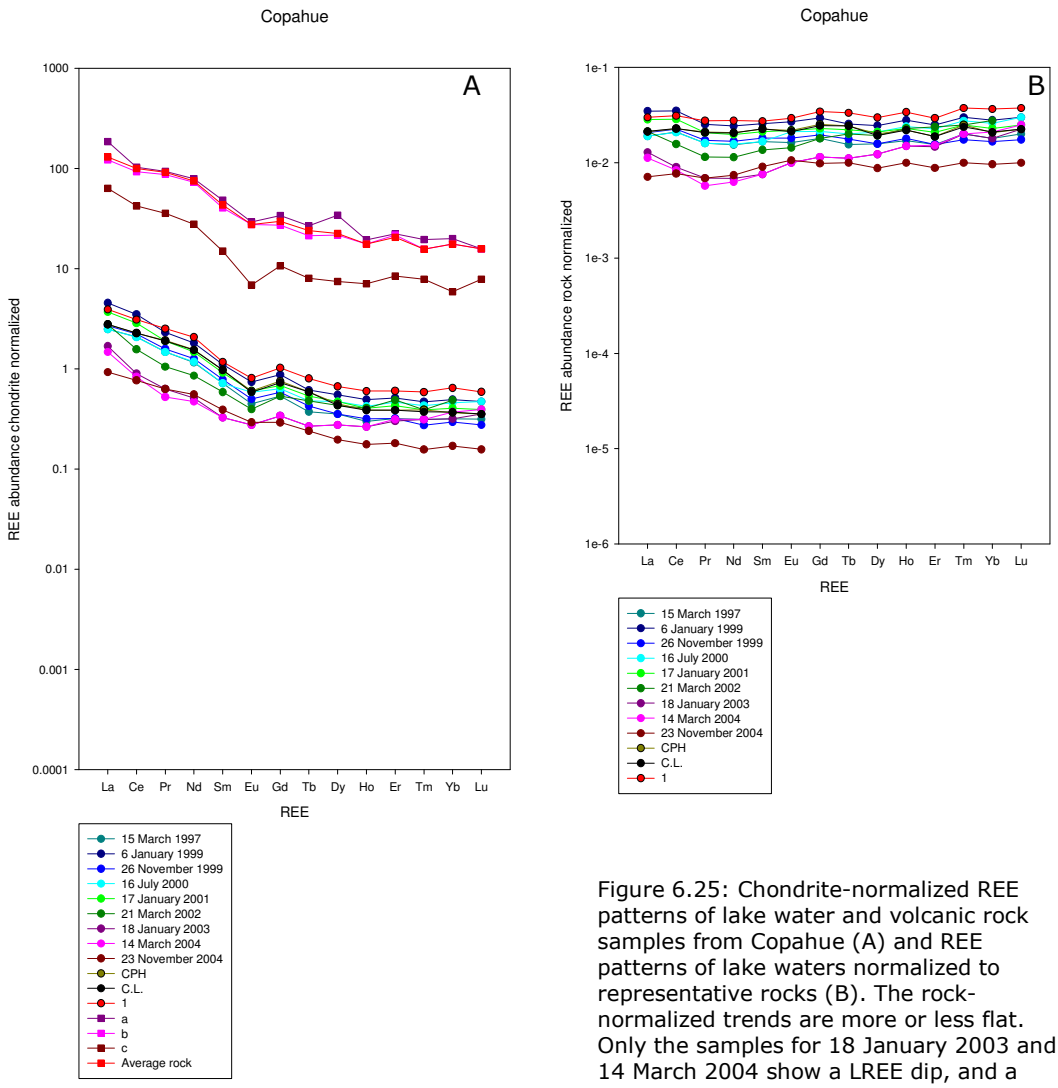

Figure 6.25: Chondrite-normalized REE patterns of lake water and volcanic rock samples from Copahue (A) and REE patterns of lake waters normalized to representative rocks (B). The rock-normalized trends are more or less flat. Only the samples for 18 January 2003 and 14 March 2004 show a LREE dip, and a steady increase towards HREE from Pr onwards. Note that a negative Eu anomaly is visible in the chondrite-normalized patterns of both the rocks and the waters. Data from Varekamp et al. (2009); Gammons et al. (2005); Takano et al. (2004).

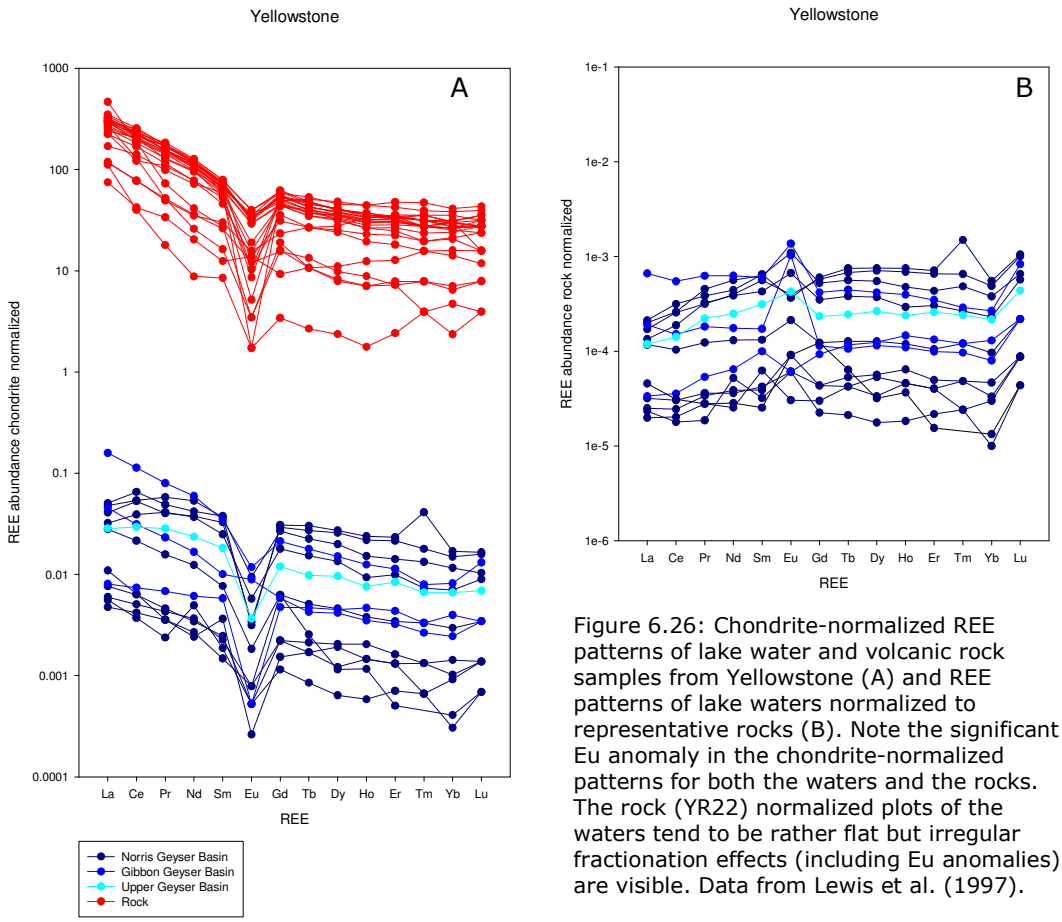

Figure 6.26: Chondrite-normalized REE patterns of lake water and volcanic rock samples from Yellowstone (A) and REE patterns of lake waters normalized to representative rocks (B). Note the significant Eu anomaly in the chondrite-normalized patterns for both the waters and the rocks. The rock (YR22) normalized plots of the waters tend to be rather flat but irregular fractionation effects (including Eu anomalies) are visible. Data from Lewis et al. (1997).

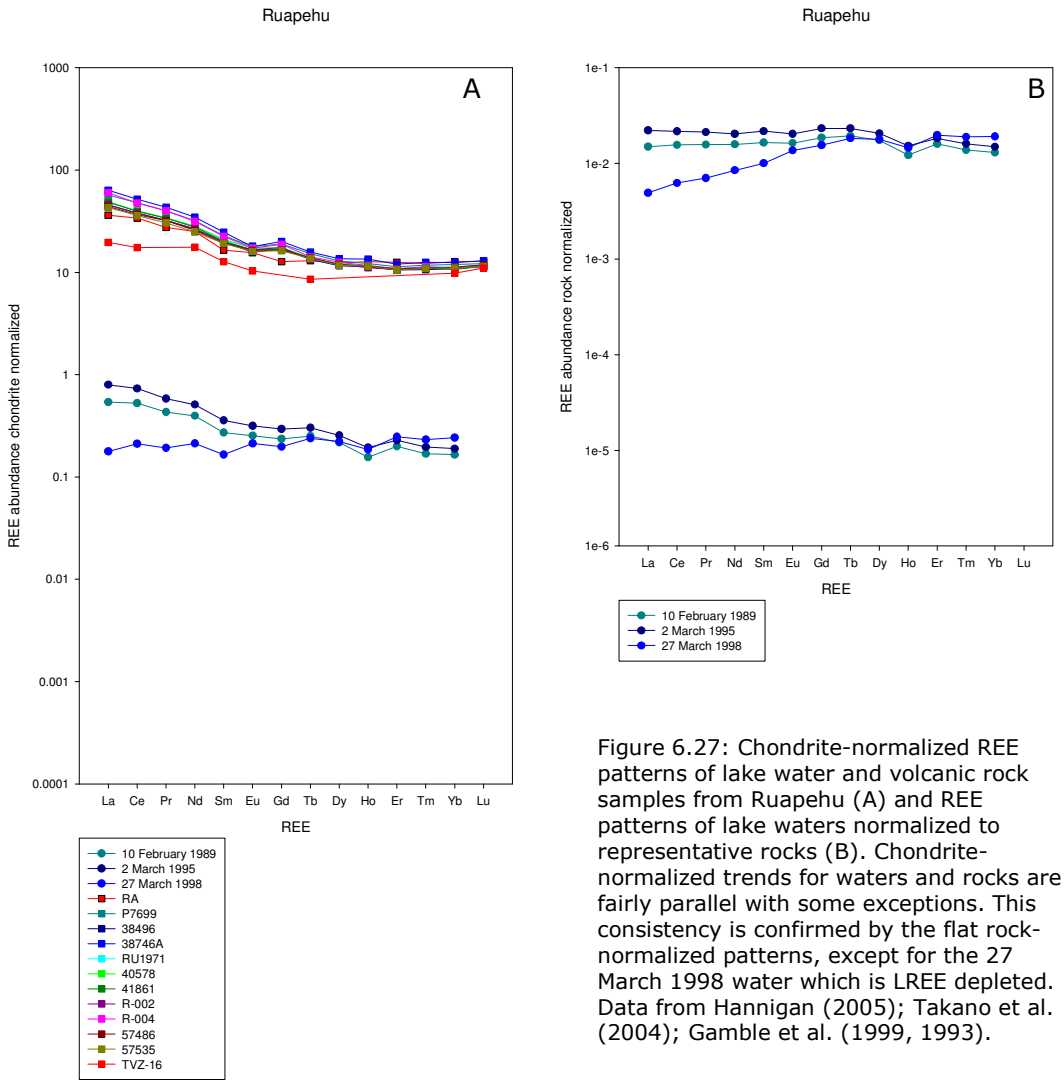

Figure 6.27: Chondrite-normalized REE patterns of lake water and volcanic rock samples from Ruapehu (A) and REE patterns of lake waters normalized to representative rocks (B). Chondrite-normalized trends for waters and rocks are fairly parallel with some exceptions. This consistency is confirmed by the flat rock-normalized patterns, except for the 27 March 1998 water which is LREE depleted. Data from Hannigan (2005); Takano et al. (2004); Gamble et al. (1999, 1993).

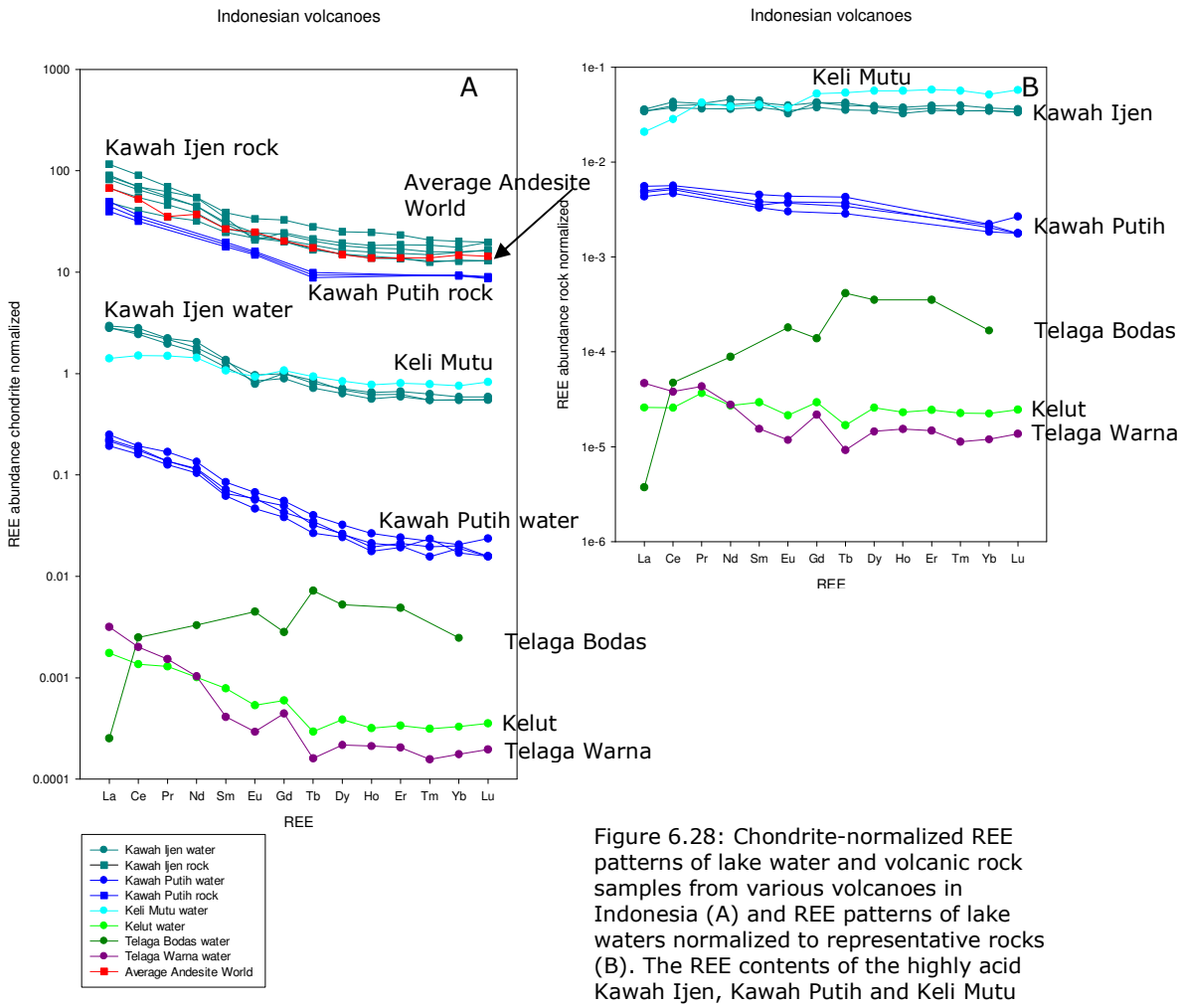

Figure 6.28: Chondrite-normalized REE patterns of lake water and volcanic rock samples from various volcanoes in Indonesia (A) and REE patterns of lake waters normalized to representative rocks (B). The REE contents of the highly acid Kawah Ijen, Kawah Putih and Keli Mutu lakes are higher than those of the other lakes which are less acid to near neutral. Concentrations of some elements in the latter can be close to detection limits which could partly explain their irregular patterns. The rock normalized patterns for Kawah Ijen are flat. The apparent LREE depletion for Keli Mutu could be a true feature or due to an inadequate choice of the normalizing rock. The Kawah Putih waters show a regular LREE over HREE enrichment. The rock-normalized trend for Kelut is rather flat, for Telaga Warna showing a slight LREE enrichment of Telaga Warna, and for Telaga Bodas a steep HREE enrichment, which may be unreliable because of the low concentrations and/or the use of an unrepresentative rock composition. The Gd anomaly is ignored. Data from the Geochemical Earth Reference Model (2011), Van Hinsberg et al (2010), Takano et al. (2004) (original Dy and Er data for Kawah Ijen multiplied by 10; Keli Mutu: Varekamp (2000, personal communication); Kelut and Telaga Warna: Apfelbeck (2000, personal communication)); Sriwana et al. (2000).

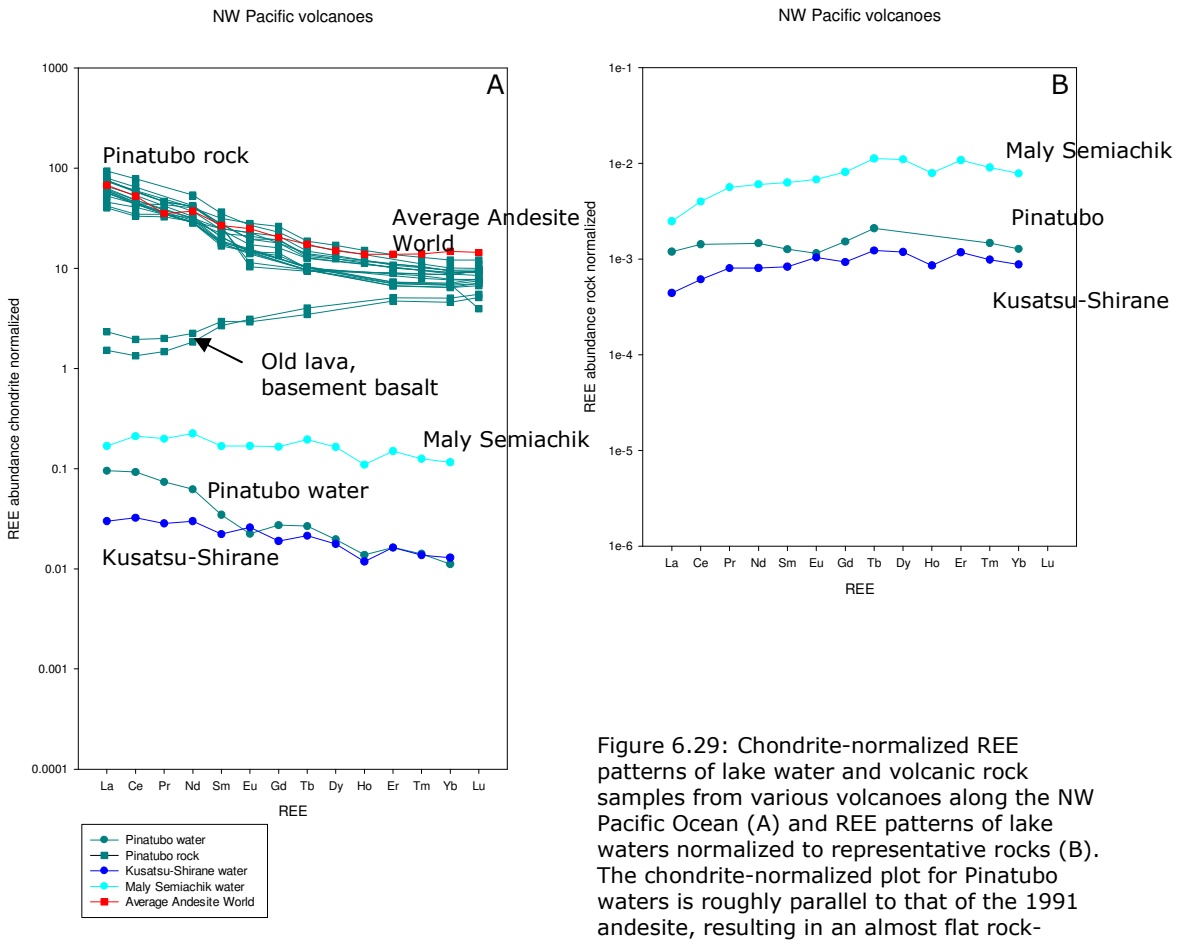

Figure 6.29: Chondrite-normalized REE patterns of lake water and volcanic rock samples from various volcanoes along the NW Pacific Ocean (A) and REE patterns of lake waters normalized to representative rocks (B). The chondrite-normalized plot for Pinatubo waters is roughly parallel to that of the 1991 andesite, resulting in an almost flat rock-normalized trend with only a slight LREE depletion and a small negative Eu anomaly. No rock data are available for Kusatsu-Shirane and Maly Semiachik. Their rock-normalized plots are based on average andesite, implying that the apparent slight LREE depletions must be interpreted with care. Data from the Geochemical Earth Reference Model (2011), Di Muro et al. (2008), Takano et al. (2004), Castillo and Punongbayan (1996), and Daag (1996).

6.5 Time related ratios and anomaly

Time-series for REE ratios and Eu anomalies are described here for selected volcanoes for which sufficient data are available. The Eu anomalies are expressed as Eu/Eu* (chondrite-normalized values) whereby Eu* was calculated as (2xEu)/(Sm+Gd).

Figure 6.30 shows the evolution of Eu anomalies in the lake waters of Poás with time, covering almost three decades. Although data for Stage II and the early part of Stage III are limited, there is a clear jump to lower Eu/Eu* values in the second half of the stage, following the eruptions of 1994. Since then, a steady increase is seen throughout Stages IV and V, followed by a sudden drop after November 2005, associated with eruptive activity in 2005.

The Ce/Yb ratios (figure 6.31) also show significant variations but they do not follow the systematics of the Eu anomalies. From 1995 on, a gradual fluctuation is seen, with lowest values corresponding to quiet intervals of the lake's activity (e.g., Substages C and E). Subsequently, following the eruptive activity in 2005, the Ce/Yb ratios steadily increase, reaching the highest values observed at Poás.

The La/Sm and Tb/Yb ratios (figures 6.32 and 6.33) tend to show variation patterns similar to Ce/Yb but with a different behaviour. There is a rough gradual decrease in La/Sm until 2006 with superimposed fluctuations, followed first by a steep increase and since mid-2007 by a more gradual decreasing trend. Variations in Tb/Yb ratios are also significant but are partly inverse to the La/Sm behaviour. A rough overall decrease since 1995 is followed by strong fluctuations culminating in a steady increase since the eruptive activity in 2006.

The Rincón de la Vieja samples (2004-2009) have fairly stable Eu/Eu* and Ce/Yb ratios. Both are relatively close to the ratios in the local rocks (figure 6.30 and 6.31).

The ratios for the El Chichón samples (1998 and 2006-2010) are variable, showing little systematic changes with time (figure 6.30 and 6.31). Values both higher and lower than the ratios in the rocks are observed.

The plots for Copahue (1997-2004, figures 6.30 and 6.31) show different behaviour before and after the eruption in 2000. Prior to the eruption, the Ce/Yb ratio was higher than that of the local rocks, whereas after the eruption it was lower. Systematics are less clear for the Eu anomaly, but before the eruption all values were lower than the rocks and several were higher after the eruption started

The available Ruapehu data (1989-1998) tend to show similar behaviour (figures 6.30 and 6.31), although they are limited and represent infrequent sampling. Before the 1995 eruption, the Ce/Yb ratios were higher than the reference rock and after the eruption lower. Likewise, the Eu anomaly shifted from slightly lower to slightly higher than that of the rock.

Poás

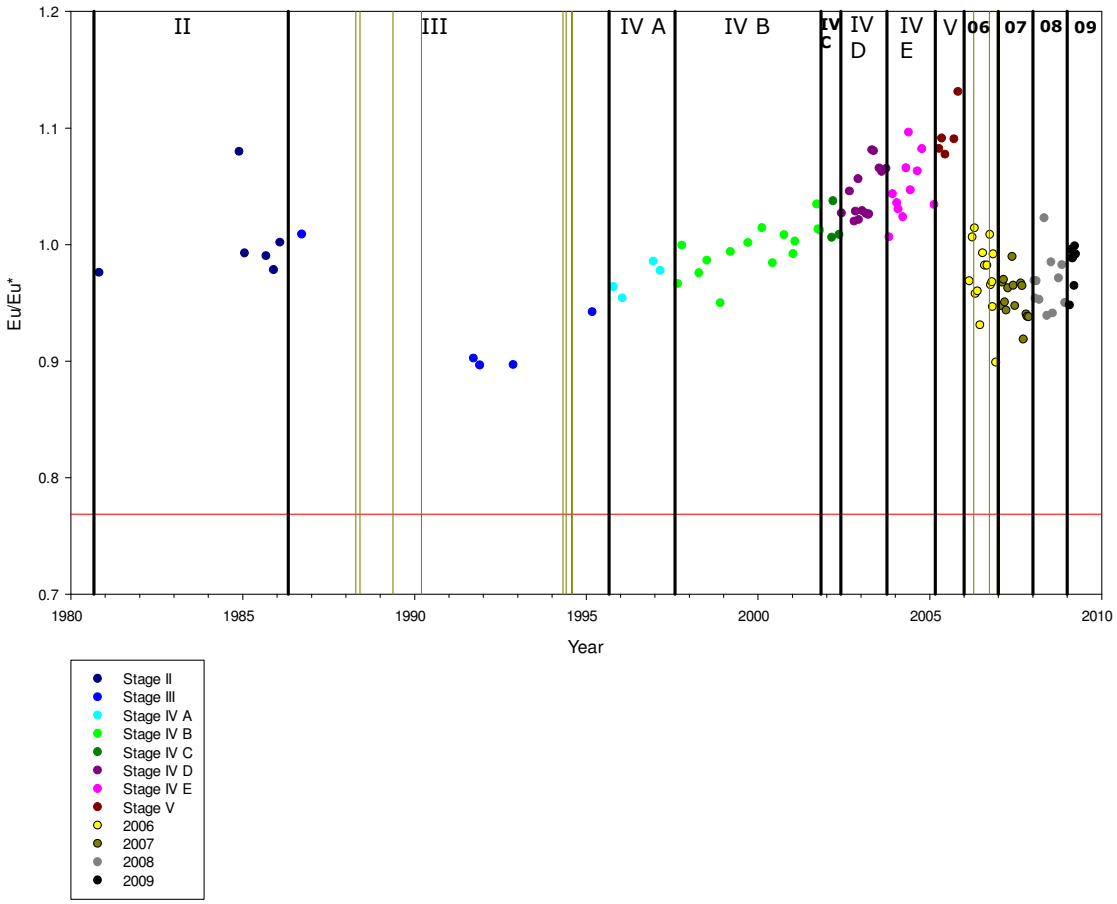

Rincón de la Vieja

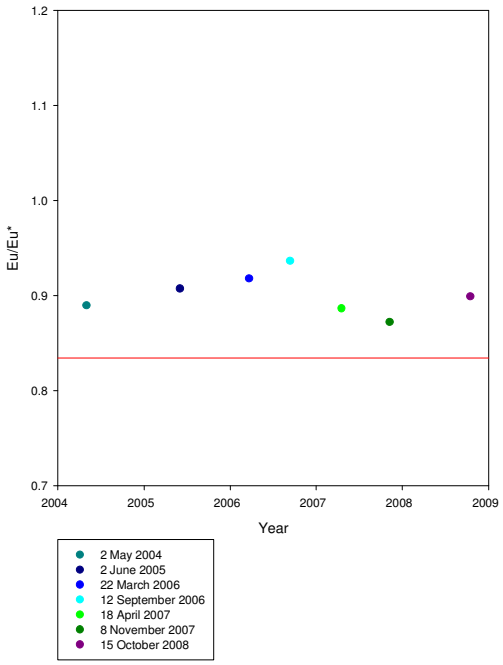

El Chichón

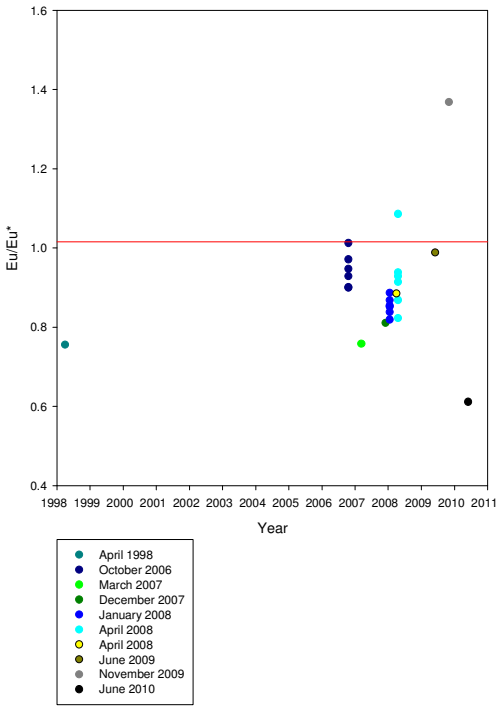

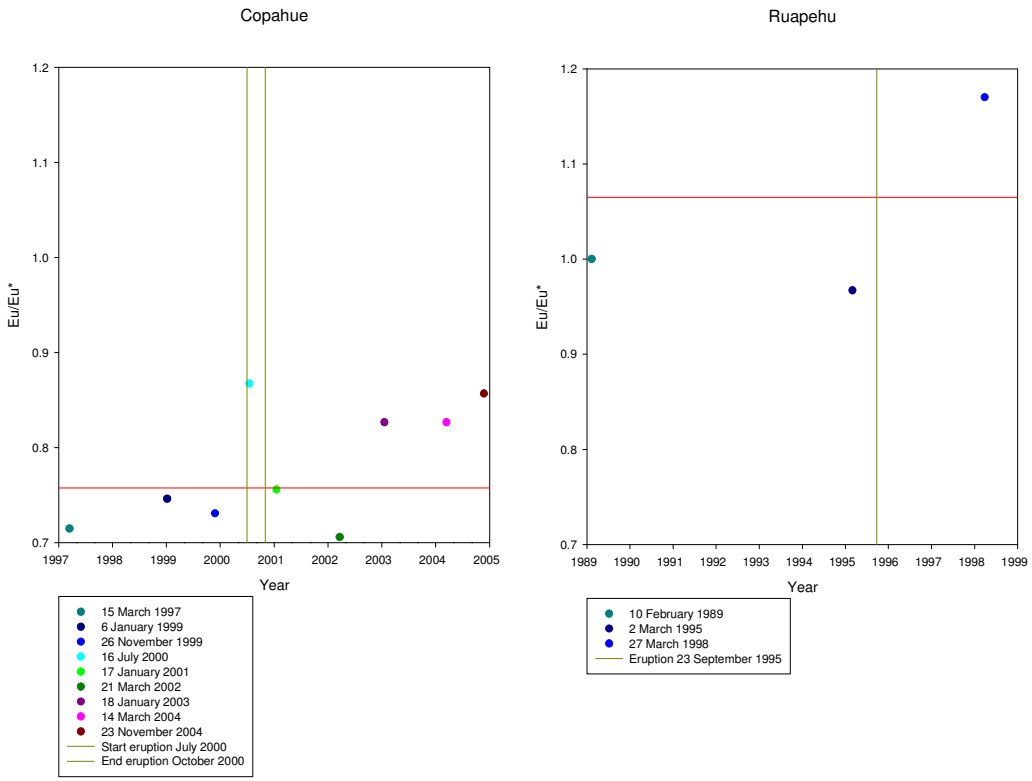

Figure 6.30: Time-series trends of Eu anomalies (expressed as Eu/Eu*, chondrite normalized) for the lake water of Poás. Intervals represent stages as defined by Martínez (2008) and calendar years since 2006. Thin vertical lines indicate phreatic eruptions and the red horizontal line shows a composition taken to represent the local rocks. Data from appendices A and B, Martínez (2008) and Prosser and Carr (1987). The trend of the water samples of Rincón de la Vieja changes from increase to decrease between 12 September 2006 and 18 April 2007. Sample 15 October 2008 suggests an increase again. There is no eruption during the plotted years. Data from appendix A and Soto et al. (2003). Both Poás and Rincón de la Vieja show water higher than rock samples. The El Chichón plot shows a lot of scatter even within the same dataset. Data from Peiffer et al. (2011); Morton-Bermea et al. (2010) and Taran et al. (2008). Both Copahue and Ruapehu show a higher than rock value after the eruption and a lower than rock value before the eruption. Data from Varekamp et al. (2009) and Gammons et al. (2005); Hannigan (2005); Takano et al. (2004) and Gamble et al. (1999).

Poás

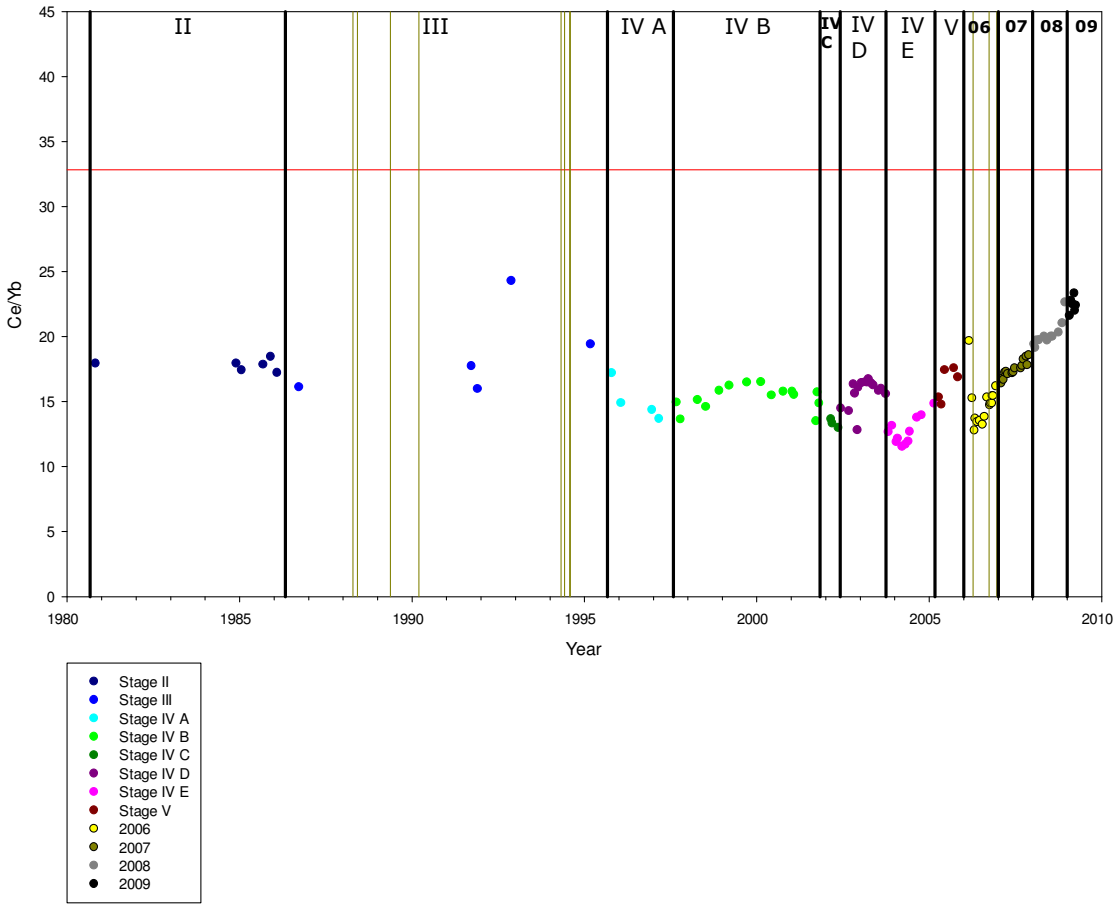

Rincón de la Vieja

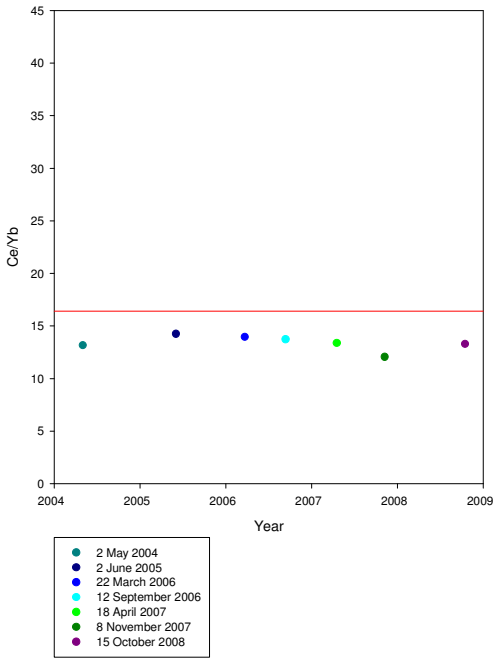

El Chichón

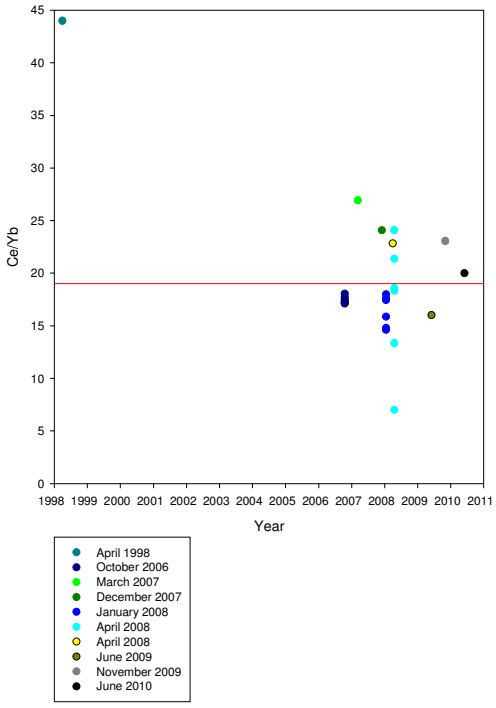

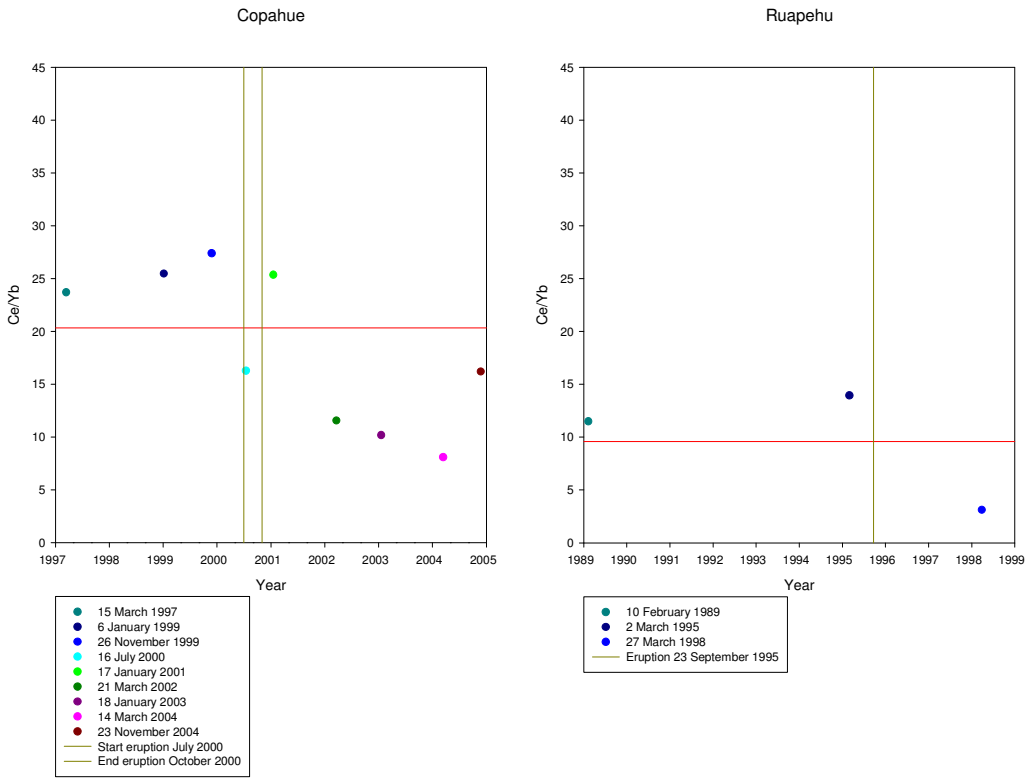

Figure 6.31: Time-series trends of Ce/Yb ratios for the lake water of Poás, indicating the degree of enrichment of LREE over HREE. Intervals represent stages as defined by Martínez (2008) and calendar years since 2006. Thin vertical lines indicate phreatic eruptions and the red horizontal line shows a composition taken to represent the local rocks. Data from appendices A and B, Martínez (2008) and Prosser and Carr (1987). Rincón de la Vieja shows in general a flat pattern with a dip on 2 May 2004 and on 8 November 2007. Like Poás, all data are below rock. Data from appendix A and Soto et al. (2003). The El Chichón plot shows a lot of scatter even within the same dataset. Data from Peiffer et al. (2011); Morton-Bermea et al. (2010) and Taran et al. (2008). Both Copahue and Ruapehu show a lower than rock value after the eruption and a higher than rock value before the eruption. Data from Varekamp et al. (2009); Gammons et al. (2005); Hannigan (2005); Takano et al. (2004) and Gamble et al. (1999).

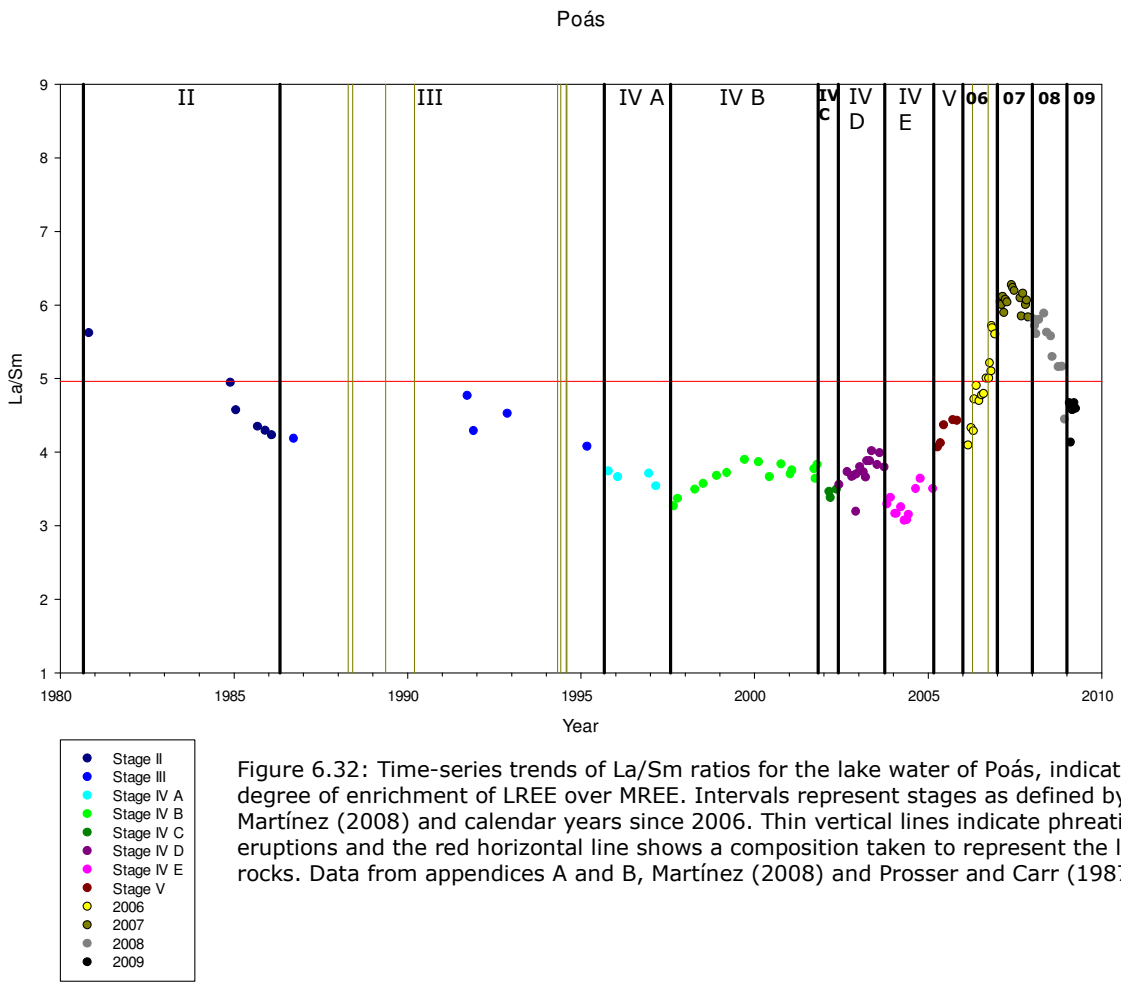

Figure 6.32: Time-series trends of La/Sm ratios for the lake water of Poás, indicating the degree of enrichment of LREE over MREE. Intervals represent stages as defined by Martínez (2008) and calendar years since 2006. Thin vertical lines indicate phreatic eruptions and the red horizontal line shows a composition taken to represent the local rocks. Data from appendices A and B, Martínez (2008) and Prosser and Carr (1987).

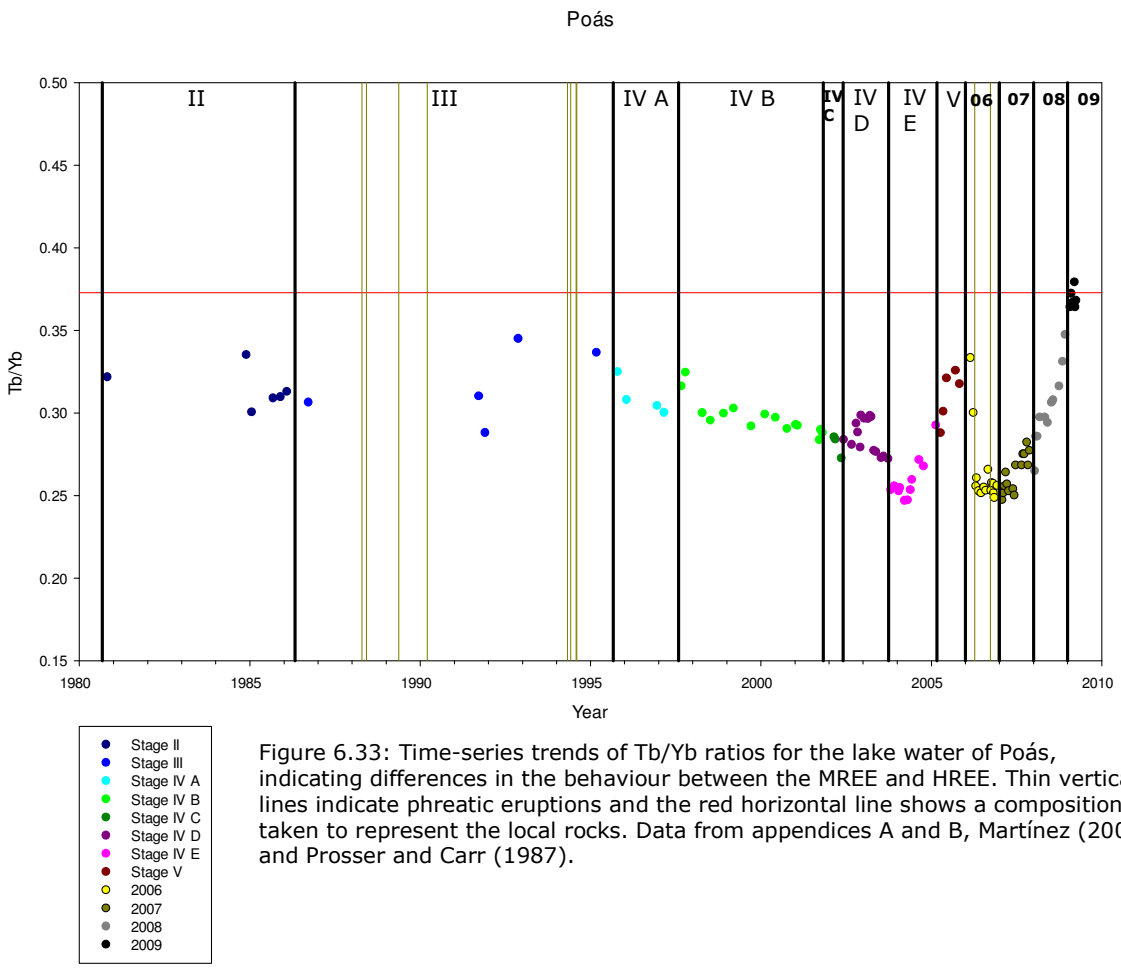

Figure 6.33: Time-series trends of Tb/Yb ratios for the lake water of Poás, indicating differences in the behaviour between the MREE and HREE. Thin vertical lines indicate phreatic eruptions and the red horizontal line shows a composition taken to represent the local rocks. Data from appendices A and B, Martínez (2008) and Prosser and Carr (1987).

7. Speciation modelling

The PHREEQC routine (version 2.17) has been used to explore the saturation state of minerals and the nature of prevailing dissolved species. The scope of the modelling is the REE behaviour. The two subchapters below treat the minerals (7.1) and the dissolved species (7.2). Each stage of the lake evolution is represented by a sample that is considered to reflect the average REE behaviour of that period. The selection was made on the basis of the second plot in figure 6.19 showing representative samples for each stage. Because of the internal scatter, two different samples were used for stage III as no useable average would be valid to describe the REE behaviour during this high-activity interval.

The tables below list the selected samples (table 7.1). These samples are not the same as the samples Martínez (2008) used to model. Another difference is that Martínez (2008) used SOLVEQ to model and in this thesis uses PHREEQC 2.17.

Stage	**Sample**
II	September 1985
III (highest REE)	November 1992
III (lowest REE)	March 1995
IV A	March 1997
IV D	February 2003
2006	August 2006

Table 7.1: Selected representative samples for the different stages

7.1 Saturation indices

The PHREEQC 2.17 routine has been used to construct the plots below, that predict if and under which conditions relevant minerals will be saturated in the lake or in the subsurface hydrothermal system below it. Eight minerals have been taken into account. They are alunite ($KAl_3(OH)_6(SO_4)_2$), anhydrite ($CaSO_4$), diaspore ($AlHO_2$), kaolinite ($Al_2Si_2O_5(OH)_4$), pyrophyllite ($Al_2Si_4O_{10}(OH)_2$), quartz (SiO_2), amorphous silica (SiO_2), and native sulphur (S).

Figures 7.1-7.6 show plots of the saturation state (expressed as log Q/K) as a function of temperature (up to 300°C) for three different pH values. One is the measured pH, two others (pH=-0.85 and pH=1.75) were arbitrarily adopted to explore the influence of pH.

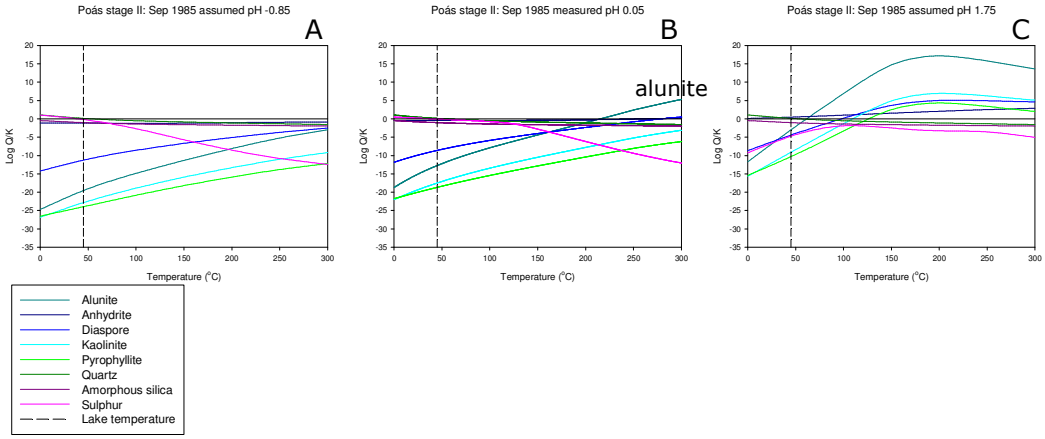

Figure 7.1: Saturation states for relevant mineral phases (expressed as log Q/K) as a function of temperature in three pH scenarios, valid for the sample of September 1985 (Stage II). At the measured temperature (45°C) and pH (0.05) quartz, anhydrite, amorphous silica and sulphur are close to saturation (panel B). Temperature has little influence on the saturation state of these minerals. In contrast, the Log Q/K values for alunite, diaspore, kaolinite and pyrophyllite increase with increasing temperature, whereas the value for sulphur decreases. Except for the latter, these minerals are undersaturated at the measured lake temperature but their trends indicate that alunite will be oversaturated from 200°C onwards and that diaspore might become saturated at the highest end of the investigated temperature range. The plot for lowered pH conditions (panel A) does not show much difference, except that alunite and diaspore do not reach saturation.
The effect of increasing the pH is modest for quartz, anhydrite and amorphous silica (panel C), but oversaturation of alunite, diaspore, kaolinite, pyrophyllite is reached at much lower temperatures than in scenario B. At the adopted pH (1.75) and measured temperature, quartz is close to saturation.

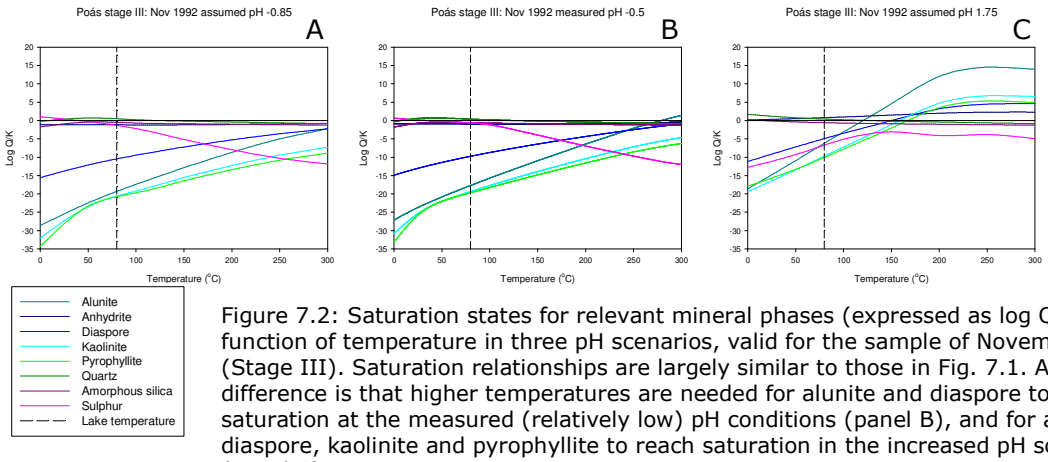

Figure 7.2: Saturation states for relevant mineral phases (expressed as log Q/K) as a function of temperature in three pH scenarios, valid for the sample of November 1992 (Stage III). Saturation relationships are largely similar to those in Fig. 7.1. A notable difference is that higher temperatures are needed for alunite and diaspore to reach saturation at the measured (relatively low) pH conditions (panel B), and for alunite, diaspore, kaolinite and pyrophyllite to reach saturation in the increased pH scenario (panel C).

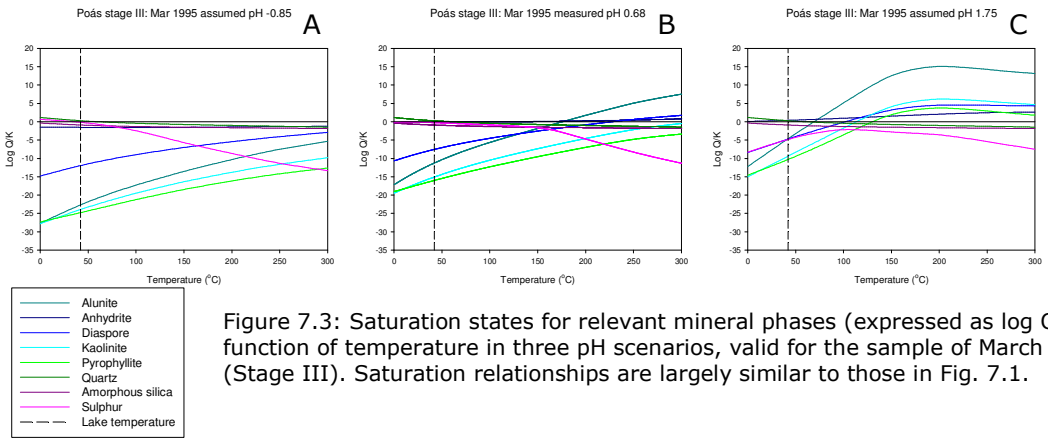

Figure 7.3: Saturation states for relevant mineral phases (expressed as log Q/K) as a function of temperature in three pH scenarios, valid for the sample of March 1995 (Stage III). Saturation relationships are largely similar to those in Fig. 7.1.

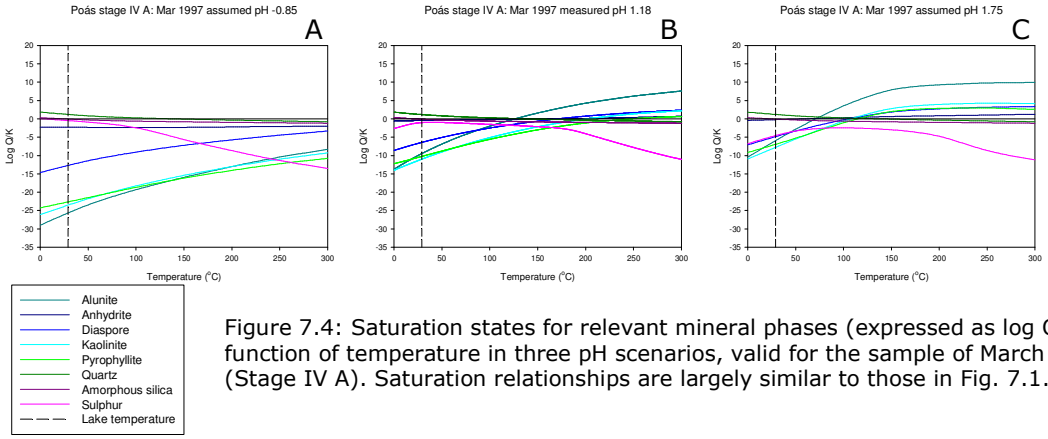

Figure 7.4: Saturation states for relevant mineral phases (expressed as log Q/K) as a function of temperature in three pH scenarios, valid for the sample of March 1997 (Stage IV A). Saturation relationships are largely similar to those in Fig. 7.1.

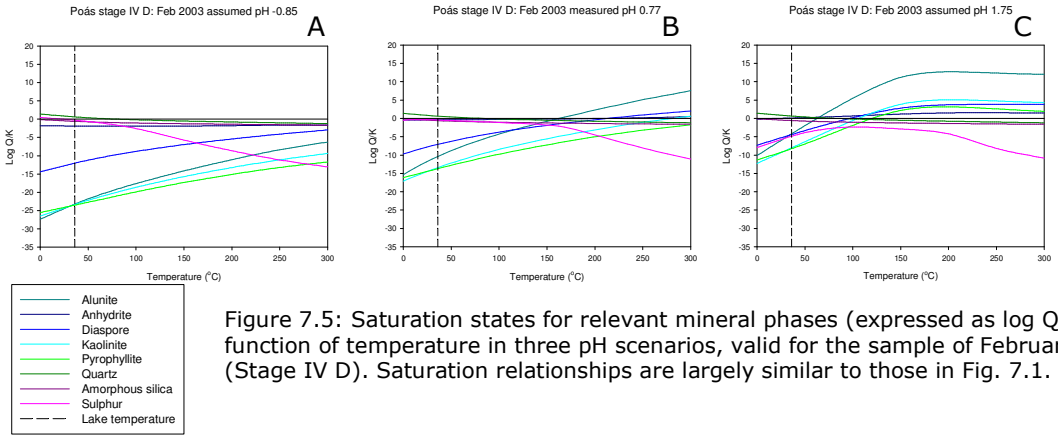

Figure 7.5: Saturation states for relevant mineral phases (expressed as log Q/K) as a function of temperature in three pH scenarios, valid for the sample of February 2003 (Stage IV D). Saturation relationships are largely similar to those in Fig. 7.1.

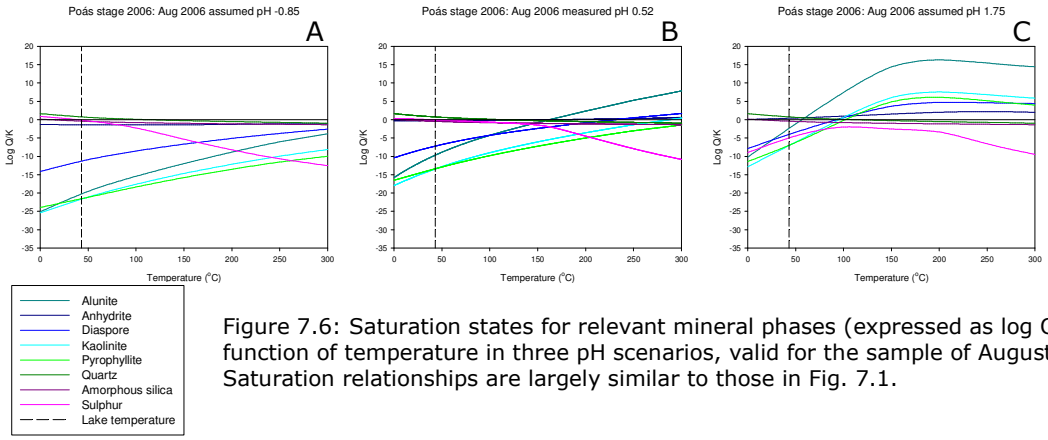

Figure 7.6: Saturation states for relevant mineral phases (expressed as log Q/K) as a function of temperature in three pH scenarios, valid for the sample of August 2006. Saturation relationships are largely similar to those in Fig. 7.1.

In summary, at measured temperature and pH values (B panels), the crater lake waters show quartz, anhydrite, amorphous silica and sulphur being close to saturation or slightly undersaturated. At lowered pH values (A panels) similar systematics are valid, but none of the minerals reaches saturation at higher temperatures. The saturation state of alunite steadily increases with temperature so that oversaturation is reached, which starts at temperatures varying between 125 and 300°C, being always much higher than the measured lake temperature. Alunite is the only mineral that reaches strong oversaturation (at elevated temperatures), except for the November 1992 sample (Stage III) for which oversaturation starts at 300°C. Anhydrite remains saturated or slightly undersaturated over the whole temperature range. Log Q/K values of diaspore steadily increase like those of alunite, but at a slower rate, so that it becomes

slightly oversaturated at higher temperatures (except for the November 1992 sample). All other investigated minerals remain slightly to highly undersaturated at the high-temperature end of the plots. Quartz and amorphous silica are in general slightly undersaturated, and pyrophyllite and kaolinite highly undersaturated. The August 2006 sample shows a slight kaolinite oversaturation.

The plots valid for the adopted pH values of 1.75 (C panels) show that minerals become oversaturated at lower temperatures than is observed for the measured pH conditions. Again alunite stands out because this mineral becomes saturated at lower temperatures than other minerals and reaches the highest degree of oversaturation when temperature increases. Alunite, diaspore (except for November 1992), kaolinite and pyrophyllite tend to show a maximum in the saturation curve at approximately 200°C (250°C for the November 1992 sample). Anhydrite (and diaspore in November 1992) is the only mineral that shows a continuously increasing trend. The anhydrite curve is steeper for the C than for the B scenarios. Quartz and amorphous silica are always slightly undersaturated or close to saturation, whereas the curves for sulphur indicate a strong undersaturation at high temperatures in the A and B scenarios, and a maximum that approaches saturation in the C scenarios. In general, the saturation trends valid for the November 1992 sample (Stage III) deviate most from the other curves.

7.2 REE speciation

The REE in the lake water will be distributed among different dissolved species, the presence and proportions of which depend on the water composition, temperature and pH. Speciation modelling using PHREEQC 2.17 was performed to investigate the distribution of REE species for different scenarios using the same selection of samples as taken for the mineral saturation calculations described above. The same different pH conditions were adopted to model the distribution of REE species as a function of temperature. In this way, the REE speciation is explored not only for the observed lake conditions but also at the higher temperatures that are more consistent with subsurface conditions in the hydrothermal system below the lake. Lanthanum, europium and ytterbium were taken to represent the light, middle and heavy REE, respectively. Figures 7.7-7.30 illustrate the results.

7.2.1 La species

The species of lanthanum are taken to represent all LREE, although in detail differences among the LREE may exist. For example, part of the dissolved lanthanum is present as $LaSO_4^+$, but this sulphate species was not detected for cerium. The distribution of La species shows a strong variation with temperature. At measured temperatures and pH conditions $LaSO_4^+$, La^{3+}, $LaCl_2^+$ are usually the dominant species but their proportions change with changing lake conditions. This is illustrated by the stage II sample (T=45°C), which shows the distribution $LaSO_4^+ > La^{3+} > LaCl^{2+}$, and by the stage III sample of November 1992 (T=80°C), which shows $LaCl^{2+}$ as the most abundant species. In general, it can be seen that increasing temperatures lead to a decrease in importance of $LaSO_4^+$ and an increase in importance of $LaCl^{2+}$. Lowering the pH ("A" scenarios) suppresses $LaSO_4^+$ and increases the importance of La^{3+}, whereas the reversed case is seen when increasing the pH ("C" scenarios).

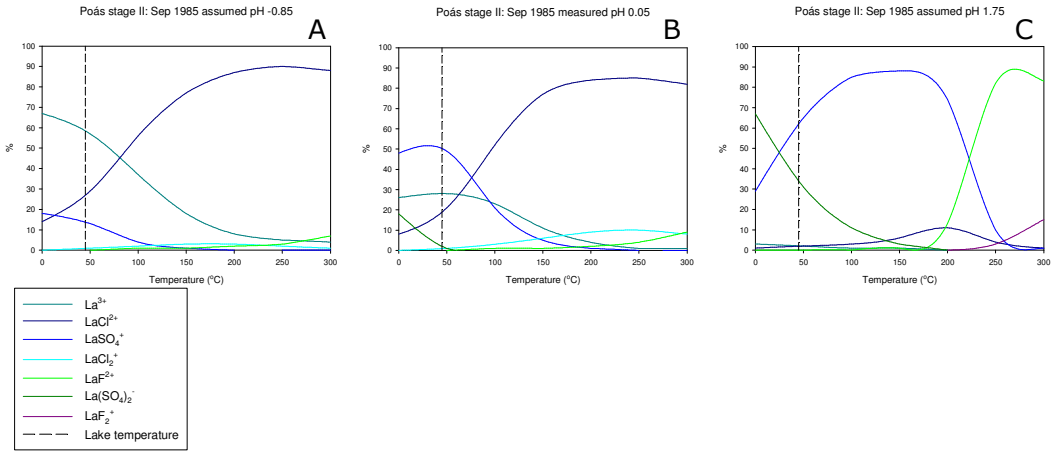

Figure 7.7: La species distributions in three scenarios for the sample of September 1985 (Stage II). At the measured temperature (45°C) and pH (0.05) $LaSO_4^+$, La^{3+}, $LaCl^{2+}$ are the main species (panel B). At lower pH (panel A) the same species are important, but their proportions are different. In both scenarios $LaCl^{2+}$ gradually increases with temperature and becomes the main species when temperatures are high. At the assumed pH 1.75 (panel C) a different behaviour is seen, because $La(SO_4)_2^-$ is an important species at the measured lake temperature (in contrast to the A and B scenarios) and $LaSO_4^+$ has a peak at around 150°C. The latter is replaced by LaF^{2+} as the main species when temperatures become higher than 220°C.

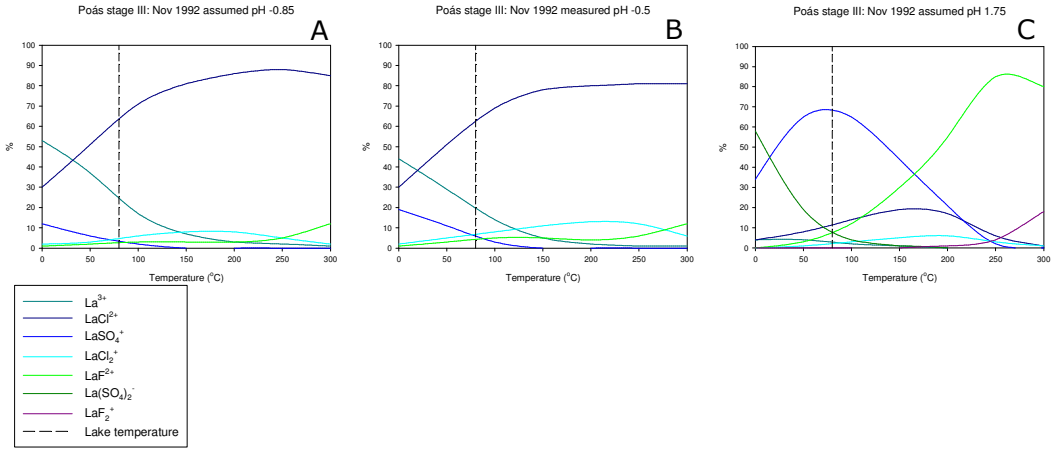

Figure 7.8: La species distributions in three scenarios for the sample of November 1992 (Stage III). At the measured temperature (80°C) and pH (-0.5) $LaCl^{2+}$ and La^{3+} are the main species (panel B). At lower pH (panel A) the same species are important and their proportions remain roughly the same, with $LaCl^{2+}$ being dominant. For higher temperatures (panel B) the share of $LaCl^{2+}$ remains more or less stable. At the assumed pH value of 1.75 (panel C) this species shows a maximum around 150°C, but it is subordinate to $LaSO_4^+$ and LaF^{2+} in importance. In all three scenarios, $LaCl_2^+$ is fairly significant though less abundant than other species, showing a maximum around 200°C. Panel C shows an increase of LaF^{2+} at high temperatures.

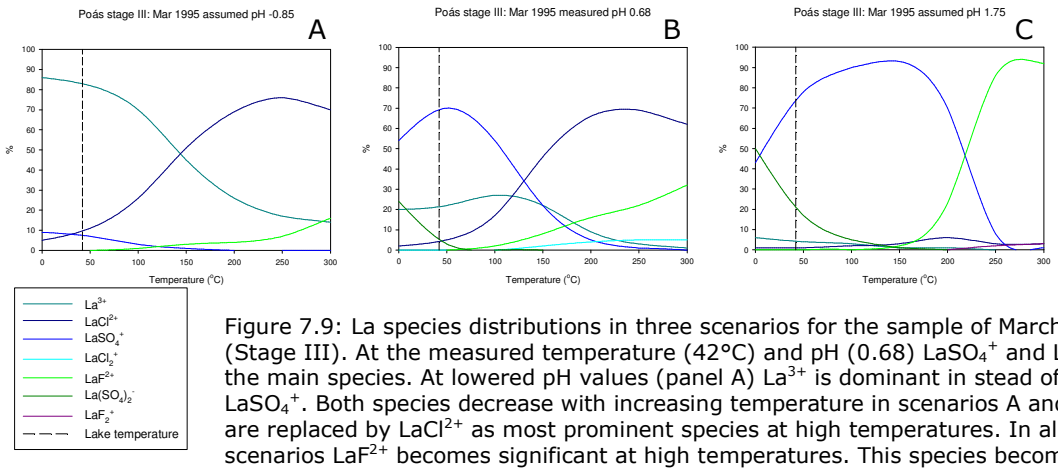

Figure 7.9: La species distributions in three scenarios for the sample of March 1995 (Stage III). At the measured temperature (42°C) and pH (0.68) $LaSO_4^+$ and La^{3+} are the main species. At lowered pH values (panel A) La^{3+} is dominant in stead of $LaSO_4^+$. Both species decrease with increasing temperature in scenarios A and B, and are replaced by $LaCl^{2+}$ as most prominent species at high temperatures. In all three scenarios LaF^{2+} becomes significant at high temperatures. This species becomes even dominant at higher assumed pH values (scenario C), taking the place of $LaSO_4^+$ as most abundant species when temperatures are high.

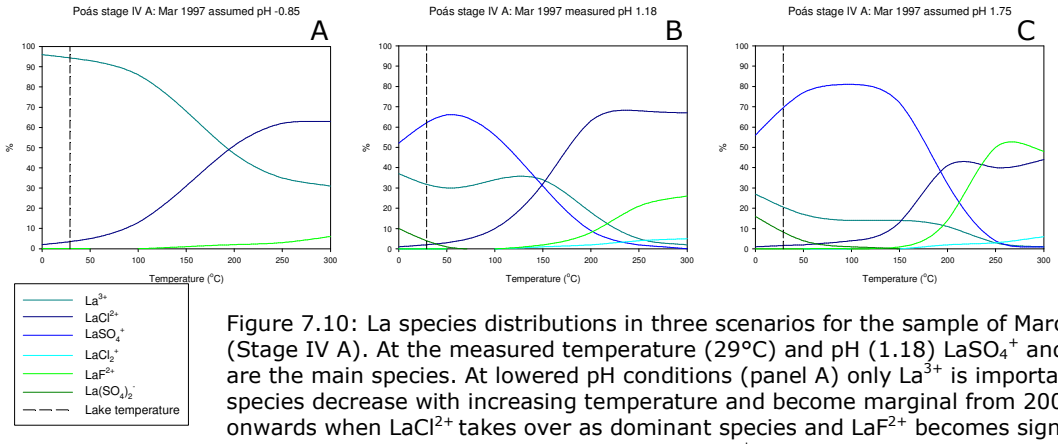

Figure 7.10: La species distributions in three scenarios for the sample of March 1997 (Stage IV A). At the measured temperature (29°C) and pH (1.18) $LaSO_4^+$ and La^{3+} are the main species. At lowered pH conditions (panel A) only La^{3+} is important. Both species decrease with increasing temperature and become marginal from 200-225°C onwards when $LaCl^{2+}$ takes over as dominant species and LaF^{2+} becomes significant as well. For elevated pH values (panel C) $LaSO_4^+$ is dominant at low temperatures, whereas $LaCl^{2+}$ and LaF^{2+} are most important at high temperatures.

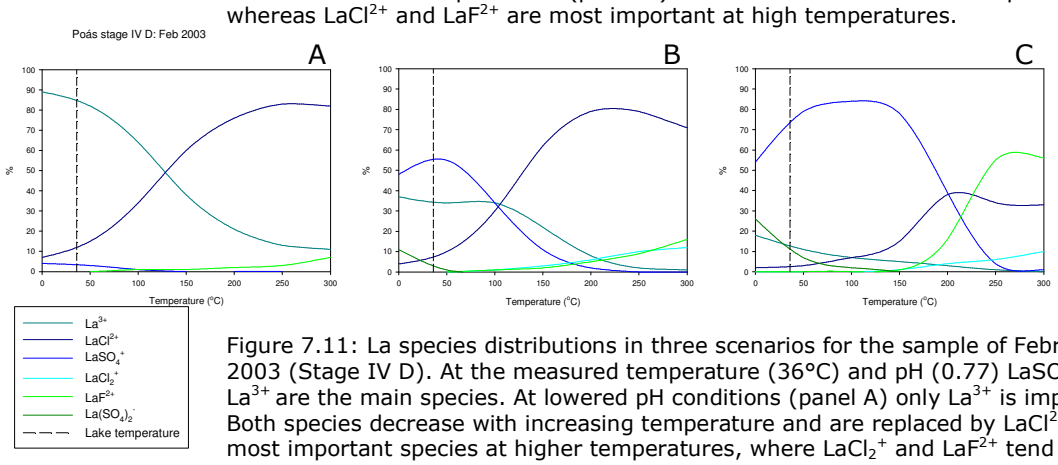

Figure 7.11: La species distributions in three scenarios for the sample of February 2003 (Stage IV D). At the measured temperature (36°C) and pH (0.77) $LaSO_4^+$ and La^{3+} are the main species. At lowered pH conditions (panel A) only La^{3+} is important. Both species decrease with increasing temperature and are replaced by $LaCl^{2+}$ as most important species at higher temperatures, where $LaCl_2^+$ and LaF^{2+} tend to become significant as well. For the more elevated pH conditions (panel C) $LaSO_4^+$ is the only relevant species at lower temperatures, while $LaCl^{2+}$ and LaF^{2+} become important at higher temperatures.

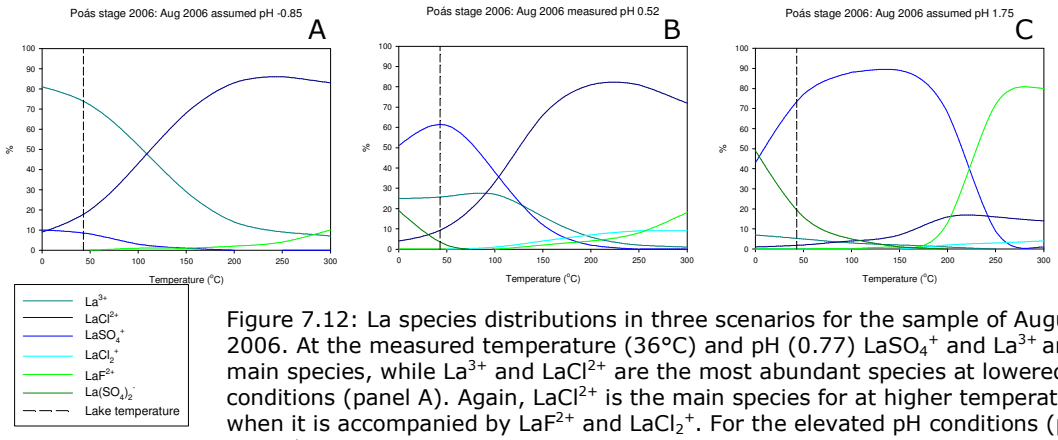

Figure 7.12: La species distributions in three scenarios for the sample of August 2006. At the measured temperature (36°C) and pH (0.77) $LaSO_4^+$ and La^{3+} are the main species, while La^{3+} and $LaCl^{2+}$ are the most abundant species at lowered pH conditions (panel A). Again, $LaCl^{2+}$ is the main species for at higher temperatures when it is accompanied by LaF^{2+} and $LaCl_2^+$. For the elevated pH conditions (panel C) $LaSO_4^+$ is again prominent at low temperatures (when it is accompanied by $La(SO_4)_2^-$), whereas LaF^{2+} is important at high temperatures.

In summary:

Except for the extreme conditions (September 1985 and November 1992) $LaSO_4^+$ and La^{3+} are the most prominent species at the temperature and pH conditions of the lake as measured during sampling. These species may be accompanied by modest abundances of $LaCl_2^+$ and/or $La(SO_4)_2^-$. Gradually increasing the temperatures to values higher than the measured one results in a distribution whereby $LaCl_2^+$ eventually becomes the dominant species. At the highest temperatures, LaF^{2+} and $LaCl_2^+$ appear as significant species as well.

The effect of lowering the pH relative to the measured values (pH=-0.85 scenarios) is that La^{3+} will be the only dominant species and that $LaSO_4^+$ is significantly reduced. This picture is valid for the measured temperatures. Increasing the temperature will decrease the importance of La^{3+} and increase the importance of $LaCl_2^+$, roughly following the same pattern as seen in the scenarios for the measured pH values.
The effect of increasing the pH relative to the measured values (pH=1.75 scenarios) is that La^{3+} becomes significantly reduced in importance and that $La(SO_4)_2^-$ becomes an additional species accompanying $LaSO_4^+$. Increasing the temperature for these elevated pH scenarios shows that LaF^{2+} eventually may replace $LaSO_4^+$ as most prominent species.

7.2.2 Eu species

The Eu species may be particularly relevant because of the possible presence of a Eu anomaly indicating that the behaviour of this element is different from the other REE. The behaviour of the Eu species was explored for the same samples and scenarios as mentioned above for La.

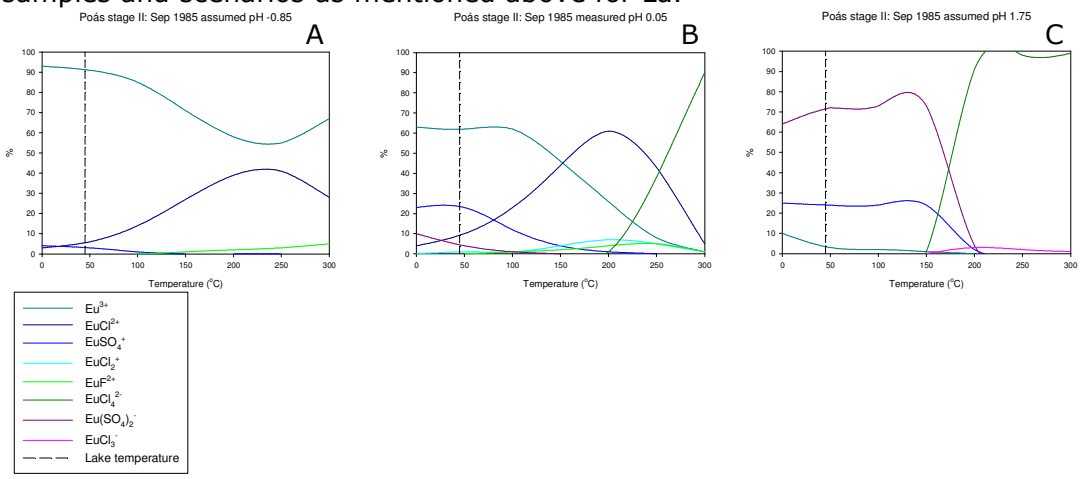

Figure 7.13: Eu species distributions in three scenarios for the sample of September 1985 (Stage II). At the measured temperature (45°C) and pH (0.05) Eu^{3+} and $EuSO_4^+$ are the main species (panel B). At lowered pH conditions (panel A) only Eu^{3+} is important. In both cases the $EuCl^{2+}$ species becomes important at increasing temperature. In the "B" scenario it reaches a peak and is the dominant species around 200°C, whereas at higher temperatures $EuCl_4^{2-}$ takes over. In the "A" scenario the $EuCl^{2+}$ peak is reached at about 240°C, but it remains subordinate to Eu^{3+}. At elevated pH conditions (panel C) $Eu(SO_4)_2^-$ is the most abundant species for the measured lake temperature, whereas $EuCl_4^{2-}$ is dominant at increased temperatures

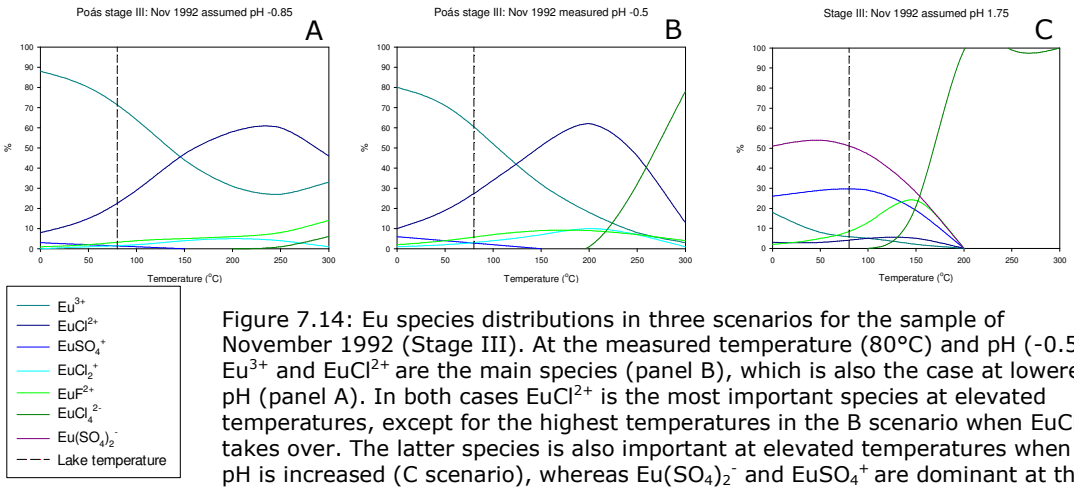

Figure 7.14: Eu species distributions in three scenarios for the sample of November 1992 (Stage III). At the measured temperature (80°C) and pH (-0.5) Eu^{3+} and $EuCl^{2+}$ are the main species (panel B), which is also the case at lowered pH (panel A). In both cases $EuCl^{2+}$ is the most important species at elevated temperatures, except for the highest temperatures in the B scenario when $EuCl_4^{2-}$ takes over. The latter species is also important at elevated temperatures when the pH is increased (C scenario), whereas $Eu(SO_4)_2^-$ and $EuSO_4^+$ are dominant at the measured crater lake temperature.

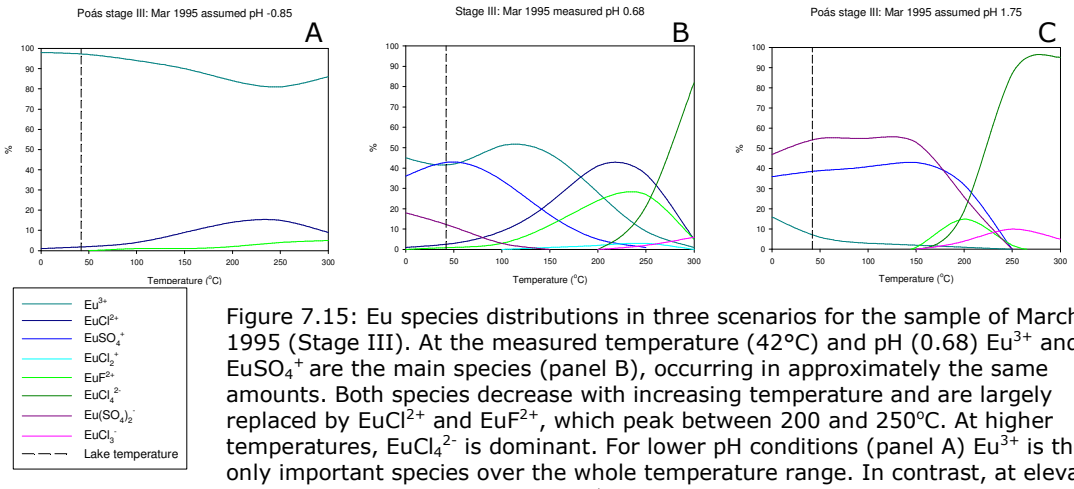

Figure 7.15: Eu species distributions in three scenarios for the sample of March 1995 (Stage III). At the measured temperature (42°C) and pH (0.68) Eu^{3+} and $EuSO_4^+$ are the main species (panel B), occurring in approximately the same amounts. Both species decrease with increasing temperature and are largely replaced by $EuCl^{2+}$ and EuF^{2+}, which peak between 200 and 250°C. At higher temperatures, $EuCl_4^{2-}$ is dominant. For lower pH conditions (panel A) Eu^{3+} is the only important species over the whole temperature range. In contrast, at elevated pH (C panel) $Eu(SO_4)_2^-$ and $EuSO_4^+$ are prominent at the measured lake temperature, and $EuCl_4^{2-}$ at more elevated temperatures.

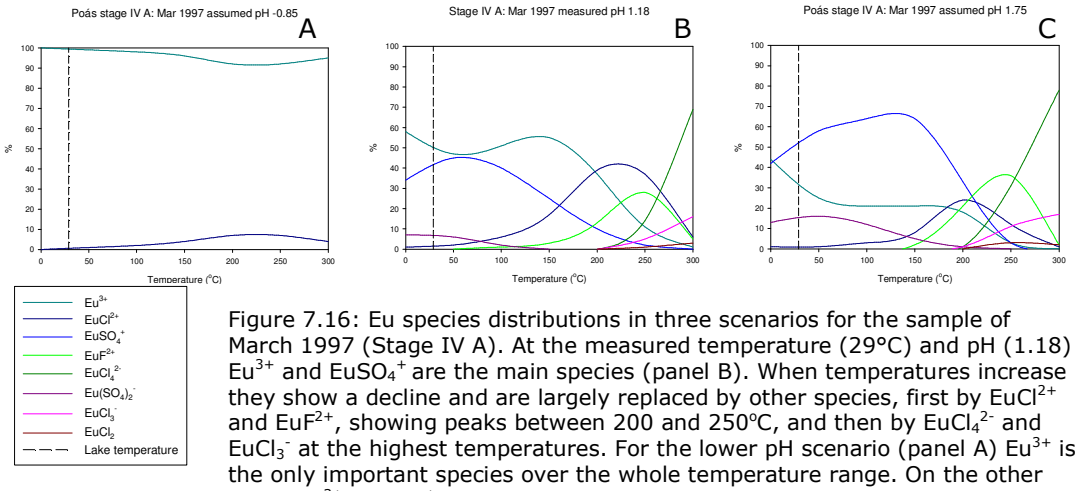

Figure 7.16: Eu species distributions in three scenarios for the sample of March 1997 (Stage IV A). At the measured temperature (29°C) and pH (1.18) Eu^{3+} and $EuSO_4^+$ are the main species (panel B). When temperatures increase they show a decline and are largely replaced by other species, first by $EuCl^{2+}$ and EuF^{2+}, showing peaks between 200 and 250°C, and then by $EuCl_4^{2-}$ and $EuCl_3^-$ at the highest temperatures. For the lower pH scenario (panel A) Eu^{3+} is the only important species over the whole temperature range. On the other hand, Eu^{3+}, $EuSO_4^+$ and $Eu(SO_4)_2^-$ are the most significant species at the measured temperature in the higher pH scenario (C panel). At higher temperatures they are replaced by $EuCl^{2+}$, $EuCl_4^{2-}$, EuF^{2+} and $EuCl_3^-$.

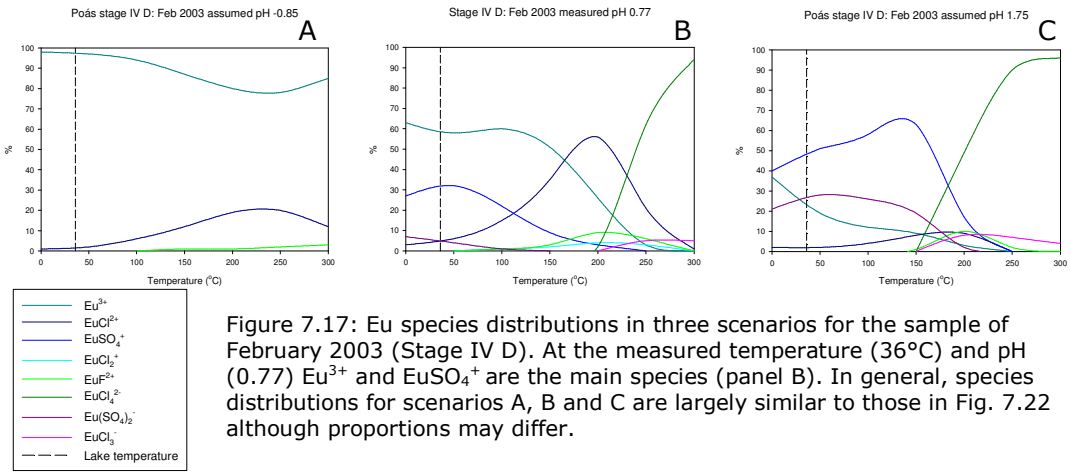

Figure 7.17: Eu species distributions in three scenarios for the sample of February 2003 (Stage IV D). At the measured temperature (36°C) and pH (0.77) Eu^{3+} and $EuSO_4^+$ are the main species (panel B). In general, species distributions for scenarios A, B and C are largely similar to those in Fig. 7.22 although proportions may differ.

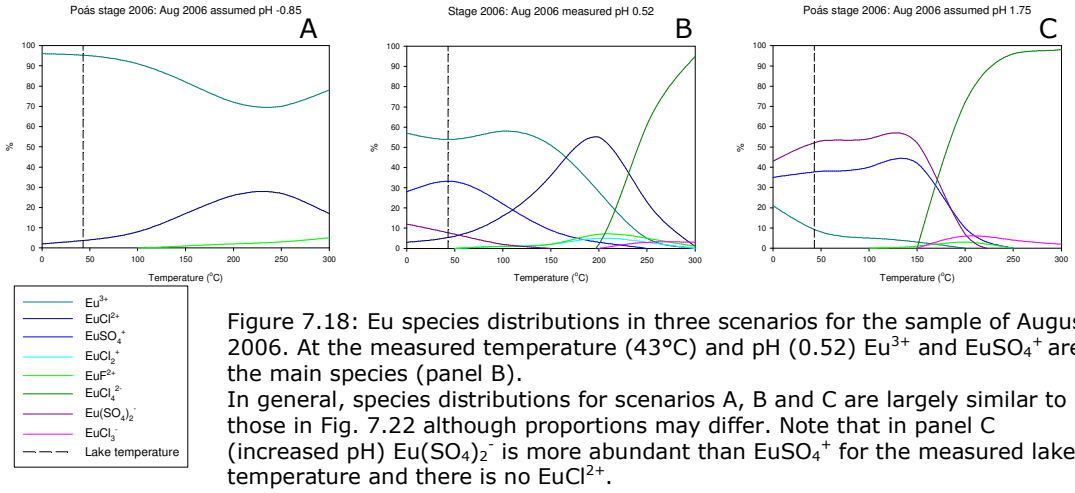

Figure 7.18: Eu species distributions in three scenarios for the sample of August 2006. At the measured temperature (43°C) and pH (0.52) Eu^{3+} and $EuSO_4^+$ are the main species (panel B).
In general, species distributions for scenarios A, B and C are largely similar to those in Fig. 7.22 although proportions may differ. Note that in panel C (increased pH) $Eu(SO_4)_2^-$ is more abundant than $EuSO_4^+$ for the measured lake temperature and there is no $EuCl^{2+}$.

In summary:

Except for the extreme conditions of November 1992, Eu^{3+} and $EuSO_4^+$ are the most prominent species at the temperature and pH conditions of the lake as recorded during sampling. These species may be accompanied by modest abundances of $EuCl_2^+$ and/or $Eu(SO_4)_2^-$. Gradually increasing the temperatures to values higher than the measured one results in a distribution whereby $EuCl_2^+$ eventually becomes the dominant species, usually accompanied by lesser amounts of EuF^{2+} and $EuCl_2^+$. At the highest temperatures, $EuCl_4^{2-}$ appears and rapidly increases so that it becomes the most abundant species.

The effect of lowering the pH relative to the measured values (pH=-0.85 scenarios) is that Eu^{3+} will be the only dominant species and that $EuSO_4^+$ is significantly reduced. This picture is valid for all temperatures, although Eu^{3+} tends to decrease in favour of $EuSO_4^+$ when temperatures are higher than the measured values.

The effect of increasing the pH relative to the measured values (pH=1.75 scenarios) is that Eu^{3+} becomes significantly reduced in importance and that $Eu(SO_4)_2^-$ becomes an additional species accompanying $EuSO_4^+$. Increasing the temperature for these elevated pH scenarios shows that $EuCl_4^{2-}$ eventually becomes the most prominent species.

7.2.3 Yb species

The species of ytterbium are taken to represent the HREE. Again, the species distributions strongly depend on temperature. At measured temperatures and pH conditions Yb^{3+} and $YbSO_4^+$ are usually the dominant species. Other species can be present as well, such as $YbCl^{2+}$ and YbF^{2+} particularly during high activity (November 1992 sample). In general, it can be seen that increasing temperatures lead to a decrease in importance of Yb^{3+} and $YbSO_4^+$ and an increase in importance of $YbCl^{2+}$ and YbF^{2+}. Lowering the pH ("A" scenarios) suppresses $YbSO_4^+$ and favours the importance of Yb^{3+}. The reversed case is seen at increased pH ("C" scenarios), when significant amounts of $Yb(SO_4)_2^-$ appear as well.

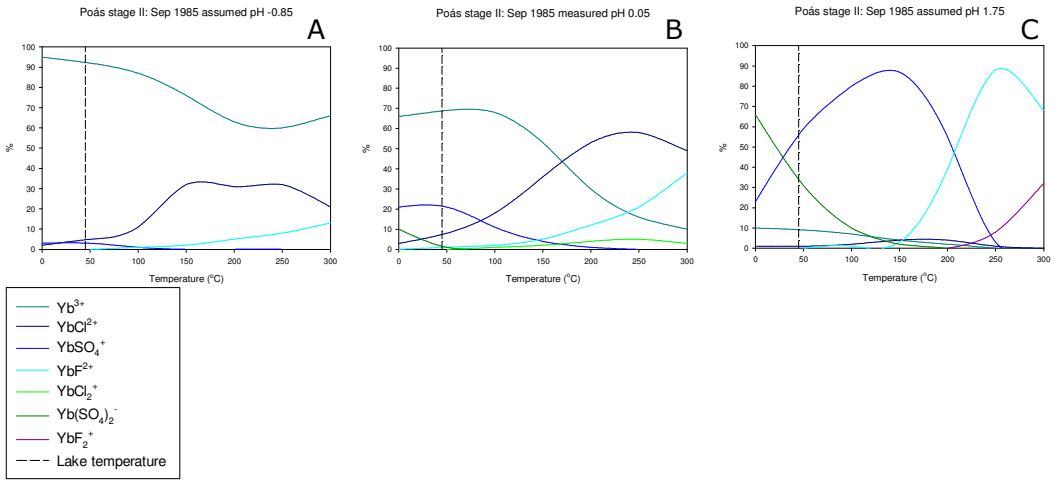

Figure 7.19: Yb species distributions in three scenarios for the sample of September 1985 (Stage II). At the measured temperature (45°C) and pH (0.05) Yb^{3+} is the main species while $YbSO_4^+$ and $YbCl^{2+}$ occur as well (panel B). The latter is important at high temperatures, peaking at 250°C. It is accompanied by increasing amounts of YbF^{2+} which is almost equally abundant at 300°C. For lowered pH values (panel A) only Yb^{3+} is significant with somewhat lower abundances at higher temperatures whereby $YbCl^{2+}$ and YbF^{2+} increase. The plot for increased pH values (panel C) shows peaks for $Yb(SO_4)_2^-$ at the lowest temperatures, for $YbSO_4^+$ around 140°C and for YbF^{2+} around 250°C.

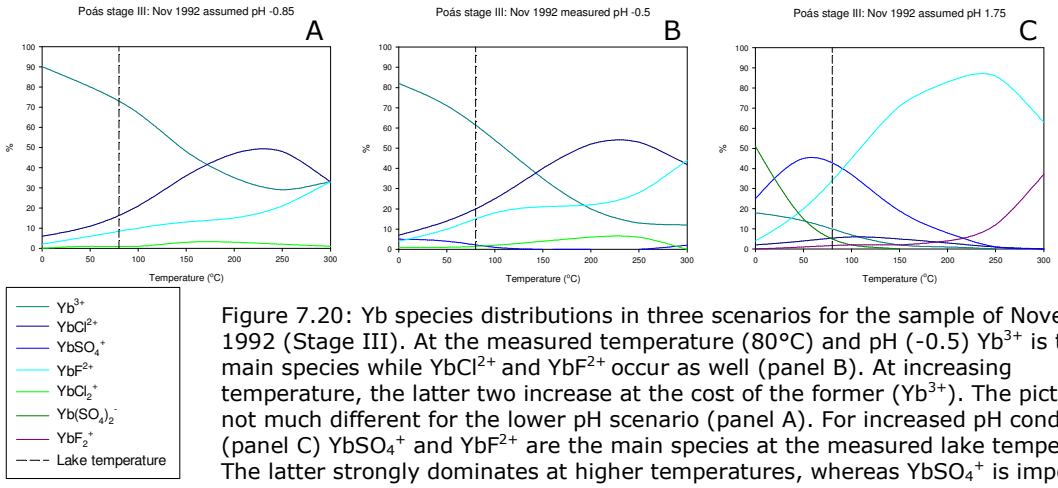

Figure 7.20: Yb species distributions in three scenarios for the sample of November 1992 (Stage III). At the measured temperature (80°C) and pH (-0.5) Yb^{3+} is the main species while $YbCl^{2+}$ and YbF^{2+} occur as well (panel B). At increasing temperature, the latter two increase at the cost of the former (Yb^{3+}). The picture is not much different for the lower pH scenario (panel A). For increased pH conditions (panel C) $YbSO_4^+$ and YbF^{2+} are the main species at the measured lake temperature. The latter strongly dominates at higher temperatures, whereas $YbSO_4^+$ is important at the lowest temperatures.

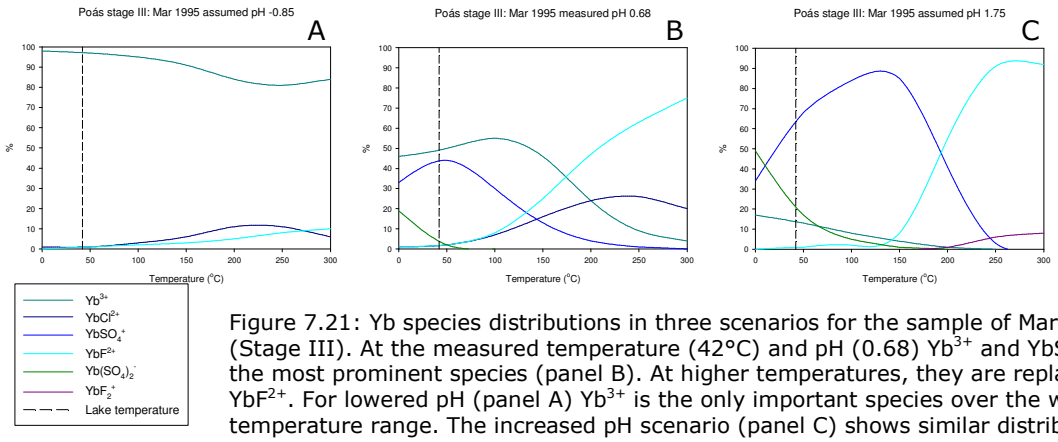

Figure 7.21: Yb species distributions in three scenarios for the sample of March 1995 (Stage III). At the measured temperature (42°C) and pH (0.68) Yb^{3+} and $YbSO_4^+$ are the most prominent species (panel B). At higher temperatures, they are replaced by YbF^{2+}. For lowered pH (panel A) Yb^{3+} is the only important species over the whole temperature range. The increased pH scenario (panel C) shows similar distribution peaks as in Fig. 7.19.

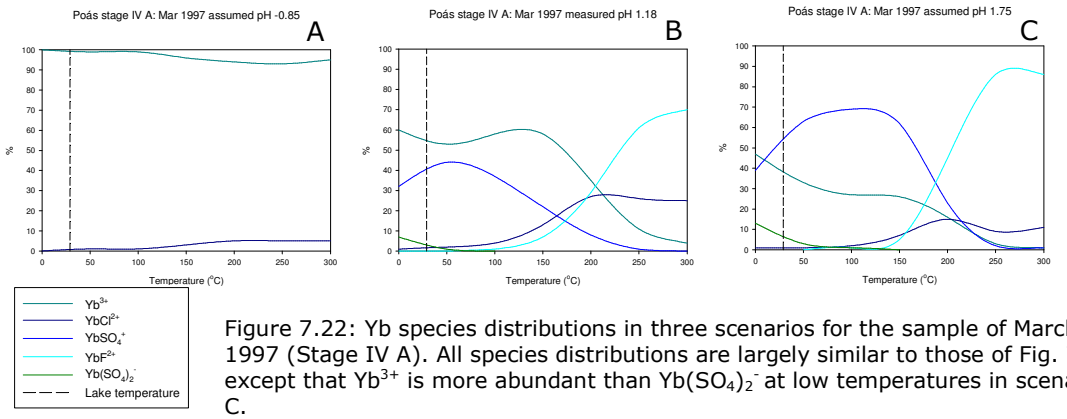

Figure 7.22: Yb species distributions in three scenarios for the sample of March 1997 (Stage IV A). All species distributions are largely similar to those of Fig. 7.21, except that Yb^{3+} is more abundant than $Yb(SO_4)_2^-$ at low temperatures in scenario C.

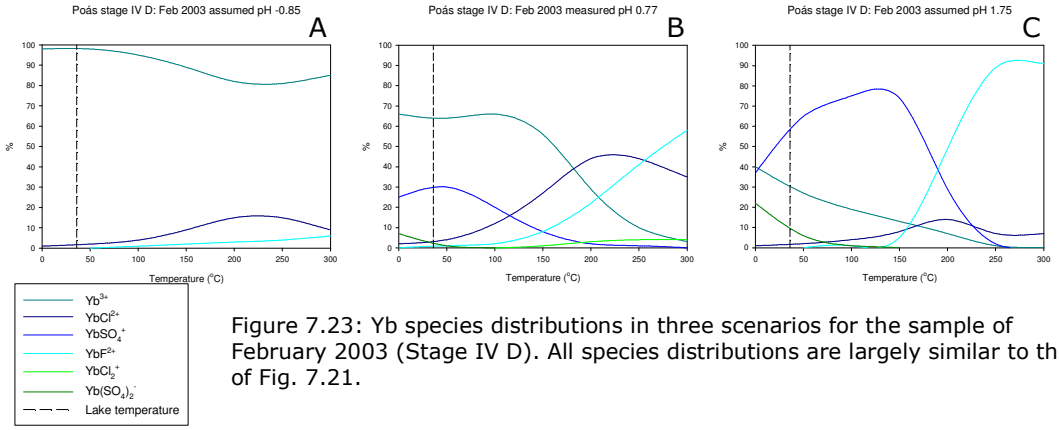

Figure 7.23: Yb species distributions in three scenarios for the sample of February 2003 (Stage IV D). All species distributions are largely similar to those of Fig. 7.21.

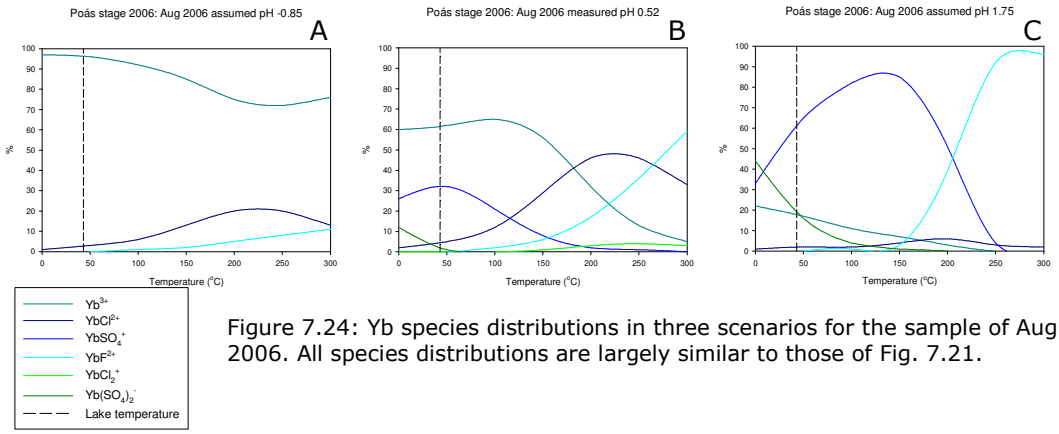

Figure 7.24: Yb species distributions in three scenarios for the sample of August 2006. All species distributions are largely similar to those of Fig. 7.21.

In summary:

The La^{3+} and $LaSO_4^+$ species are prominent at the temperature and pH as measured during sampling. Other species tend to be insignificant under these conditions. The exception is November 1992 when LaF^{2+} and $LaCl_2^+$ were clearly more abundant than $LaSO_4^+$. Gradually increasing the temperatures to values higher than the measured one results in a distribution whereby LaF^{2+} and $LaCl_2^+$ eventually become the dominant species.

The effect of lowering the pH relative to the measured values (pH=-0.85 scenarios) is that Yb^{3+} will be the only significant species over the entire temperature range.

The effect of increasing the pH relative to the measured values (pH=1.75 scenarios) is that Yb^{3+} becomes significantly reduced relative to $YbSO_4^+$ and that $Yb(SO_4)_2^-$ becomes an additional species. Increasing the temperature for these elevated pH scenarios shows that YbF^{2+} eventually may replace $YbSO_4^+$ as most prominent species.

8. Discussion

This discussion will focus on the observed REE systematics, on their significance for water-rock interaction processes and for monitoring volcanic/hydrothermal activity. The volcanic lakes will be treated separately, with emphasis on those with the most abundant data.

8.1 Poás, Costa Rica

The comparison of major element proportions in lake water and volcanic rock indicates that whole-rock dissolution is largely responsible for the lake-water composition during part of stage III and in 2006-2008 (a complete data set for 2009 was not available). During the other stages the composition deviates significantly, suggesting that rock dissolution was not congruent or that alteration minerals influenced the water chemistry. The ternary diagrams Mg-K-Na and Mg-K+Na-Al indicate that (natro-)alunite is a likely candidate given the trends towards and away from this mineral. In detail, however, the diagrams are not consistent with the composition for (natro-)alunite. Either the alunite has not the adopted 50-50% composition for K and Na, or other (Al-bearing) minerals played a role as well. Because most of the data fall on a line extrapolated between the rock and the (natro-)alunite, it appears that the elements were retained by precipitation of the (natro-)alunite during water-rock interaction. Stage IV and especially the substages A, C, and E show the most extreme behaviour in this respect.

The REE contents of the water samples confirm the systematics described above, as their chondrite-normalized trends are closest to those of the rocks during Stage III (figure 6.22A). Still, the rock normalized REE patterns of the water samples (figure 6.22B) show an enrichment of HREE over LREE and a positive Eu anomaly. An explanation could be that the LREE are preferentially retained in the rocks and Eu is preferentially released during rock dissolution. It is uncertain that a specific primary magmatic minerals is responsible. For example, residual plagioclase would not only retain LREE but also Eu. However, glass is a possible candidate. Chondrite-normalized REE plots for basalt and andesite (figure 8.1), calculated from modal rock compositions (table 8.1), indicate that Poás glass will be enriched in LREE and may have a negative Eu anomaly. If, during water-rock interaction, glass is more stable than other phases so that dissolved REE in the water will obtain roughly an opposite trend.

Alternatively, newly-formed alunite may play a role, since this mineral is rich in REE with a large LREE/HREE ratio and a negative Eu anomaly. Its formation will thus lead to an apparent enrichment in HREE and Eu in the water.

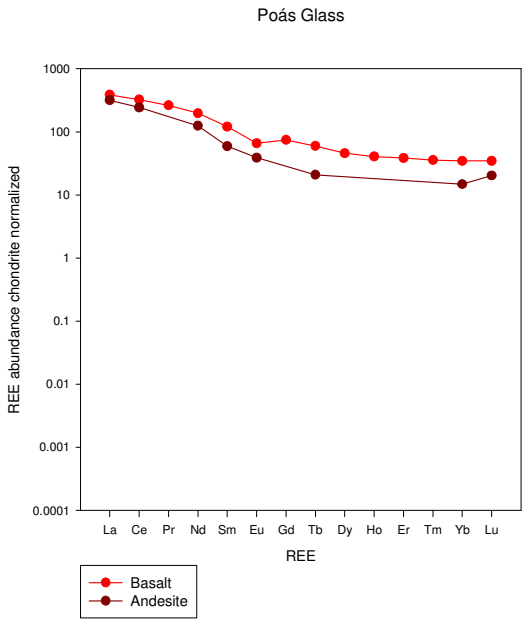

Figure 8.1: Calculated REE trends for glass compositions of an andesite and a basalt from Poás (data from Geochemical Earth Reference Model (2011) and Shaw, 1970).

	plagioclase			olivine		cpx		opx (low calcium pyroxene)		
	basalt	dacite	andesite	basalt	andesite	basalt	andesite	basalt	dacite	andesite
La	0.158	-	0.18	0.005858	0.01	0.090175	0.28	0.001167		0.26
Ce	0.09375	0.241	0.12	0.0049	-	0.16115	0.47	0.002	0.362	0.165
Pr	0.17			0.002		0.104		0.0034		
Nd	0.05775	0.172	0.09	0.003325	-	0.394358	0.86	0.0059	0.94	0.2595
Sm	0.04675	0.125	0.06	0.00282	0.01	0.597833	1.6	0.0125	1.52	0.28
Eu	0.4905	2.11	0.75	0.00363		0.481571	1.1	0.0185	1.11	0.204
Gd	0.03425	0.1095	-	0.0041		1.083333	-	0.023	-	0.155
Tb	0.033	-	0.15	0.004436	-	0.5575	2.7	0.03		0.69
Dy	0.0365	0.086	-	0.003567	0.01	0.731125	-	0.022	2.63	0.225
Ho	0.0295			0.0179		0.45		0.051		
Er	0.0305	0.084	-	0.004		0.4906	-	0.0555	2.25	0.318
Tm	0.036			0.0045		1.09		0.08		
Yb	0.0215	0.077	0.1	0.053743	0.03	0.731727	2	0.0945	2.01	0.585
Lu	0.031	0.062	0.1	0.02928	-	0.60925	1.0355	0.115	1.81	0.5815

Table 8.1: To calculate modal rock compositions: phenocryst (0-42%), plagioclase (0-27%), olivine (0-2.5%), clinopyroxene (0-5%), orthopyroxene (0-10%). (Data from Geochemical Earth Reference Model (2011).

The time-series ratios of the REE ratios (figure 6.30 - 6.33) show significant variations. In general, the Ce/Yb, La/Sm, Tb/Yb ratios fall below those of the rock, in agreement with the apparent depletion of the LREE. The La/Sm ratio is an exception, as it becomes higher than rock from 2007.

All Eu anomalies in the water samples are higher than those of the rock, supporting a preferential release of bivalent Eu, presumably controlled to a large extent by the stability of plagioclase. Whole rock dissolution is supported for the 2006-2009 samples by the observation that ratios in waters and the rock were close during that period and that temperature were high and pH low (figure 8.2 and 8.3).

Phreatic eruptions are probably important in controlling the dissolution regime, because after such event, often an immediate change in behaviour visible. They may create space for new batches of deep water to move to the

surface and enter at the bottom of crater lake. The higher temperatures during stage III, 2006 and 2007 are an indication of hot input from below the lake.

It has been proposed that magmatic intrusions have occurred during the last 30 years of monitoring but their effect on the water composition is difficult to trace, apart from the alleged release of heat and volatiles. One reason is that subsurface water will only be exposed to fresh rock of an intrusion after sufficient time has passed for cooling. Also, the water may not become in contact with the rock at all if the volume of the intrusion is too small or if it does not reach sufficiently shallow levels.

However, the Eu anomalies may provide a clue to this issue. They form a conspicuous trend with drops to low values (closest to the rock) during periods of high activity (Stage III and 2006). Figure 8.2 demonstrates the existence of an inverse relationship between Eu/Eu* and the measures lake-water temperature. The lowest Eu/Eu* values can be interpreted to indicate high-temperatures, low-pH interaction of the water with fresh rock, possibly a cooled newly emplaced magma batch. Presumably, the intrusions occurred some time earlier. The gradual increasing Eu anomaly between 1996 and 2006 can be explained by interaction with increasingly altered rock, whereby plagioclase becomes gradually less stable.

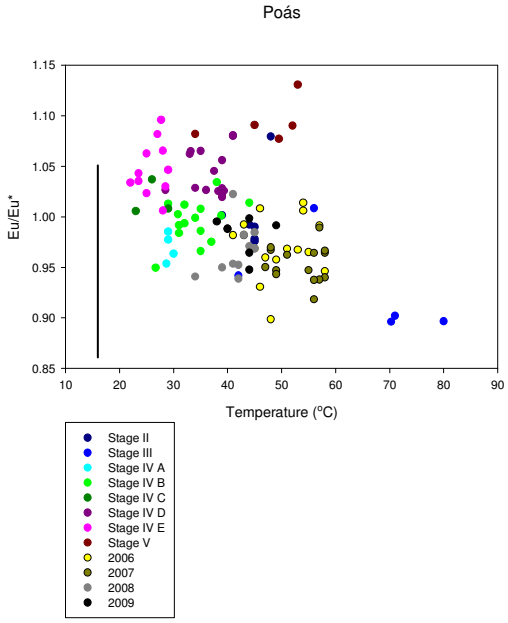

Figure 8.2: Inverse correlation between Eu/Eu* ratio and temperature. Note that values for Stage V do not fit in the general trend. Black bar indicates estimated error. Data from appendix A and Martínez (2008).

Stage IV (no whole rock dissolution) and the 2006-2008 period (close to whole rock dissolution) were selected to discuss the significance of the REE data in more detail.

Martínez (2008) proposed that Substages A, C, E of stage IV are quiet periods due to sealing processes in the sub-lake system that diminished the free supply of hot and acidic hydrothermal water to the lake. The lake geochemistry is consistent with retention of elements by alunite, which, according to the saturation models can only be stable at temperatures higher than observed in the lake. It is therefore reasonable to suppose that the sealing of pores and conduits is associated with the formation of alunite below the lake.

The REE data support this idea because Substages A, C, E are marked by relatively low Ce/Yb ratios, presumably due to the preferential uptake of LREE by alunite. Higher ratios and the steady increase from 2006 onwards can either be explained by dissolution of previously formed alunite, or by conditions promoting congruent rock dissolution.

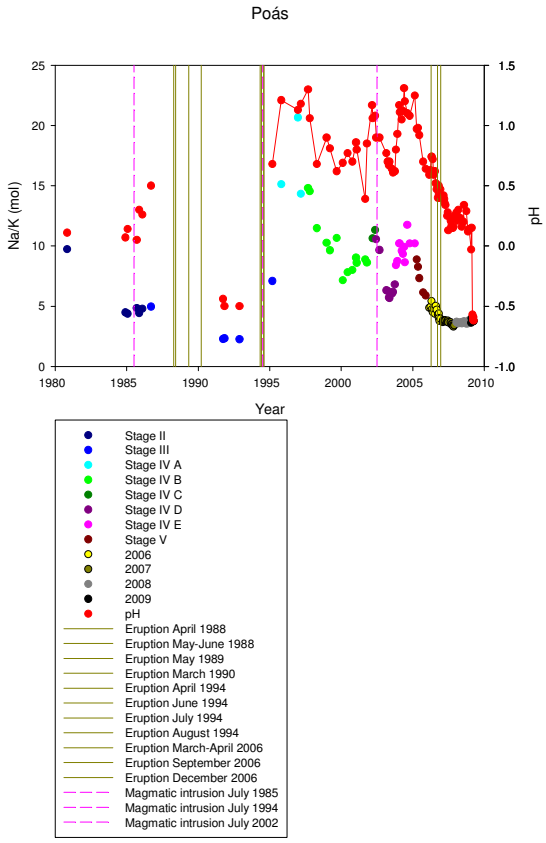

Figure 8.3: Relationships between Na/K and pH of lake-water and phreatic eruptions at Poás (OVSICORI)

Obvious relationships between the molar Na/K ratio and pH of the lake waters (Figure 8.3) further confirm the inferred role of alunite. The coinciding fluctuations seem independent from phreatic eruptions or magmatic intrusion. Relatively high Na/K ratios in Substages A, C, E of stage IV when the partial sealing occurred are consistent with the formation of alunite which is expected to retain more K than Na. Increased pH results from less input of deep, acidic water and a larger contribution of meteoric water in the lake. The years since 2006 are marked by low pH and low Na/K ratios, close to that of the rock (2.6-2.8), which argues again in favour of (near-)congruent rock dissolution.

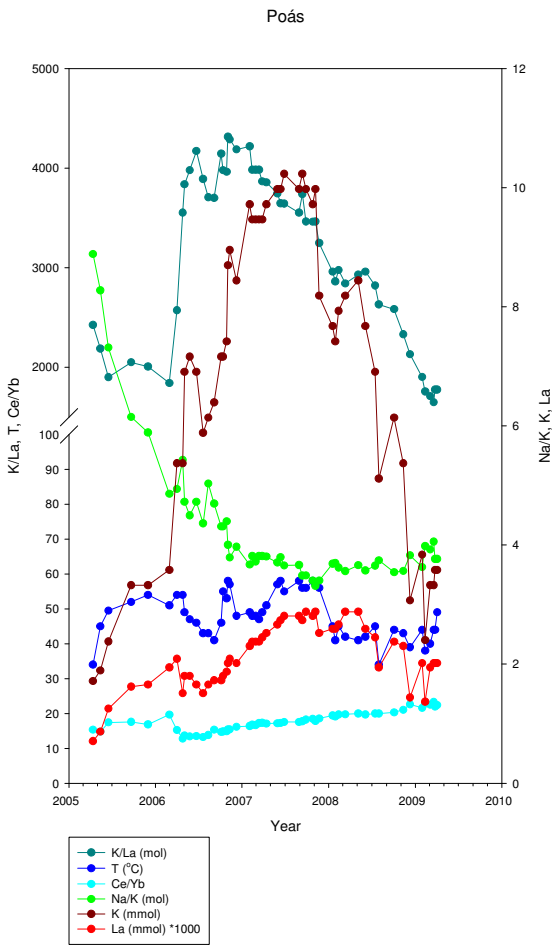

Figure 8.4: Relationships between K/La, temperature, Ce/Yb, Na/K, K, and La for Poás lake water. Data from appendix A and Martínez (2008).

Figure 8.4 highlights the effects of alunite on major and rare earth elements dissolved in the lake. The plot shows a maximum for K, La and temperature in 2007, a drop in Na/K to almost constant values from 2007 on, and a steady increase in Ce/Yb since 2006. The drop in element concentrations since mid-2007 can be explained by dilution of the system with meteoric water in the subsurface. As this may be accompanied by cooling this may have induced the dissolution of alunite which resulted in a gradual decrease in K/La down to values corresponding with a possible composition of this mineral (just above 2000), as well as in an increasing Ce/Yb trend. The near constant Na/K ratio since 2007 is consistent with dilution, but suggests that it is relatively insensitive to alunite dissolution.

A final confirmation for the role of alunite comes from the altered rock sample that was studied to investigate the assemblage of secondary minerals. The presence of this mineral and the probably origin of the ejected rock from deeper parts below the lake are further evidence for the importance of alunite.

8.2 Rincón de la Vieja, Costa Rica

The 1999-2001 samples plot in different parts of the Mg-K-Na and Mg-K+Na-Al diagrams (figure 6.11) than the other samples, as they are relatively depleted in Al and K, suggesting retention of these elements by an Al and K-bearing phase. Because they plot on the extrapolated line between the rocks and (natro)alunite, this mineral is probably responsible for the depletion in the water. In absence of data for these samples (February 1999-2001) this interpretation cannot be tested with REE results. These samples, however, point to a different behaviour of Rincón de la Vieja in the past. This suggests that some event

between March 2001 and May 2004 changed the properties of the lake quite drastically. This was probably not an eruption, because the latest eruptive activity ended in September 1998 (Venzke et al. (2002-)). OVSICORI-UNA reported fumarolic and seismic activity from March 2000 to August 2001.

The other samples, which are more recent, plot close to the rock samples in the Mg-K-Na and Mg-K+Na-Al ternary diagrams, suggesting almost complete rock dissolution as principal control. In the Mg-K+Na-Al diagram the water samples are slightly enriched in Al relative to the rock samples. If the rock data are representative, this may suggest an extra dissolution of an alteration mineral like alunite and perhaps another Al-rich phase (kaolinite, gibbsite, diaspore, or pyrophyllite).

Chondrite-normalized REE trends of the water samples are comparable to those of the rocks (figure 6.23) except that they show less enrichment in the lightest REE and a less pronounced negative Eu anomaly. In the rock-normalized REE patterns for the water samples this expresses as a dip for La and Ce and a slightly positive Eu anomaly. Based on these observations complete congruent dissolution of fresh rock cannot explain the water compositions, again if the rock data are sufficiently representative. Instead, La and Ce may have been retained by a LREE-rich phase. Alunite or another alteration mineral is unlikely in view of the major element relationships in the ternary diagrams. A primary volcanic phase that hosts LREE may have escaped (complete) dissolution (e.g. glass). This retention did not affect Eu in the same way, suggesting that the minor relative enrichment is due to the more mobile Eu^{2+}.

The time-series plots of REE ratios (figure 6.30-6.33) support this interpretation, as the Ce/Yb ratio of the water samples is consistently lower than that of the rocks and Eu/Eu* consistently higher. Over the 5-years period of monitoring the ratios show only minor variations. Several ratios (Eu/Eu*, La/Sm, Tb/Yb) show a modest jump in the trend between September 2006 and April 2007, suggesting a change in the subsurface water-rock interaction, possibly related to a minor modification in the behaviour of the magmatic/hydrothermal system. There are no obvious relationships between REE ratios and either pH or temperature of the lake.

Figure 8.5 suggests a positive correlation between Na/K and pH, similar to what has been observed at Poás. Whether this shoud also be attributed to alunite is questionable, since the ternary diagrams and flat rock-normalized REE trends argue in favour of (near-)congruent rock dissolution.

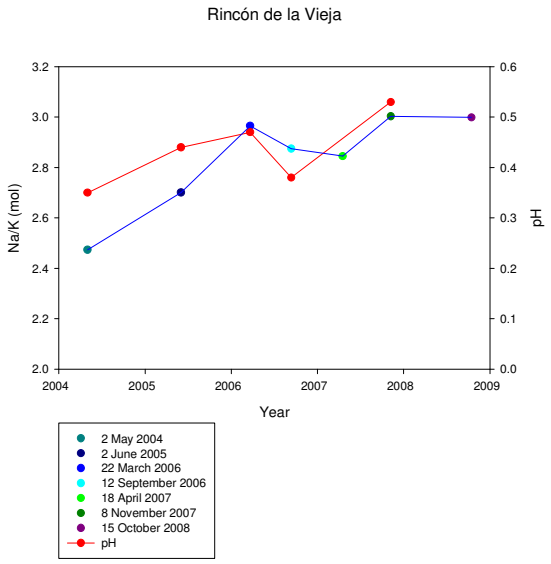

Figure 8.5: The possible (time-)relation between Na/K and pH (appendix A).

8.3 El Chichón, Mexico

The water compositions plot away from the rocks in the ternary diagrams (Figure 6.12), which preclude a role for alunite for the chemistry of the crater lake of El Chichón. There is also no evidence for controls by other secondary minerals. The lake chemistry thus deviates from that of typical hyperacid lakes.

Chondrite-normalized REE trends for waters and rocks tend to be similar and rock-normalized patterns tend to be rather flat, but because of the considerable scatter, the REE signatures are difficult to interpret. However, congruent rock dissolution is an unlikely mechanism to explain the REE, since it is inconsistent with the major element chemistry.

According to Morton-Bermea et al. (2010) a relationship would exist between Mg and HREE, but this is difficult to verify with the available data. It can be speculated that mobilization of salt deposits that are presumed to be present below the volcano could have an influence on the speciation and behaviour of the REE.

8.4 Copahue, Argentina

The Copahue data are from hot springs close to the crater lake, because essential crater lake data are missing. These hot spring data are taken as representative for the crater lake signatures.

Because of the eruption in 2000, a distinction can made between pre-eruptive (old) samples and post-eruptive (young) samples. The ternary diagrams (figure 6.13A,B,C) indicate that the pre-eruptive samples can be explained by (near-)congruent rock dissolution, consistent with the lower pH at that time (figure 8.6). In contrast, the younger samples deviate from whole-rock dissolution and point to a role of natro-alunite in retaining K, Na and Al.

Chondrite normalized REE patterns of pre-eruption waters are comparable to those of the rocks (figure 6.25), showing LREE enrichment and a negative Eu anomaly. They are thus consistent with whole-rock dissolution. The shape for the post-eruption samples is different, particularly in showing a steeper trend for the lightest REE. The overall REE concentrations in these samples are also lower and Eu anomalies are weak or absent. These features are in agreement with a deviation from whole-rock dissolution. If alunite precipitated from the same water that was present before the eruption as the major element relationships suggest, this should have resulted in a less steep LREE trend considering the strong enrichment in LREE in alunite (Fig 3.4). Hence, either the system hosted different water with a much stronger LREE enrichment before alunite precipitated, or other phases regulating the REE behaviour were involved.

The time-series plot of REE ratios (figure 6.30-6.33) further highlights the chemical contrast before (1997-2000) and after (2000-2005) the eruption. Before the eruption the negative Eu anomaly was closer to that of the rock and the Ce/Yb ratio only somewhat higher. After the eruption the differences are stronger.

The Na/K ratio roughly correlates with pH (Figure 8.6). Similar to the observations at Poás, this can be attributed to the role of alunite. Before the eruption, when both parameters were low, rock dissolution dominated, whereas after the eruption alunite formed, retaining more K and thus causing an increase in Na/K in the waters.

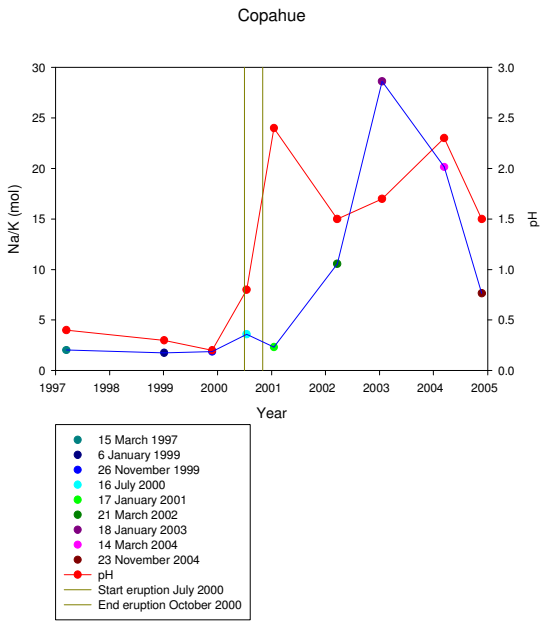

Figure 8.6: Relationship between Na/K and pH for Copahue waters. Note the difference before and after the eruption in 2000. Data from Venzke et al. (2002-) and Varekamp et al. (2006 and 2009).

8.5 Yellowstone, USA

The Yellowstone water samples are from three different areas, Norris Geyser Basin, Gibbon Geyser Basin, and Upper Geyser Basin. The water and rock samples are poor in Mg, relative to the alkalies, in agreement with the rhyolitic composition of the volcanis of the area. In general, rock and water compositions do not coincide which rules out that whole-rock dissolution is a plausible mechanism.

Chondrite normalized REE trends of the water samples are comparable to the rock samples (figure 6.26). Both water and rock show a distinct negative Eu anomaly, but the water samples show a small positive Eu anomaly in rock normalized patterns. There is relatively less LREE in the water than in the rocks, which means that probably a LREE-retaining mineral that preferentially rejects Eu precipitated. Alunite is a potential candidate, since it is commonly marked by high LREE/HREE ratios and a negative Eu anomaly. Inspection of more parameters is needed to confirm this.

8.6 Ruapehu, New Zealand

The Mg-K-Na and Mg-K+Na-Al ternary diagrams (figure 6.15) point to (near-) congruent rock dissolution for the period 1988-1996 (prior to the eruptions in 1995-1997) and possible alunite precipitation for the 2006-2008 period.

Chondrite-normalized REE trends of the older samples are comparable to the rock samples (figure 6.27A). Nearly flat REE rock-normalized trend suggest whole-rock dissolution. The water after the eruption is LREE depleted compared to the rock (figure 6.27B). None of the water samples shows a Eu anomaly, despite a slightly negative one in some of the rock samples.

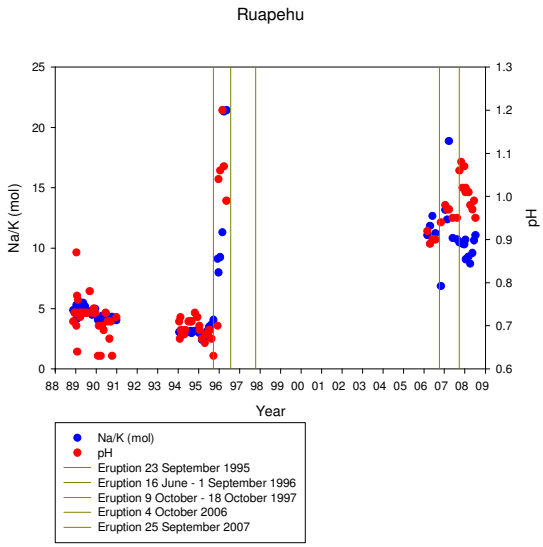

Figure 8.7: Relationship between Na/K and pH and indicated eruptions for Ruapehu. Data from Christenson et al. (2010), Christenson (2000) and Christenson and Wood (1993).

Figure 8.7 demonstrates a clear correlation between Na/K and pH, confirming previous observations for Poás and Copahue. The change after the onset of eruptions in 1995 marks a transition from whole-rock dissolution to alunite precipitation.

8.7 Indonesian volcanoes

The limited data available for the Indonesian volcanoes do not allow an in-depth evaluation of the REE signatures. Only some brief comments are given here.

The rock-normalized REE trends indicate that the chemistry of the Kawah Ijen lake is largely determined by (near-)congruent rock dissolution in agreement with its hyperacid nature. It also tends to be confirmed by the ternary diagrams. The REE trend for Keli Mutu is close, but the limited amount of data precludes a definite assessment. The patterns for Kawah Putih show a slight enrichment of the REE. Considering the ternary diagrams as well, it cannot be excluded that the lake chemistry is influenced by alunite dissolution. Because the REE abundances in the other lakes are very low and rather erratic, they will not be further discussed here.

8.8 NW Pacific volcanoes

Again, due to the limited REE data available for the waters and rocks of these volcanoes, they cannot be treated in detail. Slight depletions in LREE that are visible in rock-normalized patterns might point to an influence of precipitating alunite. The ternary plots tend to confirm this for Kusatsu-Shirane but the evidence is not clear.

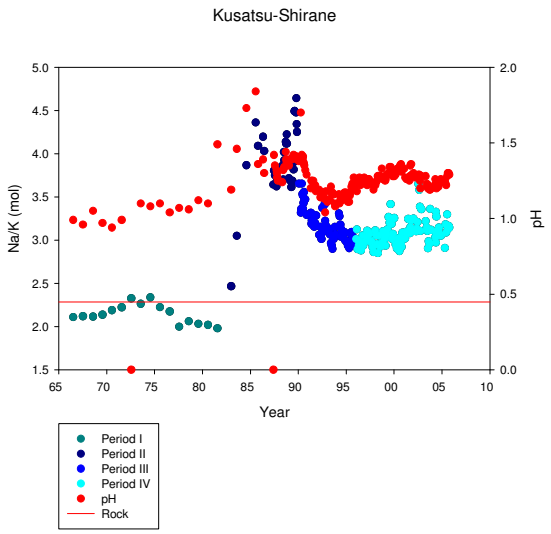

Figure 8.8: Relationship between Na/K and pH for Kusatsu-Shirane lake. Data from Ohba et al. (2008) and references therein.

Figure 8.8 suggests a different behaviour between period I and the other periods. The Na/K ratio during period I is low, and together with observations in the ternary diagrams they suggest (figure 6.21) dissolution of alunite. The reasonably good correlation between the Na/K ratio and the pH for periods II and III would again point to an occasionally operating alunite control. The relatively low Na/K ratios during Period IV might be due to a stronger influence of rock dissolution. Obviously, these interpretations remain speculative.

9. Summary and conclusions

This thesis documents the results of a study on rare earth elements (REE) in active, crater-lake hosting volcanic-hydrothermal systems worldwide. Particular attention has been paid to Poás and Rincón de la Vieja, two Costa Rican volcanoes for which new analytical data are presented. A literature survey covered geochemical information available for volcanic lakes across the globe.

The main objective of this research was to explore how REE that are dissolved in crater lake water can be used to gain insights into water-rock interaction processes and to monitor activity in the underlying hydrothermal system. For this purpose, the newly acquired data and those from the literature compilation were evaluated to discern systematics in the behaviour of the REE and other elements, whereby the compositions of local rocks were taken in account as well.

The REE concentrations and their normalized trends show significant variations for the investigated lakes. There is a rough correlation between REE patterns of the lake waters and the local rocks, testifying that lavas and other solid volcanic products are the principal source of the REE. In general, the correspondence is best for highly acidic lakes. The observed systematics indicate that rock dissolution plays an important role but fractionation among the REE shows that complete, congruent dissolution is rare and only occurs under extreme conditions. In general, water-rock interaction in these volcanic-hydrothermal settings affects individual igneous minerals in different ways, some being more resistant than others. The collected data indicate that the REE signatures in lake waters are controlled by preferential retention or release from REE hosting phases, either primary igneous minerals or glass in volcanic materials, or secondary phases formed as alteration product.

An important discovery is the apparent role of alunite in regulating the signatures of dissolved REE in lake waters. This is surprising because this mineral is an alteration product that is commonly not stable in acidic volcanic lakes. However, as could be confirmed in PHREEQC models, the saturation state of alunite in these waters is inversely correlated with temperature. This implies that alunite can be present in hotter parts of the hydrothermal system below the lake, and that the REE signatures in the lake may be inherited from inflow of water that had interacted with alunite present at depth. Changes in REE patterns in lakes that have been monitored over longer times indicate that the influence of alunite may vary with time. This suggests that a lake may signal the stability of the mineral, and its formation or dissolution in response to changing conditions. Apart from the REE data, the potential role of alunite can be confirmed by comparing the concentrations of its main cation constituents with other dissolved cations in the lake.

Time-series results on REE concentrations in the highly dynamic crater lake of Poás provide evidence for an intermittent role of alunite in the subsurface system. Strong fluctuations in LREE/HREE ratios, observed over decades of monitoring, probably reflect variations in the stability of the mineral, induced by changing hydrothermal conditions. Changes in the REE concentrations sometimes coincided with phreatic eruptive events. Since alunite is a secondary, non-magmatic mineral, its presence or absence may affect the porosity and permeability of volcanic rocks and conduits that act as pathways for upflowing fluids. Evidence for Poás suggests that the formation of alunite has a sealing effect that reduces the influx of fluid and heat into its lake.

REE in volcanic lakes are a promising new instrument to study water-rock interaction and alteration processes that are active at the very present. Monitoring the REE provides a valuable new parameter in assessing changes in the state of activity of volcanic-hydrothermal systems.

10. Acknowledgements

I would like to thank dr. Manfred van Bergen, my supervisor for his support and ideas. Also, I would like María Martínez and her colleagues at OVSICORI for sending and (partially) analyzing the Poás and Rincón de la Vieja samples. I would like to thank Marc Verheul, Nora Sutton, Marjan Versluijs-Helder and Anita van Leeuwen for their help with the analyses. I am grateful to Annika Huizinga for providing the alunite rock from Poás and Alejandro Rodríguez for analyzing it.

11. References

Alvarado Induni, G.E., 1985. Consideraciones petrologicas de los estratovolcanes de Costa Rica. Revista Geológica de América Central 3, 103-128.

Andrews, B.J., Gardner, J.E., Housh, T.B., 2008. Repeated recharge, assimilation, and hybridization in magmas erupted from El Chichón as recorded by plagioclase and amphibole phenocrysts. Journal of Volcanology and Geothermal Research 175, 415-426.

Armienta, M.A., De la Cruz-Reyna, S., Macías, J.L., 2000. Chemical characteristics of the crater lakes of Popocatetetl, El Chichon, and Nevado de Toluca volcanoes, Mexico. Journal of Volcanology and Geothermal Research 97, 105-125.

Aubert, D., Stille, P., Probst, A., 2001. REE fractionation during granite weathering and removal by waters and suspended loads: Sr and Nd isotopic evidence. Geochimica et Cosmochimica Acta 65, 387-406.

Ayres, M., Harris, N., 1997. REE fractionation and Nd-isotope disequilibrium during crustal anatexis: constraints from Himalayan leucogranites. Chemical Geology 139, 249-269.

Bach, W., Irber, W., 1998. Rare earth element mobility in the oceanic lower sheeted dyke complex: evidence from geochemical data and leaching experiments. Chemical Geology 151, 309-326.

Badrudin, M., 1994. Kelut volcano monitoring: Hazards, mitigation and changes in water chemistry prior to the 1990 eruption. Geochemical Journal 28, 233-241.

Baioumy, H.M., Gharaie, M.H.M., 2008. Characterization and origin of late Devonian illitic clay deposits southwestern Iran. Applied Clay Science 42, 318-325.

Bao, Z., Zhao, Z., 2008. Geochemistry of mineralization with exchangeable REY in the weathering crusts of granitic rocks in South China. Ore Geology Reviews 33, 519-535.

Bau, M., 1996. Controls on the fractionation of isovalent trace elements in magmatic and aqueous systems: evidence from Y/Ho, Zr/Hf, and lanthanide tetrad effect. Contrib Minerl Petrol 123, 323-333.

Bau, M., Dulski, P., 1996. Distribution of yttrium and rare-earth elements in the Penge and Kuruman iron-formations, Transvaal Supergroup, South Africa. Precambrian Research 79, 37-55.

Bau, M., Usui, A., Pracejus, B., Mita, N., Kanai, Y., Irber, W., Dulski, P., 1998. Geochemistry of low-temperature water-rock interaction: evidence from natural waters, andesite, and iron-oxyhydroxide precipitates at Nishiki-numa iron-spring, Hokkaido, Japan. Chemical Geology 151, 293-307.

Bau, M., 1999. Scavenging of dissolved yttrium and rare earths by precipitating iron oxyhydroxide: Experimental evidence for Ce oxidation, Y-Ho fractionation, and lanthanide tetrad effect. Geochimica et Cosmochimica Acta 63, 67-77.

Bau, M., Romer, R.L., Lüders, V., Dulski, P., 2003. Tracing element sources of hydrothermal mineral deposits: REE and Y distribution and Sr-Nd-Pb isotopes in fluorite from MVT deposits in the Pennine Orefield, England. Mineralium Deposita 38, 992-1008.

Bea, F., Pereira, M.D., Stroh, A., 1994. Mineral/leucosome trace-element partitioning in a peraluminous migmatite (a laser ablation-ICP-MS study). Chemical Geology 117, 291-312.

Beeson, M.H., Bargar, K.E., 1984. Major and trace element analyses of drill cores from thermal areas in Yellowstone National Park, Wyoming. USGS open-file report 84-373. (preliminary report)

Bernard, A., Mazot, A., 2004. Geochemical evolution of the young crater lake of Kelud volcano in Indonesia. Water-Rock interaction (WRI-11) Wanty & Seal II eds. A.A. Balkema Publishers.

Biddau, R., Cidu, R., Frau, F., 2002. Rare earth elements in waters from the albitite-bearing granodiorites of Central Sardinia, Italy. Chemical Geology 182, 1-14.

Bolhar, R., Kamber, B.S., Moorbath, S., Fedo, C.M., Whitehouse, M.J., 2004. Characterisation of early Archaean chemical sediments by trace element signatures. Earth and Planetary Science Letters 222, 43-60.
Bonyadi, Z., Davidson, G.J., Mehrabi, B., Meffre, S., Ghazban, F., 2011. Significance of apatite REE depletion and monazite inclusions in the brecciated Se-Chahun iron oxide-apatite deposit, Bafq district, Iran: Insights from paragenesis and geochemistry. Chemical Geology 281, 253-269.
Bortnikov, N.S., Gorelikova, N.V., Korostelev, P.G., Gonevchuk, V.G., 2008. Rare Earth Elements in Tourmaline and Chlorite from Tin-Bearing Assamblages: Factors Controlling Fractionation of REE in Hydrothermal Systems. Geology of Ore Deposits 50, 445-461.
Bourdier, J.-L., Pratomo, I., Thouret, J.-C., Boudon, G., Vincent, P.M., 1997. Observations, stratigraphy and eruptive processes of the 1990 eruption of Kelut volcano, Indeonesia. Journal of Volcanology and Geothermal Research 79, 181-203.
Casadevall, T.J., De la Cruz-Reyna, S., Rose Jr., W.I., Bagley, S., Finnegan, D.L., Zoller, W.H., 1984. Crater lake and post-eruption hydrothermal activity, El Chichón volcano, Mexico. Journal of Volcanology and Geothermal Research 23, 169-191.
Castillo, P.R. and Punongbayan, R.S., 1996. Petrology and Sr, Nd, and Pb Isotopic Geochemistry of Mount Pinatubo Volcanic Rocks. In: Fire and Mud. http://pubs.usgs.gov/pinatubo/castillo/. Accessed in September 2010.
Carr, M.J., Chesner, C.A., Gemmell, J.B., 1985. New analyses of lavas and bombs from Rincón de la Vieja volcano, Costa Rica. Bol. Vulcanol. *15*, 23-30.
Carr, M.J., Patino, L.C., Feigenson, M.D., 2007a. Chapter 22: Petrology and geochemistry of lavas. 565 – 590. In: Bundschuh, J. and Alvarado, G.E., editors. Central America: geology, resources, hazards, volume 1. Taylor & Francis/Balkema Leiden, The Netherlands.
Carr, M.J., Saginor, I., Alvarado, G.E., Bolge, L.L., Lindsay, F.N., Milidakis, K., Turrin, B.D., Feigenson, M.D., Swisher III, C.C., 2007b. Element fluxes from the volcanic front of Nicaragua and Costa Rica. G^3: Geochem. Geophys. Geosyst. 8 (6), Q06001. doi: 10.1029/2006GC001396. ISSN: 1525-2027.
Caudron, C., Mazot, A., Bernard, A., 2012. Carbon dioxide dynamics in Kelud volcanic lake. Journal of Geophysical Research 117, B05102. doi:10.1029/2011JB008806.
Christenson, B.W., Wood, C.P., 1993. Evolution of a vent-hosted hydrothermal system beneath Ruapehu Crater Lake, New Zealand. Bulletin of Volcanology 55, 547-565.
Christenson, B.W., 2000. Geochemistry of fluids associated with the 1995-1996 eruption of Mt. Ruapehu, New Zealand: signatures and processes in the magmatic-hydrothermal system. Journal of Volcanology and Geothermal Research 97, 1-30.
Christenson, B.W., Reyes, A.G., Young, R., Moebis, A., Sherburn, S., Cole-Baker, J., Britten, K., 2010. Cyclic processes and factors leading to phreatic eruption events: Insights from the 25 September 2007 eruption through Ruapehu Crater Lake, New Zealand. Journal of Volcanology and Geothermal Research 191, 15-32.
Cigolini, C., Kudo, A.M., Brookins, D.G., Ward, D., 1991. The petrology of Poás Volcano lavas: basalt-andesite relationship and their petrogenesis within the magmatic arc of Costa Rica. Journal of Volcanology and Geothermal Research 48, 367-384.
Cigolini, C., 1998. Intracrustal origin of Arenal basaltic andesite in the light of solid-melt interactions and related compositional buffering. Journal of Volcanology and Geothermal Research 86, 277-310.
Coppin, F., Berger, G., Bauer, A., Castet, S., Loubet, M., 2002. Sorption of lanthanides on smectite and kaolinite. Chemical Geology 182, 57-68.

Daag, A.S., Dolan, M.T., Laguerta, E.P., Meeker, G.P., Newhall, C.G., Pallister, J.S., Solidum, R.U., 1996. Growth of a Postclimatic Lava Dome at Mount Pinatubo, July-October 1992. In: Fire and Mud. http://pubs.usgs.gov/pinatubo/daag2/. Accessed in September 2010.
Delmelle, P., Bernard, A., 1994. Geochemistry, mineralogy, and chemical modeling of the acid crater lake of Kawah Ijen Volcano, Indonesia. Geochimica et Cosmochimica Acta 58, 2445-2460.
Delmelle, P., Bernard, A., 2000. Downstream composition changes of acidic volcanic waters discharged into the Banyupahit stream, Ijen caldera, Indonesia. Journal of Volcanology and Geothermal Research 97, 55-75.
Delmelle, P., Bernard, A., Kusakabe, M., Fischer, T.P., Takano, B., 2000. Geochemistry of the magmatic-hydrothermal system of Kawah Ijen volcano, East Java, Indonesia. Journal of Volcanology and Geothermal Research 97, 31-53.
Di Muro, A., Pallister, J., Villemant, B., Newhall, C., Semet, M., Martinez, M., Mariet, C., 2008. Pre-1991 sulfur transfer between mafic injections and dacite magma in the Mt. Pinatubo reservoir. Journal of Volcanology and Geothermal Research 175, 517-540.
Fee, J.A., Gaudette, H.E., Lyons, W.B., Long, D.T., 1992. Rare-earth element distribution in Lake Tyrrell groundwaters, Victoria, Australia. Chemical Geology 96, 67-93.
Friend, C.R.L., Nutman, A.P., Bennett, V.C., Norman, M.D., 2008. Seawater-like trace element signatures (REE + Y) of Eoarchaean chemical sedimentary rocks from southern West Greenland, and their corruption during high-grade metamorphism. Contrib Minerl Petrol 155, 229-246.
Fujimaki, H., Tatsumoto, M., Aoki, K.-I., 1984. Partition coefficients of Hf, Zr, and REE between phenocrysts and groundmasses. *Proceedings of the fourteenth lunar and planetary science conference, part 2.* Journal of geophysical research 89, B662-B672.
Fulignati, P., Gioconda, A., Sbrana, A., 1999. Rare-earth element (REE) behaviour in the alteration facies of the active magmatic-hydrothermal system of Vulcano (Aeolian Islands, Italy). Journal of Volcanology and Geothermal Research 88, 325-342.
Gamble, J.A., Smith, I.E.M., McCulloch, M.T., Graham, I.J., Kokelaar, B.P., 1993. The geochemistry and petrogenesis of basalts from the Taupo Volcanic Zone and Kermadec Island Arc, S.W. Pacific. Journal of Volcanology and Geothermal Research 54, 265-290.
Gamble, J.A., Wood, C.P., Price, R.C., Smith, I.E.M., Stewart, R.B., Waight, T., 1999. A fifty year perspective of magmatic evolution on Ruapehu Volcano, New Zealand: verification of open system behaviour in an arc volcano. Earth and Planetary Science Letters 170, 301-314.
Gammons, C.H., Wood, S.A., Pedrozo, F., Varekamp, J.C., Nelson, B.J., Shope, C.L., Baffico, G., 2005. Hydrogeochemistry and rare earth element behaviour in a volcanically acidified watershed in Patagonia, Argentina. Chemical Geology 222, 249-267.
Geochemical Earth Reference Model (GERM). http://earthref.org/GERM/. Accessed in September 2011.
Georoc. http://georoc.mpch-mainz.gwdg.de/georoc/Entry.html. Accessed in October 2010.
Gimeno Serrano, M.J., Auqué Sanz, L.F., Nordstrom, D.K., 2000. REE speciation in low-temperature acidic waters and the competitive effects of aluminium. Chemical Geology 165 167-180.
Gromet, L.P., Silver, L.T., 1983. Rare earth element distributions among minerals in a granodiorite and their petrogenetic implications. Geochimica et Cosmochimica Acta 47, 925-939.
Guichard, F., Church, T.M., Treuil, M., Jaffrezic, H., 1979. Rare earths in barites: distribution and effects on aqueous partitioning. Geochimica et Cosmochimica Acta 43, 983-997.

Handley, H.K., MacPherson, C.G., Davidson, J.P., Berlo, K., Lowry, D., 2007. Constraining Fluid and Sediment Contributions to Subduction-Related Magmatism in Indonesia: Ijen Volcanic Complex. Journal of Petrology 48, 1155-1183.
Hannigan, R.E., 2005. Rare earth, major, and trace element geochemistry of surface and geothermal waters from the Taupo Volcanic Zone, North Island New Zealand. In: Johannesson, K.H. (eds.) Rare earth elements in groundwater flow systems. Water Science and Technology Library. Volume 51 Springer, Dordrecht, The Netherlands, pp 67-88.
Hanson, G.N., 1980. Rare earth elements in petrogenetic studies of igneous systems. Annual Review Earth Planet Sci. 8, 371-406.
Heaman, L.M., 2009. The application of U-Pb geochronology to mafic, ultramafic and alkaline rocks: An evaluation of three mineral standards. Chemical Geology 261, 43-52.
Karakaya, N., 2009. REE and HFS elements behaviour in the alteration facies of the Erenler Dağı Volcanics (Konya, Turkey) and kaolinite occurrence. Journal of Geochemical Exploration 101, 185-208.
Karimzadeh Somarin, A., Lentz, D.R., 2008. Mineralogy, geochemistry and fluid evolution of a fossil hydrothermal system in the Paleogene Mendejin volcanic sequence, East Azarbaijan, Iran. Miner Petrol 94, 123-143.
Kempter, K.A., Benner, S.G., Williams, S.N., 1996. Rincón de la Vieja volcano, Guanacaste province, Costa Rica: geology of the southwestern flank and hazards implications. Journal of Volcanology and Geothermal Research 71, 109-127.
Kempter, K.A., Rowe, G.L., 2000. Leakage of Active Crater lake brine through the north flank at Rincón de la Vieja volcano, northwest Costa Rica, and implications for crater collapse. Journal of Volcanology and Geothermal Research 97, 143-159.
Kersting, A.B., Arculus, R.J., 1995. Pb isotope composition of Klyuchevskoy volcano, Kamchatka and North Pacific sediments: Implications for magma genesis and crustal recycling in the Kamchatkan arc. Earth and Planetary Science Letters 136, 133-148.
Kikawada, Y., Uruga, M., Oi, T., Honda, T., 2004. Mobility of lanthanides accompanying the formation of alunite group minerals. Journal of Radioanalytical and Nuclear Chemistry 261 651-659.
Klemme, S., Prowatke, S., Hametner, K., Günter, D., 2005. Partitioning of trace elements between rutile and silicate melts: Implications for subduction zones. Geochimica et Cosmochimica Acta 69, 2361-2371.
Lewis, A.J., Palmer, M.R., Sturchio, N.C., Kemp, A.J., 1997. The rare earth element geochemistry of acid-sulphate-chloride geothermal systems from Yellowstone National Park, Wyoming, USA. Geochimica et Cosmochimica Acta 61, 695-706.
Lewis, A.J., Komninou, A., Yardley, B.W.D., Palmer, M.R., 1998. Rare earth element speciation in geothermal fluids from Yellowstone National Park, Wyoming, USA. Geochimica et Cosmochimica Acta 62, 657-663.
Leybourne, M.I., Goodfellow, W.D., Boyle, D.R., Hall, G.M., 2000. Rapid development of negative Ce anomalies in surface waters and contrating REE patterns in groundwaters associated with Zn-Pb massive sulphide deposits. Applied Geochemistry 15, 695-723.
Leybourne, M.I., Johannesson, K.H., 2008. Rare earth elements (REE) and yttrium in stream waters, stream sediments, and Fe-Mn oxyhydroxides: Fractionation, speciation, and controls over REE + Y patterns in the surface environment. Geochimica et Cosmochimica Acta 72, 5962-5983.
Lottermoser, B.G., 1990. Rare-earth element and heavy-metal behaviour associated with the epithermal gold deposit on Lihir Island, Papua New Guinea. Journal of Volcanology and Geothermal Research 40, 269-289.
Luhr, J.F., Carmichael, I.S.E., Varekamp, J.C., 1984. The 1982 eruptions of El Chichón volcano, Chiapas, Mexico: mineralogy and petrology of the anhydrite-bearing pumices. Journal of Volcanology and Geothermal Research 23, 69-108.

Luhr, J.F., 2008. Primary igneous anhydrite: Progress since its recognition in the 1982 El Chichón trachyandesite. Journal of Volcanology and Geothermal Research 175, 394-407.
Martínez Cruz, M., 2008. Geochemical evolution of the acid crater lake of Poás volcano *Insights into volcanic-hydrothermal processes*. PhD thesis Utrecht University, 162 pp.
Mayanovic, R.A., Anderson, A.J., Bassett, W.A., Chou, I.M., 2007. On the formation and structure of rare-earth element complexes in aqueous solutions under hydrothermal conditions with new data on gadolinium aqua and chloro complexes. Chemical Geology 239, 266-283.
McLennan, S.M., 1994. Rare earth element geochemistry and the "tetrad" effect. Geochimica et Cosmochimica Acta 58, 2025-2033.
Meen, J.K., 1990. Negative Ce anomalies in Archean amphibolites and Laramide granitoids, southwestern Montana, U.S.A.. Chemical Geology 81, 191-207.
Merten, D., Büchel, G., 2004. Determination of Rare Earth Elements in Acid Mine Drainage by Inductively Coupled Plasma Mass Spectrometry. Microchimica Acta 148, 163-170.
Michard, A., Albarède, F., 1986. The REE content of some hydrothermal fluids. Chemical Geology 55, 51-60.
Michard, A., 1989. Rare earth element systematics in hydrothermal fluids. Geochimica et Cosmochimica Acta 53, 745-750.
Monecke, T., Kempe, U., Monecke, J., Sala, M., Wolf, D., 2002. Tetrad effect in rare earth element distribution patterns: A method of quantification with application to rock and mineral samples from granite-related metal deposits. Geochimica et Cosmochimica Acta 66, 1185-1196.
Moore, J.N., Allis, R.G., Nemčok, M., Powell, T.S., Bruton, C.J., Wannamaker, P.E., Raharjo, I.B., Norman, D.I., 2008. The evolution of volcano-hosted geothermal systems based on deep wells from Karaha-Telaga Bodas, Indonesia. American Journal of Science 308, 1-48.
Morgan, L.A., Shanks III, W.C.P., Pierce, K.L., 2009. Hydrothermal processes above the Yellowstone magma chamber: Large hydrothermal systems and large hydrothermal explosions. Geological Society of America Special Papers 459, 1-95.
Morton-Bermea, O., Aurora Armienta, M., Ramos, S., 2010. Rare-earth element distribution in water from El Chichón Volcano Crater Lake, Chiapas Mexico. Geofísica Internacional 49, 43-54.
Négrel, P., Guerrot, C., Cocherie, A., Azaroual, M., Brach, M., Fouillac, C., 2000. Rare earth elements, neodymium and strontium isotopic systematics in mineral waters: evidence from the Massif Central, France. Applied Geochemistry 15, 1345-1367.
Ogawa, Y., Shikazono, N., Ishiyama, D., Sato, H., Mizuta, T., Nakano, T., 2007. Mechanisms for anhydrite and gypsum formation in the Kuroko massive sulfide-sulfate deposits, north Japan. Mineralium Deposita 42. 219-233.
Ohba, T., Hirabayashi, J., Nogami, K., 2008. Temporal changes in the chemistry of lake water within Yugama Crater, Kusatsu-Shirane Volcano, Japan: Implications for the evolution of the magmatic hydrothermal system. Journal of Volcanology and Geothermal Research 178, 131-144.
Ohta, A., Kawabe, I., 2001. REE(III) adsorption onto Mn dioxide (δ-MnO_2) and Fe oxyhydroxide: Ce(III) oxidation by δ-MnO_2. Geochimica et Cosmochimica Acta 65, 695-703.
Okada, T., Ehara, Y., Ogawa, M., 2007. Adsorption of Eu^{3+} to smectites and fluoro-tetrasilicic mica. Clay and Clay Minerals 55, 348-353.
OVSICORI. Open report, OVSICORI-UNA. http://www.ovsicori.una.ac.cr/vulcanologia/estado_volcanes.htm#. Accessed in February 2010.

Palmer, S.C.J., van Hisnberg, V.J., McKenzie, J.M., Yee, S., 2011. Characterization of acif river dilution and associated trace element behaviour through hydrogeochemical modelling: A case study of the Banyu Pahit River in East Java, Indonesia. Applied Geochemistry 26, 1802-1810.
Parsapoor, A., Khalili, M., Mackizadeh, M.A., 2009. The behaviour of trace and rare earth elements (REE) during hydrothermal alteration in the Rangan area (Central Iran). Journal of Asian Earth Sciences 34, 123-134.
Pasternack, G.B., Varekamp, J.C., 1994. The geochemistry of the Keli Mutu crater lakes, Flores, Indonesia. Geochemical Journal 28, 243-262.
Pasternack, G.B., Varekamp, J.C., 1997. Volcanic lake systematics I. Physical constraints. Bulletin of Volcanology 58, 528-538.
Peiffer, L., Taran, Y.A., Lounejeva, E., Solís-Pichardo, G., Rouwet, D., Bernard-Romero, R.A., 2011. Tracing thermal aquifers of El Chichón volcano-hydrothermal system (México) with $^{87}Sr/^{86}Sr$, Ca/Sr and REE. Journal of Volcanology and Geothermal Research 205, 55-66.
Philpotts, J.A., Schnetzler, C.C., 1968. Europium anomalies and the genesis of basalt. Chemical Geology 3, 5-13.
Piasecki, W., Sverjensky, D.A., 2008. Speciation of adsorbed yttrium and rare earth elements on oxide surfaces. Geochimica et Cosmochimica Acta 72, 3964-3979.
Prasad., M.B.K., Ramanathan, A., 2008. Distribution of Rare Earth Elements in the Pichavaram Mangrove Sediments of the Southeast Coast of India. Journal of Coastal Research 24, 126-134.
Prosser, J.T. and Carr, M.J., 1987. Poás volcano, Costa Rica: Geology of the summit region and spatial and temporal variations among the most recent lavas. Journal of Volcanology and Geothermal Research 33, 131-146.
Protano, G., Riccobono, F., 2002. High contents of rare earth elements (REEs) in stream waters of a Cu-Pb-Zn mining area. Environmental Pollution 117, 499-514.
Risacher, F., Alonso, H., Salazar, C., 2002. Hydrochemistry of two adjacent acid saline lakes in the Andes of northern Chile. Chemical Geology 187, 39-57.
Rouwet, D., Bellomo, S., Brusca, L., Inguaggiato, S., Jutzeler, M., Mora, R., Mazot, A., Bernard, R., Cassidy, M., Taran, Y., 2009. Major and trace element geochemistry of El Chichón volcano-hydrothermal system (Chiapas, México) in 2006-2007: implications for future geochemical monitoring. Geofísica Internacional 48, 55-72.
Sanada, T., Takamatsu, N., Yoshiike, Y., 2006. Geochemical interpretation of long-term variations in rare earth element concentrations in acidic hot spring waters from the Tamagawa geothermal area, Japan. Geothermics 35, 141-155.
Sapozhnikova, L.N., Moroshkin, V.V., Zhukova, I.A., 2007. Luminescence of Eu^{2+} in Feldspars from Muscovite Pegmatites. Geology of Ore Deposits 49, 565-572.
Scheepers, R., Rozendaal, A., 1993. Redistribution and fractionation of U, Th and rare-earth elements during weathering of subalkaline granites in SW Cape Province, South Africa. Journal of African Earth Sciences 17, 41-50.
Schönenberger, J., Köhler, J., Markl, G., 2008. REE systematics of fluorides, calcite and siderite in peralkaline plutonic rocks from the Gardar Province, South Greenland. Chemical Geology 247, 16-35.
Shaw, D.M., 1970. Trace element fractionation during anatexis. Geochimica et Cosmochimica Acta 34, 237-243.
Sholkovitz, E.R., 1995. The Aquatic Chemistry of Rare Earth Elements in Rivers and Estuaries. Aquatic Geochemistry 1, 1-34.
Smedley, P.L., 1991. The geochemistry of rare earth elements in groundwater from the Carnmenellis area, southwest England. Geochimica et Cosmochimica Acta 55, 2767-2779.

Soto, G.J., Alvarado, G.E., Goold, S., 2003. Erupciones < 3800 a.P. del volcán Rincón de la Vieja, Costa Rica. Revista Geológica de América Central 29, 67-86.
Sriwana, T., van Bergen, M.J., Varekamp, J.C., Sumarti, S., Takano, B., van Os, B.J.H., Leng, M.J., 2000. Geochemistry of the acid Kawah Putih lake, Patuha Volcano, West Java, Indonesia. Journal of Volcanology and Geothermal Research 97, 77-104.
Stimac, J.A., Goff, F., Counce, D., Larocque, A.C.L., Hilton, D.R., Morgenstern, U., 2004. The crater lake and hydrothermal system of Mount Pinatubo, Philippines: evolution in the decade after eruption. Bulletin of Volcanology 66, 149-167.
Sun, S.-s., McDonough, W.F., 1989. Chemical and isotopic systematics of oceanic basalts: implications for mantle composition and processes. In: Saunders, A.D., Norry, M.J., (eds.), 1989. *Magmatism in the Ocean Basins*. Geological Society Special Publication 42, 313-345.
Sverjensky, D.A., 1984. Europium redox equilibria in aqueous solution. Earth and Planetary Science Letters 67, 70-78.
Takano, B., Fazlullin, S.M., Delmelle, P., 2000. Analytical laboratory comparison of major and minor constituents in an active crater lake. Journal of Volcanology and Geothermal Research 97, 497-508.
Takano, B., Suzuki, K., Sugimori, K., Ohba, T., Fazlullin, S.M., Bernard, A., Sumarti, S., Sukhyar, R., Hirabayashi, M., 2004. Bathymetric and geochemical investigation of Kawah Ijen Crater Lake, East Java, Indonesia. Journal of Volcanology and Geothermal Research 135 299-329.
Tang, J., Johannesson, K.H., 2005. Adsorption of rare earth elements onto Carrizo sand: Experimental investigations and modeling with surface complexation. Geochimica et Cosmochimica Acta 69, 5247-5261.
Taran, Y., Fischer, T.P., Pokrovsky, B., Sano, Y., Aurora Armienta, M., Macias, J.L., 1998. Geochemistry of the volcano-hydrothermal system of El Chichón Volcano, Chiapas, Mexico. Bulletin of Volcanology 59, 436-449.
Taran, Y., Rouwet, D., Inguaggiato, S., Aiuppa, A., 2008. Major and trace element geochemistry of neutral and acidic thermal springs at El Chichón volcano, Mexico Implications for monitoring of the volcanic activity. Journal of Volcanology and Geothermal Research 178, 224-236.
Tassi, F., Vaselli, O., Capaccioni, B., Macias, J.L., Nencetti, A., Montegrossi, G., Magro, G., 2003. Chemical composition of fumarolic gases and spring discharges from El Chichòn volcano, Mexico: causes and implications of the changes detected over the period 1998-2000. Journal of Volcanology and Geothermal Research 123, 105-121.
Tassi, F., Vaselli, O., Capaccioni, B., Giolito, C., Duarte, E., Fernandez, E., Minissale, A., Magro, G., 2005. The hydrothermal-volcanic system of Rincon de la Vieja volcano (Costa Rica): A combined (inorganic and organic) geochemical approach to understanding the origin of the fluid discharges and its possible application to volcanic surveillance. Journal of Volcanology and Geothermal Research 148, 315-333.
Tassi, F., Vaselli, O., Fernandez, E., Duarte, E., Martínez, M., Delgado Huertas, A., Bergamaschi, F., 2009. Morphological and geochemical features of crater lakes in Costa Rica: an overview. Journal of Limnology 68, 193-205.
Taylor, S.R., McLennan, S.M., 1985. The continental crust: its composition and evolution. Blackwell, Oxford, 312 pp.
Thouret, J.-C., Abdurachman, K.E., Bourdier, J.-L., Bronto, S., 1998. Origin, characteristics, and behaviour of lahars following the 1990 eruption of Kelud volcano, eastern Java (Indonesia). Bulletin of Volcanology 59, 460-480.
Tweed, S.O., Weaver, T.R., Cartwright, I., Schaefer, B., 2006. Behavior of rare earth elements in groundwater during flow and mixing in fractured rock aquifers: An example from the Dandenong Ranges, southeast Australia. Chemical Geology 234, 291-307.

Van Hinsberg, V., Berlo, K., van Bergen, M., Williams-Jones, A., 2010. Extreme alteration by hyperacidic brines at Kawah Ijen volcano, East Java, Indonesia: I. Textural and mineralogical imprint. Journal of Volcanology and Geothermal Research 198, 253-263.
Van Wijk de Vries, B., Grosse, P., Alvarado, G.E., 2007. Chapter 4: Volcanism and volcanic landforms. 123–154. In: Bundschuh, J. and Alvarado, G.E., editors. Central America: geology, resources, hazards, volume 1. Taylor & Francis/Balkema Leiden, The Netherlands.
Varekamp, J.C., Pasternack, G.B., Rowe, G.L., 2000. Volcanic lake systematics II. Chemical constraints. Journal of Volcanology and Geothermal Research 97, 161-179.
Varekamp, J.C., Ouimette, A.P., Herman, S.W., Bermúdez, A., Delpino, D., 2001. Hydrothermal element fluxes from Copahue, Argentina: A "beehive" volcano in turmoil. Geology 29, 1059-1062.
Varekamp, J.C., deMoor, J.M., Merrill, M.D., Colvin, A.S., Goss, A.R., Vroon, P.Z., Hilton, D.R., 2006. Geochemistry and isotopic characteristics of the Caviahue-Copahue volcanic complex, Province of Neuquén, Argentina. Geological Society of America Special Papers 407, 317-342.
Varekamp, J.C., Ouimette, A.P., Herman, S.W., Flynn, K.S., Bermudez, A., Delpino, D., 2009. Naturally acid waters from Copahue volcano, Argentina. Applied Geochemistry 24, 208-220.
Veksler, I.V., Dorfman, A.M., Kamenetsky, M., Dulski, P., Dingwell, D.B., 2005. Partitioning of lanthanides and Y between immiscible silicate and fluoride melts, fluorite and cryolite and the origin of the lanthanide tetrad effect in igneous rocks. Geochimica et Cosmochimica Acta 69, 2847-2860.
Venzke, E., Wunderman, R.W., McClelland, L., Simkin, T., Luhr, J.F., Siebert, L., Mayberry, G. (eds.) (2002-). Global Volcanism, 1968 to the present. Smithsonian Institution, Global Volcanism Program Program Digital Information Series, GVP-4 (http://www.volcano.si.edu/reports/). Accessed in August 2011.
Verplanck, P.L., Nordstrom, D.K., Taylor, H.E., Kimball, B.A., 2004. Rare earth elements partitioning between hydrous ferric oxides and acid mine water during iron oxidation. Applied Geochemistry 19, 1339-1354.
Welch, S.A., Christy, A.G., Kirste, D., Beavis, S.G., Beavis, F., 2007. Jarosite dissolution I – Trace cation flux in acid sulfate soils. Chemical Geology 245, 183-197.
Welch, S.A., Christy, A.G., Isaacson, L., Kirste, D., 2009. Mineralogical control of rare earth elements in acid sulfate soils. Geochimica et Cosmochimica Acta 73, 44-64.
Weyl, R., 1980. Geology of central America. *Second, completely revised edition*. Gebrüder Borntraeger Berlin Stuttgart.
Whitford, D.J., Korsch, M.J., Porritt, P.M., Craven, S.J., 1988. Rare-earth element mobility around the volcanogenic polymetallic massive sulfide deposit at Que river, Tasmania, Australia. Chemical Geology 68, 105-119.
Yan, X.P., Kerrich, R., Hendry, M.J., 1999. Sequential leachates of multiple grain size fractions from a clay-rich till, Saskatchewan, Canada: implications for controls on the rare earth element geochemistry of porewaters in an aquitard. Chemical Geology 158, 53-79.

A. Appendix

A1 ICP analysis (UU) in ppm

Poás

Sample date	Temp (^oC)	pH	Conductivity ($mScm^{-1}$)	Volume (m^3x1000)	Depth (m)	SO_4 (a)	S (b)	Cl (a)	Cl (b)	F (a)	Br (a)
28-Feb-06	51	0.591	158	-	-	17680	8120	13400	13900	990	31.7
01-Apr-06	54	0.63	120.2	1521.926	41.8	17200	6910	15700	15100	1050	32.3
25-Apr-06	54	0.74	94.2	-	-	13820	5720	13000	13800	990	26.9
03-May-06	49	0.74	118	1496.105	41.4	17670	6900	15100	15800	1150	30.6
25-May-06	47	0.72	123.1			19510	6870	15900	16400	1130	32.6
22-Jun-06	46	0.59	132.5	1499.037	41.47	23150	7680	16300	16400	1090	31.7
20-Jul-06	43	0.62	121.4	-	-	21280	7450	13400	14900	890	-
11-Aug-06	43	0.52	144	-	-	25440	8210	16100	16100	1100	-
05-Sep-06	41	0.47	159.8	-	-	27540	8890	17100	16800	1100	-
05-Sep-06	41	-	-	-	-	-	8920	-	16500	-	-
05-Oct-06	46	0.4	162.5	1489.646	41.38	28400	9410	16700	17000	1140	-
12-Oct-06	55	0.46	158.8	-	-	29000	9030	16300	15800	1170	-
28-Oct-06	53	0.5	157.6	-	-	24930	9100	13600	16000	740	31
02-Nov-06	58	0.43	180.4	-	-	29100	11000	13200	17600	950	-
10-Nov-06	57	0.4	-	-	-	34330	11300	13200	18000	1030	35
08-Dec-06	48	0.47	187	1444.519	40.6	33950	11500	14900	17900	1100	30
02-Feb-07	49	0.4	218	1396.361	39.8	44300	14200	17500	20200	1300	45
13-Feb-07	48	0.4	216	-	-	-	14000	-	19800	-	-
27-Feb-07	48	0.42	230	-	-	-	14300	-	20300	-	-
13-Mar-07	47	0.39	237	1385.28	39.6	-	14900	-	20600	-	-
27-Mar-07	49	0.36	246	-	-	-	15300	-	21200	-	-
13-Apr-07	51	0.34	260	-	-	53000	16000	20400	21700	1500	42
30-May-07	57	0.25	290	-	-	50900	17900	18700	23200	1400	40
12-Jun-07	58	0.28	302	1121.221	34.6	-	18600	-	24000	-	47
27-Jun-07	55	0.13	313	-	-	67300	19500	23900	24900	1530	-

Sample date	Temp (°C)	pH	Conductivity ($mScm^{-1}$)	Volume (m^3x1000)	Depth (m)	SO_4 (a)	S (b)	Cl (a)	Cl (b)	F (a)	Br (a)
29-Aug-07	58	0.21	354	-	-	84400	21100	36000	26200	1500	53
12-Sep-07	56	0.16	371	-	-	98300	21700	40300	27800	1800	61
27-Sep-07	56	0.22	311	-	-	98900	21900	40800	27600	1750	64
26-Oct-07	58	0.15	375	-	-	84500	22300	30300	28100	1850	60
06-Nov-07	57	0.16	385	-	-	73000	23000	26100	28500	1700	40
22-Nov-07	56	0.25	339	-	-	72540	19600	25600	23300	1740	85
18-Jan-08	45	0.28	313	-	-	67950	18400	23870	22100	1630	55
29-Jan-08	41	0.26	314	-	-	67580	18300	23450	21400	1540	35
12-Feb-08	45	0.21	324	-	-	72000	19100	25500	22800	1700	55
11-Mar-08	42	0.3	334	910	26	68800	19600	25200	23900	1640	47
05-May-08	41	0.23	348	833	23	87700	20600	36300	25200	1650	45
04-Jun-08	42	0.16	323	-	-	75200	18500	31300	22500	1450	80
15-Jul-08	45	0.2	301	919.58	24.2	65400	17300	27900	21400	1360	70
31-Jul-08	34	0.34	229	-	-	49500	13100	20700	15900	1100	20
03-Oct-08	44	0.29	264	898	23.7	-	15900	-	19100	-	-
11-Nov-08	43	0.12	255	-	-	41100	14600	18700	17600	960	-
09-Dec-08	39	0.14	152.7	-	-	23300	8320	10200	9880	540	-
29-Jan-09	44	-0.03	176.8	-	-	-	9900	-	11600	-	-
11-Feb-09	38	0.15	121.9	817.72	23.8	-	6790	-	7810	-	-
25-Feb-09	40			-	-	-	9830	-	11500	-	-
04-Mar-09	40	-0.57	176.7	-	-	-	9890	-	11500	-	-
19-Mar-09	44	-0.61	185.2	-	-	-	10500	-	12100	-	-
25-Mar-09	44	-0.59	187.3	-	-	-	10700	-	12400	-	-
03-Apr-09	49	-0.62	195.7	-	-	-	11000	-	12800	-	-

(a): IC analysis (OVSICORI) in mg/kg
(b): ICP analysis (UU) in ppm

Sample date	Al	Fe	Ca	Mg	Na	K	Si	Mn	P	Sc	Ti	Zn	Sr
28-Feb-06	1490	1120	1430	370	400	140	52	22.6	8.5	0.46	1.5	1.93	11.7
01-Apr-06	2470	1440	1310	560	610	210	52	23.7	15	0.69	5.5	2.87	15.2
25-Apr-06	2360	1410	1250	780	670	210	66	30.3	13	0.63	1.98	2.91	13.1
03-May-06	2860	1530	1220	610	750	270	57	27	18	0.77	2.18	3.32	16.4
25-May-06	2890	1520	1150	660	740	280	47	27.9	17	0.77	1.74	3.15	15.8
22-Jun-06	2770	1500	1180	640	750	270	64	28.7	17	0.77	1.35	3.22	15.4
20-Jul-06	2410	1340	1240	580	590	230	55	23.5	14	0.65	1.36	2.54	12.9
11-Aug-06	2540	1390	1180	620	710	240	62	26.9	15	0.72	1.18	2.97	14.2
05-Sep-06	2540	1330	1170	580	690	250	52	25.4	16	0.7	1.22	2.86	14
05-Sep-06	2560	1340	1170	580	700	260	53	25.7	16	0.7	1.21	2.94	14.3
05-Oct-06	2790	1400	1160	620	710	280	61	26.5	17	0.73	1.48	2.96	14.6
12-Oct-06	2780	1320	1080	600	710	280	44	26.1	17	0.74	1.37	2.93	14.9
28-Oct-06	2830	1400	1050	680	750	290	44	28.8	17	0.79	1.13	3.07	15.5
02-Nov-06	3190	1420	1110	640	800	340	52	27.9	20	0.84	1.24	3.3	17.4
10-Nov-06	3210	1440	1080	630	780	350	39	27.3	20	0.82	1.24	3.27	17.3
08-Dec-06	3110	1390	1050	620	770	330	42	27	20	0.83	1.43	3.19	17
02-Feb-07	3420	1520	1060	680	820	380	40	28.7	22	0.89	1.72	3.32	18
13-Feb-07	3320	1480	1010	660	830	370	39	29	23	0.89	1.73	3.38	18.2
27-Feb-07	3310	1470	1020	680	810	370	38	28.5	22	0.88	1.8	3.29	17.6
13-Mar-07	3350	1500	1020	680	830	370	37	29.1	22	0.89	1.88	3.31	18
27-Mar-07	3360	1510	1010	680	830	370	37	29.6	23	0.89	2.09	3.37	18.1
13-Apr-07	3420	1530	1000	710	850	380	36	30.1	23	0.91	2.17	3.41	18.3
30-May-07	3460	1570	980	700	850	390	34	30.1	24	0.92	2.87	3.44	18.1
12-Jun-07	3530	1600	970	720	870	390	33	30.7	24	0.93	2.84	3.52	18.4
27-Jun-07	3560	1630	940	740	860	400	31	30.4	23	0.93	3.09	3.49	18.2
29-Aug-07	3430	1630	900	740	840	390	33	30.4	23	0.92	4.02	3.48	17.5
12-Sep-07	3480	1650	920	730	820	400	31	29.8	23	0.89	4.05	3.46	17.5
27-Sep-07	3470	1640	910	730	800	390	31	28.5	22	0.86	4.08	3.33	17
26-Oct-07	3370	1610	890	740	760	380	29	27.6	21	0.83	4.23	3.26	15.9

Sample date	Al	Fe	Ca	Mg	Na	K	Si	Mn	P	Sc	Ti	Zn	Sr
06-Nov-07	3420	1610	890	730	760	390	30	28.3	22	0.84	4.37	3.26	16.1
22-Nov-07	2860	1370	940	610	640	320	32	23.4	18	0.71	3.81	2.73	13.7
18-Jan-08	2660	1260	960	580	650	300	36	23.9	18	0.72	3.58	2.64	14.5
29-Jan-08	2610	1250	970	580	630	290	41	23.3	17	0.7	3.52	2.8	14.1
12-Feb-08	2740	1300	950	590	660	310	36	24.5	18	0.74	3.82	2.71	14.8
11-Mar-08	2800	1340	970	620	670	320	35	24.9	18	0.74	3.92	2.73	15.3
05-May-08	2910	1390	990	650	710	330	36	26.2	20	0.8	4.67	2.88	16
04-Jun-08	2620	1250	1020	580	630	300	38	23.5	17	0.7	4.55	2.59	14.3
15-Jul-08	2440	1170	1050	540	580	270	39	21.5	16	0.65	4.27	2.33	13.5
31-Jul-08	1800	900	1100	420	440	200	58	16.9	12	0.5	3.18	1.73	10.7
03-Oct-08	2130	1020	1080	480	500	240	45	18.9	14	0.58	3.49	1.98	12.2
11-Nov-08	1920	930	1110	440	440	210	53	16.6	12	0.5	2.97	1.76	11.1
09-Dec-08	1100	530	1030	260	270	120	58	10.1	7.1	0.32	1.68	1.03	7.56
29-Jan-09	1320	620	1060	300	320	150	63	12.2	8.7	0.38	1.52	1.23	9.86
11-Feb-09	870	410	1010	200	220	94	80	8.11	5.9	0.28	1.01	0.84	7.08
25-Feb-09	1240	590	1080	290	280	130	59	11	7.8	0.35	1.25	1.12	9.01
04-Mar-09	1220	580	1110	280	300	130	67	11.6	8.2	0.37	1.27	1.17	9.65
19-Mar-09	1250	590	1170	280	310	130	68	11.7	8.2	0.37	1.29	1.19	9.96
25-Mar-09	1270	600	1200	290	310	140	65	11.6	8.3	0.37	1.35	1.19	9.96
03-Apr-09	1290	610	1100	290	310	140	66	11.7	8.3	0.37	1.3	1.2	9.87

Rincón de la Vieja

Sample date	Temp (°C)	pH	S (b)	Cl (b)	Al	Fe	Ca	Mg	Na	K	Si
15-Oct-08	37	-	8850	19700	3110	1630	1330	680	670	380	49
08-Nov-07	43	0.53	8980	20900	4000	2200	1110	870	830	470	44
18-Apr-07	45	-	9360	22200	4220	2210	1150	890	870	520	41
12-Sep-06	39	0.38	9330	21500	3430	1860	1240	710	710	420	39
22-Mar-06	36	0.47	8690	18800	3070	1670	1260	690	680	390	44
02-Jun-05	41	0.44	10100	21900	3830	2040	1180	790	810	510	40
02-May-04	36	0.35	11500	24800	4730	2450	1130	930	960	660	36

Sample date	Mn	P	Sc	Ti	Zn	Sr
15-Oct-08	28.4	26	0.94	2.33	4.25	12.8
08-Nov-07	36.2	34	1.22	1.89	5.3	14.5
18-Apr-07	36.3	37	1.25	2.38	5.48	16.4
12-Sep-06	29.3	30	1.03	2.52	4.79	14.4
22-Mar-06	28.5	27	0.94	2.53	4.33	13.6
02-Jun-05	32	34	1.1	2.02	5.03	15.5
02-May-04	36.8	43	1.32	1.92	5.86	17.5

A2 ICP-MS analysis (UU) in ppb

Poás Sample date	Temp (°C)	pH	Li	Be	B	V	Cr	Co	Ni	Cu	Ga	As	Se	Rb	Y	Zr	Nb	Mo
28-Feb-06	51	0.591	210	11	5660	4280	77000	880	36300	680	280	1290	110	370	270	260	27	350
01-Apr-06	54	0.63	270	19	6640	6300	320	320	140	370	450	2710	160	620	300	330	0.46	15
25-Apr-06	54	0.74	300	20	6040	6350	310	250	110	290	390	2240	110	590	240	190	0.38	5.7
03-May-06	49	0.74	300	22	7370	7950	390	330	140	380	530	2860	130	770	300	300	0.58	9.5
25-May-06	47	0.72	310	22	7740	7810	350	330	150	370	530	2760	150	800	270	310	0.54	8
22-Jun-06	46	0.59	300	22	7640	7870	380	350	150	430	490	2750	180	780	300	360	0.56	9.6
20-Jul-06	43	0.62	260	19	6660	6350	310	280	130	540	420	2390	87	660	210	300	0.49	10
11-Aug-06	43	0.52	290	20	7200	7270	340	330	140	470	440	2890	94	700	300	360	0.57	11
05-Sep-06	41	0.47	280	21	7620	7330	340	300	130	500	460	2890	170	740	270	410	0.76	11
05-Sep-06	41	-	290	21	7790	7010	360	310	130	490	460	2900	93	730	280	400	0.47	11
05-Oct-06	46	0.4	300	22	8040	7460	360	310	140	480	520	2990	130	780	240	450	0.56	23
12-Oct-06	55	0.46	280	22	7320	7430	370	300	140	480	510	2910	210	750	280	430	0.57	13
28-Oct-06	53	0.5	310	23	7340	8150	380	340	150	510	520	3150	89	760	250	440	0.7	15

Sample date	Temp (°C)	pH	Li	Be	B	V	Cr	Co	Ni	Cu	Ga	As	Se	Rb	Y	Zr	Nb	Mo
02-Nov-06	58	0.43	320	24	8430	8240	450	330	150	560	610	3490	180	880	270	550	0.88	19
10-Nov-06	57	0.4	310	24	8600	8650	420	320	140	590	600	3580	210	860	260	560	0.71	21
08-Dec-06	48	0.47	320	24	8650	8510	430	350	150	1420	640	4340	120	880	250	550	1	100
02-Feb-07	49	0.4	330	24	9200	8810	450	350	160	860	630	3690	240	900	270	670	0.87	18
13-Feb-07	48	0.4	350	25	9370	8770	460	370	160	850	660	3760	110	930	260	730	1	11
27-Feb-07	48	0.42	330	25	9300	8780	450	370	170	790	650	3370	91	910	280	750	1.3	9.2
13-Mar-07	47	0.39	330	25	10100	8710	460	380	170	790	640	3660	230	910	300	780	2.6	9.6
27-Mar-07	49	0.36	330	25	10300	8570	450	380	170	770	650	3440	180	900	290	810	0.85	7.7
13-Apr-07	51	0.34	320	25	10100	9100	430	350	160	770	660	3680	240	900	300	880	0.83	13
30-May-07	57	0.25	330	27	10900	9150	470	410	180	990	680	3910	220	930	300	1000	1	33
12-Jun-07	58	0.28	330	27	11000	9340	520	420	180	1000	690	3980	290	940	310	1050	1.2	35
27-Jun-07	55	0.13	340	28	11300	9690	520	440	190	1050	690	3990	220	960	310	1120	1.2	36
29-Aug-07	58	0.21	330	27	11500	9130	510	460	200	1210	680	3740	280	900	320	1180	1.4	43
12-Sep-07	56	0.16	320	27	11800	8940	470	470	200	1230	660	3770	320	930	310	1190	1.4	43
27-Sep-07	56	0.22	310	27	11700	9170	510	460	200	1250	660	4120	140	900	350	1220	1.5	43

Sample date	Temp (°C)	pH	Li	Be	B	V	Cr	Co	Ni	Cu	Ga	As	Se	Rb	Y	Zr	Nb	Mo
26-Oct-07	58	0.15	310	25	11600	8850	510	490	220	1330	660	4150	290	890	330	1230	2.1	46
06-Nov-07	57	0.16	310	27	12700	8900	510	480	200	1310	670	4340	300	900	340	1250	1.4	46
22-Nov-07	56	0.25	260	23	11000	7530	410	410	170	1160	560	3630	240	740	300	1070	1.2	40
18-Jan-08	45	0.28	250	22	10700	6890	380	390	160	1150	510	3250	260	690	280	1010	1.4	24
29-Jan-08	41	0.26	240	22	10400	6760	380	390	160	1110	510	2990	220	690	310	1010	0.96	15
12-Feb-08	45	0.21	250	22	10700	7050	400	400	240	850	550	2610	200	720	310	1070	1.3	7.4
11-Mar-08	42	0.3	260	23	11200	7350	410	420	170	500	560	1170	290	740	310	1120	1.2	5.9
05-May-08	41	0.23	260	23	11800	7550	520	520	220	360	600	430	290	770	340	1160	1.6	6.5
04-Jun-08	42	0.16	250	22	11000	6830	390	400	160	290	520	140	260	680	280	1040	1.6	4.9
15-Jul-08	45	0.2	230	20	10500	6160	360	370	150	250	480	280	170	630	270	960	1.5	4.9
31-Jul-08	34	0.34	170	15	7500	4590	270	290	120	280	350	470	220	460	220	710	1.4	4.1
03-Oct-08	44	0.29	210	16	9750	5520	310	330	140	170	450	310	250	570	270	840	1.2	4
11-Nov-08	43	0.12	190	14	9010	4830	290	300	130	160	370	290	170	520	270	760	0.96	3.5
09-Dec-08	39	0.14	110	8.4	5470	2880	170	180	79	160	220	380	170	290	170	420	0.51	2.9
29-Jan-09	44	-0.03	130	10	6490	3450	190	200	94	320	280	1240	120	360	240	490	0.7	5.5

Sample date	Temp (°C)	pH	Li	Be	B	V	Cr	Co	Ni	Cu	Ga	As	Se	Rb	Y	Zr	Nb	Mo
11-Feb-09	38	0.15	90	6.7	4500	2260	180	150	63	300	170	840	82	230	190	320	0.49	4.8
25-Feb-09	40		130	9.3	6260	3230	190	190	85	400	240	1290	130	320	210	460	0.47	8.6
04-Mar-09	40	-0.57	130	9.7	6240	3180	190	190	80	430	240	1380	210	320	230	460	0.48	9.7
19-Mar-09	44	-0.61	140	9.5	6340	3260	190	190	80	480	240	1400	24	320	250	470	1.3	12
25-Mar-09	44	-0.59	140	9.7	6330	3210	190	190	84	490	240	1460	160	330	230	470	0.9	13
03-Apr-09	49	-0.62	140	9.2	6480	3330	200	200	79	570	250	1550	250	330	250	490	1.5	16

Sample date	Ag	Cd	Sn	Sb	Cs	Ba	Bi	Te	Th	U	Hf	Tl	Pb
28-Feb-06	2.2	35	64	9.2	7.8	90	20	0.43	53	20	5.4	260	470
01-Apr-06	3.2	43	27	5.1	13	94	85	0.79	83	33	6.4	270	620
25-Apr-06	1.5	36	11	5	12	100	47	0.47	67	27	3.3	220	510
03-May-06	4.5	45	19	8.4	16	91	88	0.67	89	36	5.2	280	760
25-May-06	2.5	41	25	11	16	65	74	0.79	90	35	5.3	240	670
22-Jun-06	4.8	41	37	16	16	120	80	0.8	88	34	6.2	250	690
20-Jul-06	2.2	32	32	14	13	120	61	1.5	75	29	5.3	190	520
11-Aug-06	2.8	39	43	20	15	140	75	0.77	80	32	6.4	230	610
05-Sep-06	3.2	40	53	26	15	120	88	1.1	82	33	6.3	250	660

Sample date	Ag	Cd	Sn	Sb	Cs	Ba	Bi	Te	Th	U	Hf	Tl	Pb
05-Sep-06	2.8	40	56	26	15	120	88	0.77	81	33	7.4	260	650
05-Oct-06	3.2	39	58	24	16	120	98	1.1	88	34	8.1	260	720
12-Oct-06	3.5	37	58	23	15	56	100	1.4	87	33	7.6	240	680
28-Oct-06	5.4	37	67	26	16	58	110	1.2	90	35	7.9	210	730
02-Nov-06	7.4	43	85	38	17	130	130	1.1	100	37	10	160	890
10-Nov-06	4.6	43	87	47	18	48	130	1.4	100	36	10	290	860
08-Dec-06	5.7	44	100	88	17	68	190	4.6	99	37	10	290	860
02-Feb-07	5.9	45	130	54	18	73	150	1.5	100	38	13	280	910
13-Feb-07	5.7	48	140	53	18	78	160	1.3	110	39	14	310	960
27-Feb-07	5.4	46	140	42	18	79	140	1.2	100	38	14	320	920
13-Mar-07	6.4	48	150	45	18	75	150	1.6	110	38	15	320	980
27-Mar-07	5.9	49	150	45	18	73	150	0.97	110	39	16	370	1030
13-Apr-07	6	50	160	54	18	70	170	1.1	110	40	17	370	1030
30-May-07	7.6	53	190	67	18	67	190	1.2	110	40	19	390	950
12-Jun-07	8.4	55	200	70	19	68	190	1.2	110	40	20	390	1130
27-Jun-07	8	57	210	72	19	67	200	1.3	120	41	22	400	1130

Sample date	Ag	Cd	Sn	Sb	Cs	Ba	Bi	Te	Th	U	Hf	Tl	Pb
29-Aug-07	8.1	58	230	80	19	67	220	1.3	110	39	24	400	1190
12-Sep-07	8	57	230	78	18	64	220	1.4	110	38	24	390	1180
27-Sep-07	8.3	57	230	81	18	62	220	1.3	110	38	24	390	1140
26-Oct-07	9.3	59	240	88	18	62	220	1.6	110	37	24	400	1170
06-Nov-07	9.6	59	250	90	18	63	230	1.1	110	38	25	460	1200
22-Nov-07	7.2	51	210	75	15	69	200	1.3	95	32	22	380	1020
18-Jan-08	6.3	47	200	75	14	88	190	1.1	88	30	20	340	950
29-Jan-08	6.5	46	200	58	14	98	190	1.2	88	29	21	330	950
12-Feb-08	6.3	48	210	38	14	93	170	1.1	92	30	22	340	990
11-Mar-08	6.3	50	210	21	15	81	130	1.1	93	31	23	340	1020
05-May-08	7	51	220	6.1	15	110	110	1.3	94	31	24	350	1080
04-Jun-08	7	47	190	2.6	13	100	81	1.7	84	29	21	310	950
15-Jul-08	6.2	43	180	4.1	12	110	84	1.6	78	26	20	290	880
31-Jul-08	4.8	32	130	6.6	9.1	120	69	2.4	58	20	14	210	650
03-Oct-08	5.2	36	150	3.5	11	130	50	1.2	69	24	18	260	800

Sample date	Ag	Cd	Sn	Sb	Cs	Ba	Bi	Te	Th	U	Hf	Tl	Pb
11-Nov-08	5.5	33	130	3.4	9.8	140	40	1.1	63	22	16	230	720
09-Dec-08	3.8	19	70	4.6	5.5	93	27	0.92	37	13	8.9	130	400
29-Jan-09	5.2	22	77	18	6.6	120	61	0.89	46	16	11	150	500
11-Feb-09	3.4	15	49	14	4.3	120	40	0.79	31	11	6.8	100	340
25-Feb-09	3.2	21	72	23	6.1	92	61	0.78	45	15	10	150	470
04-Mar-09	3.3	21	72	24	6.2	100	61	0.77	44	15	10	160	470
19-Mar-09	3.5	21	74	25	5.3	110	62	0.96	45	15	10	160	470
25-Mar-09	3.5	21	74	25	6.2	110	67	0.96	45	15	10	170	480
03-Apr-09	3.9	22	79	29	6.4	140	70	1.2	45	16	10	180	510

Rincón de la Vieja

Sample date	Temp (°C)	pH	Li	Be	B	V	Cr	Co	Ni	Cu	Ga	As	Se	Rb	Y	Zr	Nb	Mo
15-Oct-08	37	-	540	28	9990	9120	520	370	230	450	580	780	210	880	380	310	0.64	16
08-Nov-07	43	0.53	700	36	11000	11700	700	510	330	660	760	1800	160	1100	420	400	1	19
18-Apr-07	45	-	710	37	11000	12300	740	540	330	640	780	1740	150	1070	520	430	1	14
12-Sep-06	39	0.38	550	29	10600	9780	720	500	610	580	640	760	230	900	390	370	1.1	60
22-Mar-06	36	0.47	530	27	9810	8860	560	450	270	300	580	510	120	830	400	350	0.88	6.7
02-Jun-05	41	0.44	600	29	10900	10700	900	560	460	320	690	1040	170	910	450	420	0.88	4.9
02-May-04	36	0.35	690	34	13200	13200	850	680	410	1500	920	2050	230	1140	540	640	1.1	5.6

Sample date	Ag	Cd	Sn	Sb	Cs	Ba	Bi	Te	Th	U	Hf	Tl	Pb
15-Oct-08	2.3	62	220	5.3	19	130	64	1.8	50	30	6.2	510	940
08-Nov-07	3.8	66	330	14	24	94	160	2.1	67	40	7.7	520	940
18-Apr-07	3	68	270	16	23	89	170	2.2	69	38	8.5	530	1080
12-Sep-06	3.4	64	230	3.3	19	79	47	2	55	31	7.7	520	810
22-Mar-06	2.3	58	180	6.3	17	79	16	1.9	52	28	7.1	450	770
02-Jun-05	3.4	60	230	3.5	18	67	60	2.2	55	30	8.3	510	940
02-May-04	4.7	72	390	11	23	74	160	1.8	65	39	13	630	1100

A3 REE; ICP-MS analysis (UU) in ppb

Poás Sample date	La	Ce	Pr	Nd	Sm	Eu	Gd	Tb	Dy	Ho	Er	Tm	Yb	Lu
28-Feb-06	270	590	75	320	66	21	65	10	56	11	33	4.5	30	4.4
01-Apr-06	290	610	74	320	67	23	72	12	67	14	41	5.9	40	6
25-Apr-06	210	460	52	220	49	17	53	9.2	54	12	36	5.2	36	5.7
03-May-06	250	520	59	250	53	18	62	9.9	58	13	38	5.6	38	6
25-May-06	250	510	58	240	51	17	57	9.6	55	12	37	5.4	38	5.9
22-Jun-06	230	500	54	230	49	16	56	9.3	55	12	37	5.4	37	5.9
20-Jul-06	210	410	45	190	44	15	48	7.9	46	10	31	4.6	31	4.9
11-Aug-06	230	470	53	220	48	16	51	8.6	50	11	34	5	34	5.4
05-Sep-06	240	490	54	220	48	16	51	8.5	50	11	32	4.9	32	4.6
05-Sep-06	250	510	54	230	48	15	50	8.7	49	11	33	4.8	34	5.3
05-Oct-06	240	500	56	230	48	17	55	8.6	50	11	33	5	34	5.3
12-Oct-06	250	490	57	240	48	16	53	8.5	49	10	32	4.8	33	5.2
28-Oct-06	260	520	61	250	51	17	56	9	52	11	34	5.1	35	5.6
02-Nov-06	280	540	61	250	49	16	54	8.8	51	11	34	5	35	5.4
10-Nov-06	290	540	63	260	51	17	53	8.7	51	11	34	5	35	5.4

Sample date	La	Ce	Pr	Nd	Sm	Eu	Gd	Tb	Dy	Ho	Er	Tm	Yb	Lu
08-Dec-06	280	550	62	250	50	16	59	8.7	50	11	33	4.9	34	5.3
02-Feb-07	320	590	67	270	53	17	56	8.9	52	11	34	5.1	36	5.5
13-Feb-07	330	620	69	280	55	18	58	9.3	53	12	35	5.3	37	5.7
27-Feb-07	330	600	68	270	54	18	59	9.2	53	11	34	5.1	36	5.6
13-Mar-07	330	620	71	290	56	18	59	9.5	55	12	35	5.3	36	5.7
27-Mar-07	340	640	71	290	56	18	60	9.5	56	12	36	5.4	37	5.8
13-Apr-07	350	650	73	290	58	19	62	9.6	57	12	37	5.5	38	5.9
30-May-07	370	670	75	300	59	20	64	9.9	59	12	38	5.6	39	6
12-Jun-07	380	690	77	310	61	20	65	10	60	13	39	5.8	40	6.1
27-Jun-07	390	720	80	320	63	20	65	11	62	13	40	6.1	41	6.3
29-Aug-07	390	720	79	330	64	21	68	11	62	13	40	5.9	41	6.3
12-Sep-07	380	710	80	320	65	21	67	11	62	13	40	6	40	6.3
27-Sep-07	400	730	82	330	65	20	67	11	63	13	40	5.9	40	6.2
26-Oct-07	390	720	80	330	65	21	71	11	63	13	40	5.9	39	6.1
06-Nov-07	400	730	82	330	66	21	70	11	65	14	41	6	41	6.3
22-Nov-07	350	650	74	300	60	19	63	9.7	57	12	35	5.1	35	5.4

Sample date	La	Ce	Pr	Nd	Sm	Eu	Gd	Tb	Dy	Ho	Er	Tm	Yb	Lu
18-Jan-08	360	660	75	310	62	20	63	9	49	9.7	34	5.2	34	5.2
29-Jan-08	360	670	77	320	63	20	64	10	58	12	35	5.1	35	5.2
12-Feb-08	370	690	79	320	66	21	65	10	60	12	36	5.3	35	5.4
11-Mar-08	400	730	84	340	69	22	71	11	62	13	37	5.4	37	5.6
05-May-08	400	740	84	340	68	24	75	11	62	13	38	5.4	37	5.6
04-Jun-08	360	670	77	320	64	20	65	10	58	12	35	5	34	5.1
15-Jul-08	340	640	73	300	61	20	62	9.8	56	11	33	4.7	32	4.8
31-Jul-08	270	520	61	260	51	16	52	8	45	9.2	27	3.8	26	3.8
03-Oct-08	330	630	74	310	64	20	60	9.8	55	11	32	4.5	31	4.5
11-Nov-08	320	610	72	300	62	20	61	9.6	53	11	30	4.3	29	4.3
09-Dec-08	200	430	50	210	45	14	44	6.6	37	7.4	21	2.9	19	2.8

Sample date	La	Ce	Pr	Nd	Sm	Eu	Gd	Tb	Dy	Ho	Er	Tm	Yb	Lu
29-Jan-09	280	540	66	280	60	18	54	9.1	50	10	28	3.8	25	3.6
11-Feb-09	190	410	51	210	46	15	45	6.7	37	7.2	20	2.7	18	2.5
25-Feb-09	270	540	65	280	59	19	57	8.8	48	9.6	26	3.6	24	3.4
04-Mar-09	270	540	65	280	59	19	57	8.8	49	9.5	27	3.6	24	3.4
19-Mar-09	280	560	68	290	60	19	59	9.1	50	9.9	27	3.7	24	3.6
25-Mar-09	280	550	68	290	61	20	60	9.1	51	10	27	3.8	25	3.6
03-Apr-09	280	560	68	290	61	20	61	9.2	51	10	28	3.8	25	3.6

Rincón de la Vieja

Sample date	La	Ce	Pr	Nd	Sm	Eu	Gd	Tb	Dy	Ho	Er	Tm	Yb	Lu
15-Oct-08	250	660	92	420	89	26	88.4	14	80	16	49	7.1	49	7.8
08-Nov-07	270	690	98	440	92.3	26	91.2	15	86	18	53	8.1	57	9
18-Apr-07	340	830	110	480	106	31	108	17	97	20	59	8.8	62	9.8
12-Sep-06	310	820	110	510	113	35	111	18	100	20	57	8.6	60	9
22-Mar-06	300	770	110	480	104	31	103	17	92	19	54	7.9	55	8.5
02-Jun-05	310	800	110	480	101	30	102	16	91	19	54	8.1	56	8.8
02-May-04	330	850	120	520	111	33	112	18	98	21	61	9.3	65	10

B. Appendix

Data from http://www-rci.rutgers.edu/~carr/index.html (accessed in October 2010) and Prosser and Carr (1987).

Country	sample	Data	pubs	Majors	Traces	Volcname	Descript.	collector/location
CR-	PO8393	5	ProsserCarr	dcp MC	dcp MC	Poas/crater section	lava	prosser/ru
CR-	PO8394	5	ProsserCarr	dcp MC	dcp MC	Poas/crater section	lava	prosser/ru
CR-	PO8395	5	ProsserCarr	dcp MC	dcp MC	Poas/crater section	lava	prosser/ru
CR-	PO8396	5	ProsserCarr	dcp MC	dcp MC	Poas/crater section	lava	prosser/ru
CR-	PO8397	10	ProsserCarr		icpms LP	Poas/crater section	lava	prosser/ru
CR-	PO8310	10	ProsserCarr		icpms LP	Poas/crater section	lava	prosser/ru
CR-	PO8340	5	ProsserCarr	dcp MC	dcp MC	Poas/crater section	lava	prosser/ru
CR-	PO8317	10	ProsserCarr		icpms LP	Poas/crater section	lava	prosser/ru
CR-	PO839	5	ProsserCarr	dcp MC	dcp MC	Poas/crater section	lava	prosser/ru
CR-	PO8369	5	ProsserCarr	dcp MC	dcp MC	Poas/crater section	lava	prosser/ru
CR-	PO838	5	ProsserCarr	dcp MC	dcp MC	Poas/crater section	lava	prosser/ru
CR-	PO8312	5	ProsserCarr	dcp MC	dcp MC	Poas/crater section	lapilli	prosser/ru
CR-	PO835	5	ProsserCarr	dcp MC	dcp MC	Poas/crater section	lava	prosser/ru
CR-	PO8398	5	ProsserCarr	dcp MC	dcp MC	Poas/crater section	lava	prosser/ru
CR-	PO8319	5	ProsserCarr	dcp MC	dcp MC	Poas/Botos	lava	prosser/ru
CR-	PO8349	5	ProsserCarr	dcp MC	dcp MC	Poas/von Frantzius	lava	prosser/ru

Country	sample	Data	pubs	Majors	Traces	Volcname	Descript.	collector/location
CR-	PO8349	25	ProsserCarr/ tLBphd		HRICPMS LB	Poas/von Frantzius	lava	prosser/ru
CR-	PO8363	5	ProsserCarr	dcp MC	dcp MC	Poas/Lapilli Tuff	lapilli	prosser/ru
CR-	PO8387	10	ProsserCarr	dcp MC	icpms LP	Poas/Lapilli Tuff	lapilli	prosser/ru
CR-	PO2	10	ProsserCarr	dcp MC	icpms LP	Poas/Laguna Hule	lava	carr/ru
CR-	PO3	5	ProsserCarr	dcp MC	dcp MC	Poas	lava	carr/ru
CR-	PO4	10	ProsserCarr	dcp MC	icpms LP	Poas	lava	carr/ru
CR-	PO1	25	ProsserCarr/ tLBphd	dcp MC	HRICPMS LB	Poas	lava	carr/ru
CR-	PO6	25	ProsserCarr/ tLBphd	dcp MC	HRICPMS LB	Poas	lava	carr/ru
CR-	PO7	25	ProsserCarr/ tLBphd	dcp MC	HRICPMS LB	Poas/Sabana Redonda	lava	carr/ru
CR-	PO8	5	ProsserCarr	dcp MC	dcp MC	Poas/Sabana Redonda	lava	carr/ru
CR-	PO9	25	ProsserCarr/ tLBphd	dcp MC	HRICPMS LB	Poas/Sabana Redonda	lava	carr/ru
CR-	PO10	10	ProsserCarr	dcp MC	icpms LP	Poas/Sabana Redonda	scoria?	carr/ru
CR-	RC	5	CarrRose87	dcp MC	dcp MC	Poas/Lavas Rio Cuarto		Alvarado/ru
CR-	PO-02-28	24	Carr et al 2007	xrf MSU	HRICPMS LB	Poas/Lavas Rio Cuarto	lava flow, rio cuarto quarry	Carr/Turrin
CR-	PO-02-29	24	Carr et al 2007	xrf MSU	HRICPMS LB	Poas/Lavas Rio Cuarto	dike or levee beneath maar deposit,rio cuarto	Carr/Turrin

sample	SiO_2	TiO_2	Al_2O_3	Fe_2O_3	FeO	MnO	MgO	CaO	Na_2O	K_2O	P_2O_5	H_2O^+
PO8393	57.55	0.72	16.79		7.72	0.14	3.35	6.94	3.28	1.66	0.171	
PO8394	57.98	0.7	16.44		7.12	0.13	3.21	6.63	3.22	1.75	0.179	
PO8395	54.88	0.73	16.71		7.61	0.15	3.47	6.61	2.91	1.44	0.16	
PO8396	56.18	0.74	16.8		8.03	0.155	3.63	7.13	3.15	1.55	0.185	
PO8397	51.47	0.83	18.32		10.09	0.18	5.59	10.23	2.56	0.86	0.17	
PO8310	50.48	0.77	17.41		6.8	0.18	5.01	9.98	2.25	0.85	0.13	
PO8340	52.52	1.03	16.89		9.8	0.18	4.44	9.03	2.81	1.46	0.274	
PO8317	49.1	1.05	15.52		9.47	0.15	7.11	9.44	2.46	1.52	0.42	
PO839	64.57	0.5	15.8		4.64	0.1	1.67	4.38	3.37	2.57	0.159	
PO8369	57.13	0.62	16.75		7.4	0.16	3.13	7.36	3.04	1.62	0.158	
PO838	53.98	0.75	17.38		9.21	0.14	4.2	7.99	2.75	1.2	0.165	
PO8312	61.54	0.58	16.37		5.6	0.13	2.38	5.35	2.94	2	0.18	
PO835	57.14	0.69	17.05		7.71	0.14	3.42	7.53	2.92	1.65	0.174	
PO8398	54.63	0.8	18.18		8.7	0.15	4.78	9.21	2.99	1.04	0.134	
PO8319	59.55	0.69	18.29		5.6	0.12	2.25	6.61	3.39	2.11	0.22	
PO8349	54.57	0.84	18.89		6.97	0.13	2.69	7.51	3.21	1.43	0.24	
PO8349	54.57	0.84	18.89	0	6.97	0.13	2.69	7.51	3.21	1.43	0.24	
PO8363	54.3	1	17.09		9.18	0.172	3.82	8.15	2.76	1.45	0.222	
PO8387	52.14	0.97	17.93		9.38	0.16	4.38	8.78	2.66	1.04	0.12	
PO2	51.13	0.75	19.64		8.99	0.18	5.55	9.61	2.89	0.75	0.15	0.3
PO3	62.15	0.62	18.78		3.77	0.1	1.17	5.96	4.05	2.51	0.23	0.26
PO4	54.21	0.79	19.35		7.71	0.16	3.84	8.61	3.09	1.06	0.19	0.24
PO1	54.07	0.99	19.81	0	7.49	0.14	2.66	8.14	3.62	1.97	0.4	0.21
PO6	58.43	0.9	16.85	0	7.17	0.16	2.8	6.38	3.64	2.12	0.26	0.46
PO7	55.66	1.06	16.76	0	8.87	0.17	3.68	7.8	3.31	2.03	0.31	0.2
PO8	58.73	0.92	17.04		7.43	0.17	2.98	6.74	3.64	2.07	0.26	0.16
PO9	56.59	1.04	16.85	0	8.85	0.17	3.11	6.95	3.09	2.01	0.28	0.56
PO10	52.36	1.11	18.24		9.92	0.19	3.89	8.25	3.16	1.24	0.26	0.45
RC	55.94	1.1	17.08		9.8	0.18	4.39	8.82	3.1	1.72	0.25	
PO-02-28	53.88	1.03	16.53	10.51		0.17	4.05	8.21	2.88	1.66	0.27	
PO-02-29	53.42	1.06	16.82	10.67		0.17	4.05	8.2	2.87	1.64	0.26	

sample	Li	Boron	Be	Sc	V	Cr	Co	Ni	Cu	Zn	Rb	Sr
PO8393				22.7	189.7	32.2		11.6	66.5		37.2	474
PO8394				23.3	198.5	32.1		14.7	97.6		25.6	489.7
PO8395				22.6	191.9	32.7		9.9	83.3		13	470.8
PO8396				26.4	227.2	45.3		21	91.4		23.5	519.4001
PO8397			0.88	31.05	271.2	24.09		21.37	111		15.8	586.5
PO8310			1	30.85	293.6	58.48		31.57	160.5		17.2	579.5
PO8340				33.9	326.2	26.9		15.7	118.4		31.2	621.5
PO8317			1.37	29.18	266.3	263.9		117.1	52.63		33.9	741.1
PO839				10.8	90.1	32.7		10.3	79.4		70.6	428
PO8369				19.3	179	26.9		12.2	110.9		36.7	565.6
PO838				23.5	245.7	33.5		12.9	109.9		18.4	598.3
PO8312				13.4	116	7		9	56		61	525
PO835				23	212.7	27.7		14.5	99.7		50	542
PO8398				28	269.2	26.8		13.9	121.2		27.1	564.5
PO8319				16.1	142	12		3	67		64.4	525
PO8349				22.5	220	25		30	102		40	584
PO8349	7.324			26.076	199.947	125.354	28.793	52.514	103.686	77.067	30.609	804.291
PO8363				30.3	281	12.4		14.2	155		44.2	536
PO8387			0.96	31.72	165.1	20.86		15.03	164.6		22.3	559.3
PO2		4.7	0.8	26.4	230	23.52		25.05	92.19		13.5	618
PO3				12.7	73.1	8.3		2.3	31		71.7	594.6
PO4			0.88	22.21	167	4.9		10.26	147.3		20.2	687.6
PO1	9.54			25.546	216.841	17.827	21.816	12.375	307.102	84.322	50.549	732.555
PO6	9.968			23.446	161.27	0.225	15.097	0.43	110.158	74.357	58.439	487.473
PO7	9.809			30.207	256.614	1.339	21.785	4.291	155.299	82.041	61.875	558.421
PO8				24.9	193.1	6.3		1.9	110.2		62.3	515.2
PO9	11.771			15.329	113.072	4.815	12.42	2.335	47.247	65.549	61.843	553.797
PO10		6.1	1.39	33.89	350.9	5.53		9.08	159		26.4	555.2

sample	Li	Boron	Be	Sc	V	Cr	Co	Ni	Cu	Zn	Rb	Sr
RC				32	324	15		12	182			532
PO-02-28	7.86			31.89	249.68	12.37	22.57	10.69	176.39	80.29	45.66	496.37
PO-02-29	7.5			33.32	248.64	9.56	22.92	6.83	169.56	79.23	39.24	500.31

sample	Y	Zr	Nb	Mo	Cs	Ba
PO8393		117.9				766.5
PO8394		144.9				828.6
PO8395		114				727.5
PO8396		132.9				767.6
PO8397	16.14	74.57	4.7			455.4
PO8310	16.83	85.29	8.4			480.3
PO8340		101.7				618.6
PO8317	25.09	164	13.5			702.2
PO839		176.8				976
PO8369		120.4				684.8
PO838		110.1				560.9
PO8312		126				814
PO835		149.1				697.7
PO8398		93.7				468.4
PO8319		150				794
PO8349		111				628
PO8349	20.551	146.773	14.854		0.376	718.156
PO8363		136				610
PO8387	20.26	105.6	7.33			494.3

sample	Y	Zr	Nb	Mo	Cs	Ba
PO2	16.19	78.02	6.1		0.283	374
PO3		198.7				1058.6
PO4	20.63	84.84	7.2		0.31	636.8
PO1	28.654	192.573	17.923		0.812	1027.086
PO6	26.815	159.917	13.708		0.811	853.667
PO7	28.185	163.868	13.928		1.156	868.183
PO8		161.1				782.2
PO9	27.998	188.082	17.859		0.606	1591.099
PO10	27.79	154.6	12.2			727.9
RC		131				635
PO-02-28	21.74	125.03	10.83	2.46	0.92	609.44
PO-02-29	22.57	128.62	11.16	2.38	0.9	642.4

sample	Hf	Ta	W	Tl	Pb	Th	U	$^{87}Sr/^{86}Sr$	$^{143}Nd/^{144}Nd$
PO8397								0.70379	
PO8310								0.703703	
PO8317								0.70379	0.51289
PO8349	3.478	0.747			3.585	5.123	1.737		
PO8387								0.703715	
PO2	1.79				5.27	1.426	0.596	0.703735	
PO4	1.956				6.54	2.886	1.028		
PO1	4.749	0.933			6.033	9.504	3.284		
PO6	4.231	0.93			7.501	9.446	3.284		
PO7	4.074	0.83			6.828	9.629	3.367		
PO9	4.592	0.966			4.219	12.431	3.798		
PO10								0.70373	0.51288
PO-02-28	3.23	0.73	0.61	0.05	5.79	6.1	2.31		
PO-02-29	3.31	0.74	0.6	0.06	5.73	6.28	2.32		

sample	La	Ce	Pr	Nd	Sm	Eu	Gd	Tb	Dy	Ho	Er	Tm	Yb	Lu
PO8397	15.44	31.07		16.08	3.4	1.06	3.41		3.72		1.69		1.4	
PO8310	15.64	31.07		14.77	3.27	0.97	3.78		3.76		1.54		1.39	
PO8317	46.14	93.32		44.99	7.77	2.26	6.77		4.99		2.4		1.98	
PO8349	32.168	64.985	8.817	31.528	6.12	1.633	5.031	0.706	3.688	0.703	1.914	0.281	1.753	0.261
PO8387	17.47	36.77		19.55	4.26	1.18	4.09		4.23		1.99		1.85	
PO2	10.71	23.95		13.05	2.71	1.02	3.18		3.58		1.65		1.46	
PO4	19.71	36.82		18.13	4.14	1.15	3.59		3.6		1.94		1.38	
PO1	40.922	87.013	11.244	40.614	8.246	1.959	6.988	0.988	5.213	1.013	2.81	0.42	2.649	0.397
PO6	28.712	60.162	7.705	27.812	5.931	1.474	5.502	0.816	4.647	0.941	2.687	0.412	2.653	0.407
PO7	32.879	70.989	8.898	32.283	6.771	1.664	6.108	0.89	4.766	0.955	2.689	0.408	2.591	0.393
PO9	50.655	102.291	12.946	43.437	7.9	1.977	6.374	0.893	4.599	0.892	2.55	0.393	2.534	0.396
PO10	29.51	59.54		28.15	6.29	1.5	5.55		5.4		2.62		2.28	
PO-02-28	23.62	51.61	5.86	23.88	5.22	1.27	4.99	0.74	4.06	0.83	2.34	0.36	2.26	0.34
PO-02-29	25.62	53.85	6.16	25.22	5.45	1.31	5.21	0.77	4.24	0.86	2.43	0.37	2.35	0.35